EXPERIMENTAL INVESTIGATION AND SIMULATION OF A FLUIDIZED-BED GASIFIER USING SWITCHGRASS

By

ASHOKKUMAR M SHARMA

Bachelor of Engineering in Mechanical Engineering
Maharaja Sayajirao University of Baroda
Vadodara, Gujarat, India
1998

Master of Technology in Mechanical Engineering
Sardar Vallabhbhai National Institute of Technology
Surat, Gujarat, India
2006

Submitted to the Faculty of the
Graduate College of the
Oklahoma State University
in partial fulfillment of
the requirements for
the Degree of
DOCTOR OF PHILOSOPHY
December, 2013

EXPERIMENTAL INVESTIGATION AND

SIMULATION OF A FLUIDIZED-BED GASIFIER

USING SWITCHGRASS

Dissertation Approved:

Dr. Ajay Kumar

Dissertation Advisor

Dr. Raymond L. Huhnke

Dissertation Co-Advisor

Dr. Krushna N. Patil

Dr. James R. Whiteley

ACKNOWLEDGEMENTS

With my great pleasure and deep sense of gratitude, I would like to thank many individuals who helped to complete this study. My to-date success would not have been possible without their guidance and support.

I would like express my great appreciation and sincere gratitude to my research advisor Dr. Ajay Kumar for his guidance, mentorship and outstanding support right from the beginning of my doctoral study at Oklahoma State University. His continuous effort has helped me to achieve set goals and objectives of this research. My research writing and project management skills considerably improved through his valuable advices and constructive suggestions. I am extremely grateful to my co-advisor Dr. Raymond L. Huhnke for the guidance and valuable advice to complete this research. He has always been a source of motivation and great supporter. His thoughtful consideration of my research studies has brought out the best of me and contributed a lot in improving my presentation skills. I feel very fortunate to work with Dr. Kumar and Dr. Huhnke, and I am greatly indebted to them for my all accomplishment during this time.

I would like to thank my research advisory committee members Dr. Krushna N. Patil and Dr. James R. Whiteley for the guidance and providing their expert advices for improving the overall quality of this research. I am grateful to Dr. Sundar Madihally for extending his technical support and guidance to complete reaction kinetics modeling of

biomass gasification.

I acknowledge BAE workshop team, Wayne R. Kiner, Mike Veldman, Robert J. Harrington and Jason Walker for their excellent support for constructing and developing the necessary experimental facilities for this research. I also appreciate the support of Mark Gilstrap regarding lab safety and management during this research. I am so grateful to Nancy Rogers and BAE administrative staff for their best support and services.

I convey my sincere thanks to graduate students Siddharth Patil, Balaji Dhamodharan, Bipul Chandra, Nitesh Rentam, Karthikragunath Mariyappan, Vamsee Pasangulapati, Pushpak Bhandari, Shaswat Dixit, Mohit Dobhal, Deepak Padaliya, Madhura Sarkar, Cody Collins, Kezhen Qian and Zixu Yang for their assistance in conducting the experiments. This work would not have been done without their hard work and continuous involvement. I appreciate the support of Mr. Prakash Bhoi, Dr. Karthikeyan Ramachandriya and Dr. Sachin Handa for the technical discussion and extending their necessary support during this period.

I would like to thank Dr. S. A. Channiwala and Prof. B. S. Pathak for sharing their expertise and developing my overall skills in the area of biomass thermochemical conversion. I thank Dr. Dinesh Babu whose continuous effort and guidance have helped me to obtain a job opportunity during this time. I am also grateful to Dr. Hiren Bhavsar, Jalpa Bhavsar, Dr. Amit Khanchi, Dr. Bhavna Sharma, Shri Harshadbhai Patel for their valuable friendship and societal support.

I am extremely thankful to my wife, Kavita. This accomplishment would not have been possible without her constant support and care. I am so thankful to my sons Dishant and Arnav for always being my source of great energy and relaxation. I am always

indebted to my parents for their support, love and sacrifice. I am thankful to my elder brother, Mr. Santosh Sharma, for mentoring my career path start from the beginning of my education. I also thank my whole family for their blessings and support throughout my career journey.

Name: ASHOKKUMAR M SHARMA

Date of Degree: DECEMBER, 2013

Title of Study: EXPERIMENTAL INVESTIGATION AND SIMULATION OF A FLUIDIZED-BED GASIFIER USING SWITCHGRASS

Major Field: BIOSYSTEMS ENGINEERING

Abstract:

The overall goal of this research was to improve and optimize yield and composition of syngas generated from biomass gasification using an autothermal lab-scale fluidized-bed gasifier, and to develop a biomass gasification model to predict the syngas composition. The first objective was to design, develop and experimentally optimize the equivalence ratio (ER) of a 5 kg/h lab-scale fluidized-bed gasifier using switchgrass as a biomass feedstock. The ER of 0.32 was found to be optimal with the maximum syngas heating value of 6.6 MJ/Nm^3, and cold and hot gas efficiencies of 71 and 75%, respectively. Our next objective was to investigate the effects of bed-materials (i.e. a mixture of sand, switchgrass and gasifier solid residues (GSR)) on fluidization characteristics (minimum fluidization velocity and bed-pressure drop) that are critical for optimizing reaction conditions in a fluidized-bed gasifier. Results showed that the fluidization characteristics were found to be strongly dependent upon mixture's effective properties, which were determined using properties of all mixture components. GSR and switchgrass present in the mixture had a highly significant (p-value < 0.001) influence on fluidization. Then, the syngas yield was further improved by optimizing steam injection location into the gasifier. Steam injection locations of 51, 152, and 254 mm above the distributor plate and steam-to-biomass ratios (SBRs) of 0.1, 0.2, and 0.3 were selected. The best syngas yields (0.018 kg H_2/kg biomass and 0.513 kg CO/kg biomass) and gasifier efficiencies (cold gas efficiency of 67%, hot gas efficiency of 72%, and carbon conversion efficiency of 96%) were obtained at the steam injection location of 254 mm and SBR of 0.2. Finally, biomass gasification models, using three modeling approaches, i.e. Gibbs equilibrium, reaction kinetics and computational fluid dynamics (CFD) with reaction kinetics, were developed and validated with experimental results. Results showed that reaction kinetics and CFD models with reaction kinetics showed considerable improvements in the prediction of syngas composition and yield, as well as gasification energy efficiency compared to the Gibbs equilibrium model. Further, the CFD model also revealed insight about distribution of syngas constituents, temperature and dominating reactions within the gasifier.

TABLE OF CONTENTS

Chapter Page

Chapter Page

Chapter Page

Chapter Page

Chapter Page

LIST OF TABLES

Table Page

LIST OF FIGURES

Figure Page

CHAPTER I

INTRODUCTION

Biomass such as plants, agro-residues, and grasses is a renewable and sustainable source of energy. Many researches have successfully demonstrated the generation of heat and power from biomass (Abelson, 1976; Jenkins and Bhatnagar, 1991; Quaark et al., 1999). However, biomass is categorized as a low-grade energy fuel (Rao and Reddy, 2010) and has limited uses as a direct feedstock for generating liquid fuels and chemicals. Thermochemical conversion process, such as gasification and pyrolysis, converts the solid biomass into gaseous or liquid fuel under high temperature (Brown et al., 1986; Kumar et al., 2009b). Gasification process yields a gaseous product, called syngas or producer gas, through partial oxidation of biomass in the presence of one or more oxidizing agent such as air, steam, and oxygen. Biomass generated syngas or producer gas consists of CO, H_2, CO_2, CH_4, C_2H_2, C_2H_4, C_2H_6, N_2 (if air is used as oxidizing agent) and impurities such as tars, H_2O, NH_3 and H_2S. Syngas is considered a building block for many liquid fuels and chemicals such as Fischer-Tropsch gasoline, methanol, and ethanol (Spath and Dayton, 2003). However, synthesis of liquid fuels and chemicals using various conversion processes requires a quality syngas with different concentrations of H_2, CO, and CO_2 (Wender, 1996), as well as H_2/CO ratio from 0.4 to 4 (Hamelinck and Faaij, 2002; Jess et al., 1999; Klasson et al., 1993; Spath and Dayton,

2003; Wender, 1996). To maximize the product (fuels, chemicals or power) yield, it is necessary that biomass gasification matches the needs of downstream conversions in terms of gas composition, levels of impurities, and yield of the syngas. Currently available experimental and modeling techniques of biomass gasification are inadequate to provide and predict syngas with gas compositions needed for production of fuels and chemicals.

The biomass-generated syngas yield and quality rely on several factors such as the properties of biomass, gasifier reactor design and operating conditions, and oxidizing agents. Biomass properties, such as size, shape, moisture content, and chemical compositions, significantly influence the quality of syngas in terms of gas composition and impurities. The biomass properties depend upon the biomass type such as switchgrass, which is a perennial grass. The physical properties and chemical composition of switchgrass varies with the geographic location, and variety.

Switchgrass is a lignocellulosic material primarily composed of cellulose, hemicellulose, and lignin. Ash and moisture are the other inorganic compounds, present in the switchgrass. All these organic and inorganic compounds of the switchgrass participate in gasification reactions and influence the overall quality of the syngas in terms of gas composition and contaminants. Literature shows numerous experimental (Bhoi et al., 2006; Boateng et al., 1992; Boateng et al., 2007; Campoy et al., 2009; Hanping et al., 2008; Kumar et al., 2009a; Kurkela and Ståhlberg, 1992; Singh et al., 2006) and simulation (Kumar et al., 2009c; Nikoo and Mahinpey, 2008; Paviet et al., 2009; Puig-Arnavat et al., 2010; Wenyi and Qin, 2010) studies on gasification using different biomass feedstocks; however, limited information is available on fluidized-bed gasification of switchgrass as a biomass feedstock.

Gasifier operating conditions such as flowrate of oxidizing agent, biomass feedrate, and gasification temperature influence syngas quality. The appropriate flow of oxidizing agent is key to maintain effective fluidization in the reactor bed, and to optimize reaction conditions in a fluidized-bed gasifier. An improper fluidization leads to inefficient conversion due to many reasons such as low heat and mass transfers, ineffective gas-solid phase reactions, and uneven reactor temperatures in autothermal gasification (Daleffe et al., 2008). Therefore, one focus of this study was on fluidization characteristics of all participating solids during gasification and optimization of gasifier reaction conditions.

Oxidizing agent, such as air, oxygen, and steam, used in biomass gasification also effects on the syngas quality. Researchers have shown that injecting steam with air in air-steam gasification yields syngas with higher H_2 and CO contents (Kumar et al., 2009a; Lv et al., 2003; Lv et al., 2004) which makes the syngas a more suitable feedstock to convert into liquid fuels and chemicals. Since reaction conditions inside the gasifier vary along the height of the gasifier reactor, we hypothesized that the location of steam injection has an influence on the syngas quality. This was another focus of this study.

With the advent of latest computational techniques and sophisticated simulation software such as ASPEN plus™ and CFD (computational fluid dynamics), biomass gasification can be optimized and syngas composition can be predicted more reliably. ASPEN plus™ software contains a wide property database of conventional materials and various reaction models, such as Gibbs equilibrium reactor model (RGIBBS) and continuous stirred-tank reactor (RCSTR), which can be used to simulate biomass gasification. There are several ASPEN plus™ based modeling studies on biomass gasification using an equilibrium reactor called ‘RGIBBS’ (Kumar et al., 2009c; Nikoo and Mahinpey, 2008; Paviet et al.,

2009; Puig-Arnavat et al., 2010; Wenyi and Qin, 2010). However, the gasification models based on the Gibbs equilibrium reactor showed large deviations between the predicted and experimental values of gas composition. The primary reason for these deviations is the unrealistic assumption made in Gibbs equilibrium model that gasification reactions reach equilibrium within the short residence time of gasification. Moreover, the model does not consider fluidization hydrodynamics that occurs in fluidized-bed gasifier along with several heterogeneous and homogeneous reactions.

By including reaction kinetics of major reactions in the gasification model, continuous stirred-tank reactor model, i.e. RCSTR of ASPEN plus™, can more reliably predict syngas composition. Nikoo and Mahinpey (2008) developed a RCSTR reactor-based gasification model using ASPEN plus™ for pine sawdust. However, authors assumed a limited number of gasification reactions that may have led to the deviations between experimental and predicted data. Further, the authors assumed that combustion of volatiles (all gaseous products from biomass devolatization) followed Gibbs equilibrium model but the volatile reactions are so fast that assuming equilibrium state during gasification is impractical and leads to deviations between predicted and experimental results. Another focus of this research was to build and evaluate a significantly improved reaction kinetics-based model by incorporating all major gasification reaction.

Reaction kinetic-based gasification model, stated above, does not predict the temperature and species distributions along the height of the gasifier reactor. Further, the reaction kinetics-based gasification model does not take into consideration the non-ideal behavior of the gasifier, which is effected by the fluidization hydrodynamics. In the last part of this study, we propose to incorporate both reaction kinetics and fluidization characteristics,

which are effected by shape and size of biomass and bed materials, in the gasification model using CFD.

1.1 Objectives

The overall goal of the proposed research was to improve and optimize composition of syngas generated from switchgrass gasification using a lab-scale fluidized-bed gasifier and to develop a biomass gasification model to predict the syngas composition. The specific objectives of proposed studies were as follows:

1. The objective of study-1 was to design, develop and evaluate performance of a 5 kg/h laboratory-scale fluidized bed biomass gasifier (FBBG) in terms of reactor temperature profile, yield, composition, and heating value of producer gas, as well as gasifier efficiencies by varying the equivalence ratio.
2. The objective of study-2 was to investigate effect of reactor bed composition, i.e. a mixture of gasifier solid residues, switchgrass, and inert material, on fluidization.
3. The objective of study 3 was to investigate effect of steam injection location on syngas composition and yield, gas tar and particulates contents, as well as gasifier efficiencies.
4. The objective of study 4 was to develop a reaction kinetics-based gasification model using continuous stirred-tank reactor (CSTR) to predict syngas composition and yield, and validate model prediction with the experimental results obtained using the experimental results obtained on our lab-scale fluidized-bed gasifier.
5. The objective of study 5 was to develop a CFD-based gasification model by incorporating fluidization hydrodynamics and gasification reaction kinetics to predict

reliable gas composition and yield, and validate model prediction using the experimental results obtained on our lab-scale fluidized-bed gasifier.

1.2 References

Abelson, P.H. 1976. Energy from biomass. *Science*, **191**(4233), 1221.

Bhoi, P.R., Singh, R.N., Sharma, A.M., Patel, S.R. 2006. Performance evaluation of open core gasifier on multi-fuels. *Biomass and Bioenergy*, **30**(6), 575-579.

Boateng, A., Walawender, W., Fan, L., Chee, C. 1992. Fluidized-bed steam gasification of rice hull. *Bioresource Technology*, **40**(3), 235-239.

Boateng, A.A., Banowetz, G.M., Steiner, J.J., Barton, T.F., Taylor, D.G., Hicks, K.B., El-Nashaar, H., Sethi, V.K. 2007. Gasification of Kentucky bluegrass (Poa pratensis l.) straw in a farm-scale reactor. *Biomass & Bioenergy*, **31**(2-3), 153-161.

Brown, M., Baker, E., Mudge, L. 1986. Environmental design considerations for thermochemical biomass energy. *Biomass*, **11**(4), 255-270.

Campoy, M., Gómez-Barea, A., Vidal, F., Ollero, P. 2009. Air-steam gasification of biomass in a fluidised bed: Process optimisation by enriched air. *Fuel Processing Technology*, **90**(5), 677-685.

Daleffe, R.V., Ferreira, M.C., Freire, J.T. 2008. Effects of binary particle size distribution on the fluid dynamic behavior of fluidized, vibrated and vibrofluidized beds. *Brazilian Journal of Chemical Engineering*, **25**, 83-94.

Hamelinck, C.N., Faaij, A.P.C. 2002. Future prospects for production of methanol and hydrogen from biomass. *Journal of Power Sources*, **111**(1), 1-22.

Hanping, C., Bin, L., Haiping, Y., Guolai, Y., Shihong, Z. 2008. Experimental investigation of biomass gasification in a fluidized bed reactor. *Energy & Fuels*, **22**(5), 3493-3498.

Jenkins, B.M., Bhatnagar, A.P. 1991. On the Electric-Power Potential from Paddy Straw in the Punjab and the Optimal Size of the Power-Generation Station. *Bioresource Technology*, **37**(1), 35-41.

Jess, A., Popp, R., Hedden, K. 1999. Fischer-Tropsch-synthesis with nitrogen-rich syngas - Fundamentals and reactor design aspects. *Applied Catalysis a-General*, **186**(1-2), 321-342.

Klasson, K.T., Ackerson, M.D., Clausen, E.C., Gaddy, J.L. 1993. Biological Conversion of Coal and Coal-Derived Synthesis Gas. *Fuel*, **72**(12), 1673-1678.

Kumar, A., Eskridge, K., Jones, D.D., Hanna, M.A. 2009a. Steam-air fluidized bed gasification of distillers grains: Effects of steam to biomass ratio, equivalence ratio and gasification temperature. *Bioresource Technology*, **100**(6), 2062-2068.

Kumar, A., Jones, D.D., Hanna, M.A. 2009b. Thermochemical biomass gasification: A review of the current status of the technology. *Energies*, **2**(3), 556-581.

Kumar, A., Noureddini, H., Demirel, Y., Jones, D., Hanna, M. 2009c. Simulation of corn stover and distillers grains gasification with Aspen Plus. *Transactions of the ASAE*, **52**(6), 1989-1995.

Kurkela, E., Ståhlberg, P. 1992. Air gasification of peat, wood and brown coal in a pressurized fluidized-bed reactor. I. Carbon conversion, gas yields and tar formation. *Fuel Processing Technology*, **31**(1), 1-21.

Li, X., Grace, J., Lim, C., Watkinson, A., Chen, H., Kim, J. 2004. Biomass gasification in a circulating fluidized bed. *Biomass and Bioenergy*, **26**(2), 171-193.

Lv, P., Chang, J., Xiong, Z., Huang, H., Wu, C., Chen, Y., Zhu, J. 2003. Biomass Air- Steam Gasification in a Fluidized Bed to Produce Hydrogen-Rich Gas. *Energy Fuels*, **17**(3), 677-682.

Lv, P., Xiong, Z., Chang, J., Wu, C., Chen, Y., Zhu, J. 2004. An experimental study on biomass air-steam gasification in a fluidized bed. *Bioresource Technology*, **95**(1), 95-101.

Nikoo, M.B., Mahinpey, N. 2008. Simulation of biomass gasification in fluidized bed reactor using ASPEN PLUS. *Biomass and Bioenergy*, **32**(12), 1245-1254.

Paviet, F., Chazarenc, F., Tazerout, M. 2009. Thermo chemical equilibrium modelling of a biomass gasifying process using Aspen Plus. *International Journal of Chemical Reactor Engineering*, **7**(7), 40.

Puig-Arnavat, M., Bruno, J.C., Coronas, A. 2010. Review and analysis of biomass gasification models. *Renewable and Sustainable Energy Reviews*, **14**(9), 2841-2851.

Quaark, P., Knoef, H., Stassen, H.E. 1999. Energy from biomass: a review of combustion and gasification technologies. *World Bank-free PDF*.

Rao, K.V.N.S., Reddy, G.V. 2010. Cold Flow Studies of Rice Husk, Saw Dust, and Groundnut Shell Fuels in a Fluidized Bed. *Energy Sources, Part A: Recovery, Utilization, and Environmental Effects*, **32**(18), 1701 - 1711.

Sharma, A.M., Kumar, A., Patil, K.N., Huhnke, R.L. 2011. Performance evaluation of a lab-scale fluidized bed gasifier using switchgrass as feedstock. *Transactions of the ASABE*, **56**(6), 2259-66.

Singh, R., Sharma, A., Jena, U., Bhave, A., Vyas, D. 2006. Case study of open core down draft gasifier system for cooking applications. *Agricultural Engineering Today*, **30**(3-4), 19-25.

Spath, P.L., Dayton, D.C. 2003. Preliminary screening - technical and economic assessment of synthesis gas to fuels and chemicals with emphasis on the potential for biomass-derived syngas. NREL Report, Contract No. DE-AC36-99-GO10337.

Wender, I. 1996. Reactions of synthesis gas. *Fuel Processing Technology*, **48**(3), 189-297.

Wenyi, T., Qin, Z. 2010. Simulation of Hydrogen Production in Biomass Gasifier by ASPEN PLUS. *Power and Energy Engineering Conference (APPEEC), 2010 Asia-Pacific*, 28-31 March 2010. pp. 1-4.

CHAPTER II

PERFORMANCE EVALUATION OF A LAB-SCALE FLUIDIZED BED GASIFIER USING SWITCHGRASS AS FEEDSTOCK

This research paper was published as "Sharma, A.M., Kumar, A., Patil, K.N., Huhnke, R.L. 2011. Performance evaluation of a lab-scale fluidized bed gasifier using switchgrass as feedstock. *Transactions of the ASABE*, **56**(6), 2259-66."

Abstract

The goal of present study was to evaluate performance of a 5 kg/h laboratory-scale fluidized bed biomass gasifier (FBBG) using switchgrass as a biomass feedstock. The main components of the FBBG system were a biomass feeding unit, a fluidized bed gasifier, an air supply unit with preheater, an air pressure regulator, two cyclone separators, an orifice plate, and a jet-type self-aerated producer gas burner. Silica sand was used as a bed material. Experiments were conducted to evaluate the effect of equivalence ratio (ER) on the reactor temperature profile, energy efficiencies, and producer gas yield and quality such as gas composition and particulate contents. An ER of 0.32 was found to be optimal with a producer gas higher heating value of 6.6MJ/Nm^3 and tar and particulates contents of 4.28 and 0.13 g/Nm^3, respectively. The cold and hot gas efficiencies at the optimal condition were 71% and 75%, respectively, and these efficiencies decreased on either side of the optimal value of ER. Both gas yield and carbon conversion efficiency were found to be in positive correlation with ER, with maximum values of 2.5 Nm^3/kg biomass (d.b.) and 96%, respectively, at an ER of 0.45.

Keywords: Biomass; equivalence ratio; fluidized bed gasifier; particulates; producer gas; switchgrass; tar

2.1 Introduction

Gasification and pyrolysis are the two primary thermochemical conversion processes that convert a solid biomass into gaseous and liquid fuels with the help of high temperature (Brown et al., 1986). The gasification process yields a gaseous product, called producer gas or syngas, through partial oxidation of biomass in the presence of one or more oxidizing agents such as air, steam, and oxygen (Li et al., 2004). The producer gas can be used for various thermal and power applications or, after cleaning and conditioning, can be further processed into liquid fuels and chemicals (Wang et al., 2008). Several gasifier designs, such as fluidized bed, updraft, downdraft, and crossed draft, accept a wide variety of biomass feedstocks for conversion into gaseous fuel, which makes the gasification process a more viable route for using numerous biomass resources for fuel and power production (Overend, 2004). Fluidized bed gasifiers are more commonly used for gasifying low-density, irregularly shaped, poor flowability, high ash content or powdery biomass feedstocks such as pine sawdust, chopped wheat straw, rice hulls, and almond shells (Boateng et al., 1992; Ergudenler and Ghaly, 1993; Kurkela and Ståhlberg, 1992; Natarajan et al., 1998; Rapagnà and Latif, 1997). Even a low-grade feedstock of non-uniform size with varying moisture content (3.5% to 25%) can easily be gasified using fluidized bed reactors (Natarajan et al., 1998). Moreover, fluidized bed reactors have inherent advantages of high heat and mass transfers because of better biomass mixing and efficient gas-solid phase reactions, which result in isothermal operating condition and high conversion efficiency (Buragohain et al., 2010).

A fluidized bed gasifier consists of a cylindrical reactor column with a bed of inert material, such as sand or a mixture of sand and catalysts, supported by a distributor

plate. Initially, the sand bed is preheated by an external heat source. Air or another oxidizing agent is then made to flow through the gasifier for fluidization of the bed materials and for partial oxidation of the biomass. The temperature of the gasifier varies in the range of 700°C to 900°C (Buragohain et al., 2010). An auger is used to introduce biomass into the gasifier. The biomass particles then flow upward through the fluidized bed, undergo a series of gasification reactions and finally convert primarily into producer gas. Steam generation, power production using internal combustion engine or gas turbine, and production of fuels and chemicals are possible applications of producer gas. The gasifier performance parameters such as yield, composition, and heating value of producer gas, amount of tar and particulates in the producer gas, and energy efficiencies depend upon both the biomass properties and the gasification operating conditions. The biomass properties include particle size, composition, and moisture content. The operating conditions include flow rate and type of oxidizing agent, and reactor temperature and pressure. For gasification with air as an oxidizing agent, the gasifier performance is highly dependent on the equivalence ratio (ER), which is the ratio of air supplied to air needed for complete combustion. In addition, inert materials or catalysts used in the gasifier bed, and the type of the fluidized reactor design, such as bubbling bed, circulatory bed, and dual bed, also influence the performance.

Switchgrass, a perennial grass, is locally available in the state of Oklahoma and can be a potential biomass feedstock for gasification. It is estimated that 377 million dry tons of perennial crops can be produced on a sustainable basis in the U.S. with changes in land use patterns (Perlack et al., 2005). The physical properties and chemical composition of switchgrass significantly depend upon the geographic location where it grows, and the

variety such as Kanlow and Alamo. Gasification studies for several biomass feedstocks are reported in the literature; however, little information is available on gasification of switchgrass as a biomass feedstock. The goal of this study was to evaluate performance of a 5 kg/h laboratory-scale fluidized bed biomass gasifier (FBBG) in terms of reactor temperature profile, yield, composition, and heating value of producer gas, as well as gasifier efficiencies by varying the ER using Kanlow switchgrass as the biomass feedstock.

2.2 Materials and methods

2.2.1 Experimental setup

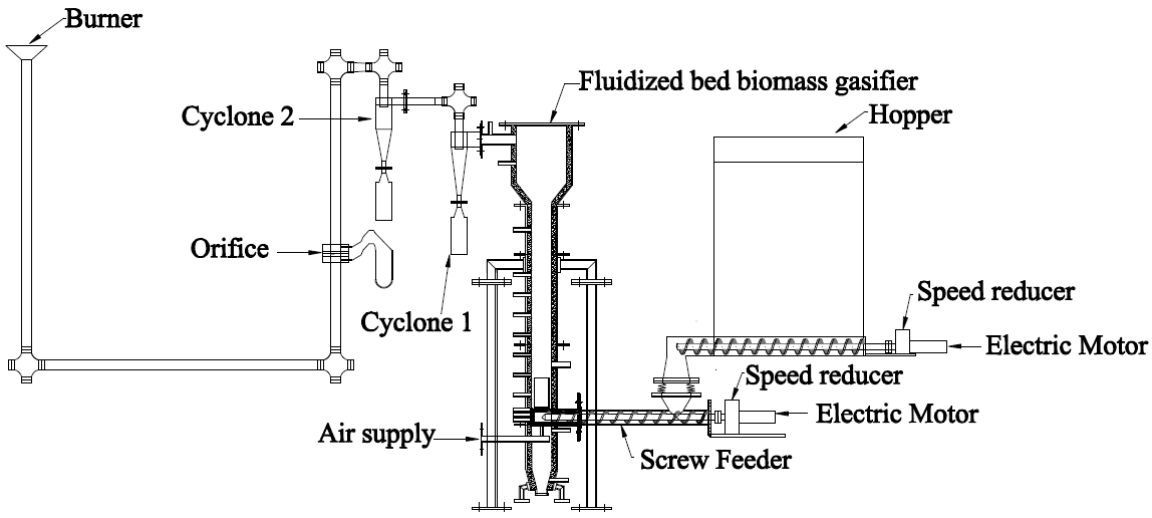

Fig. 2.1. Schematic of the fluidized bed gasifier setup

Fig. 2.1 shows the experimental setup of the laboratory-scale fluidized bed gasifier. A hopper was used to store and feed the biomass into a screw feeder. The screw feeder injects the biomass into the gasifier. The inside and outside of the gasifier were thermally insulated with a 25.4 mm thick refractory lining and a 25.4 mm thick cerawool layer, respectively. Air supplied into the gasifier was measured with a mass flowmeter (model 8059MPNH, Eldridge Products, Inc., Monterey, Cal.). During startup, air was

preheated with a heat torch (model HT150, Farnam Custom Products, Arden, N.C.). Two cyclone separators were connected in series for removal of soot and particulate matter from the producer gas. A calibrated orifice plate was fitted in the gas line for measuring the flow rate of tar-laden producer gas. The producer gas was finally combusted in a gas burner.

2.2.2 Gasifier components

2.2.2.1 Lab-scale fluidized bed gasifier

The reactor is the main component of the gasifier where the gasification process takes place. Many design parameters, such as thermal power output, biomass consumption rate, ER, and superficial velocity, were considered for determining the reactor dimensions (Fig. 2.1). Based on the maximum thermal power output of 20 kW, a biomass consumption rate was estimated by assuming gasifier efficiency of 77% and gas heating value of 5.7 MJ/Nm^3 (van den Enden and Lora, 2004). The gasifier reactor was designed for a biomass throughput of 5 kg/h. The reactor diameter was determined by assuming air superficial velocity of 0.3 m/s (Mansaray et al., 1999; Patil et al., 2005) at an ER of 0.3 (Cateni, 2007; Gabra et al., 2001; van den Enden and Lora, 2004). Other reactor dimensions, such as height of freeboard and disengagement zones, were calculated by assuming a height to diameter ratio of 14.5, as reported by (Cateni, 2007) for our pilot-scale bubbling fluidized bed gasifier. The gasifier reactor (102 mm i.d. × 1118 mm height) and disengagement zone (250 mm i.d. × 310 mm height) were fabricated of SS 316 steel.

2.2.2.2 Hopper and screw feeder

The biomass hopper was used to store the biomass, and the screw feeder was used to inject the biomass into the gasifier reactor. Biomass feed rate, physical characteristics (Dai and Grace, 2008a, b) of chopped switchgrass, and desired test duration were considered in designing the hopper and the screw feeder (Fig. 2.1). Physical characteristics of chopped switchgrass included particle size, shape, bulk density, and angle of repose. The biomass hopper was designed to store 20 kg of chopped switchgrass. The hopper (610 mm length × 305 mm width × 914 mm height) was fabricated of SS 316 steel. The diameter, pitch, depth, and length of the feeder screw were 46.7 mm, 50.8 mm, 10.7 mm, and 762 mm, respectively. The feeder screw was fabricated of 4140 HT alloy steel. The hopper screw was designed to run at variable speeds in the range of 0 to 9.43 rad/s, whereas the speed of the screw feeder was kept constant at 3.14 rad/s.

2.2.2.3 Cyclones

Standard cyclone designs called 1D3D and 2D2D, as reported by Parnell et al. (1982), were used to design cyclone separators for removing soot and particulate materials from the producer gas (Parnell and Guzman, 1982). The above design notations represent the lengths of the barrel (upper cylindrical section) and the cone (lower conical section) of the cyclone, respectively. In this notation, D stands for the diameter of the barrel; therefore, 1D3D notation means that the lengths of the barrel and cone are one time and three times the barrel diameter, respectively. Producer gas flow rate of 12.5 Nm^3/h and gas velocity of 15.4 m/s at the inlet of the cyclone were assumed to calculate the inlet cross-sectional area for both cyclones. Both cyclones were fabricated of SS 316 steel.

2.2.2.4 Orifice plate

A maximum gas flow rate of 12.5 Nm^3/h was assumed for designing the orifice plate (Miller, 1996). The orifice plate was fabricated of SS 304 steel and was installed in-line with the gas pipeline for measuring producer gas flow rate.

2.2.2.5 Producer gas burner

A jet-type self-aerated atmospheric burner was designed for the combustion of the producer gas (Priestley, 1973). The burner was fabricated of SS 316 steel. The central part of the burner was composed of a converging pipe that increased the gas velocity, which allowed self-aeration of the gas through two air ports. The air ports were aligned at 30° tangentially in the horizontal direction to produce a swirling gas flame. A maximum gas flow rate of 12.5 Nm^3/h was assumed to design the burner.

2.2.2.6 Distributor plate and gas pipeline

A distributor plate (280 mm o.d. × 5 mm thick) was used to support the silica sand (bed material) and to uniformly distribute the inlet air flowing through the gasifier bed. The distributor plate was made of SS 316 steel and contained 37 equally spaced holes (3 mm i.d.). A wire mesh (30 × 30 mesh size) was placed on top of the distributor plate to prevent sand from falling through the plate. The gasifier exit port was connected to the cyclone separators using a gas pipeline of 50.8 mm. The cyclones and the producer gas burner were connected with a gas pipeline of 38.1 mm i.d. The gas pipelines were made of SS 316 steel.

2.2.3 Material characteristics

2.2.3.1 Silica sand

Silica sand (supplied by Oglebay Norton Industrial Sands, Inc., Brady, Tex.) was used as the bed material for all experiments. Particle size distribution of the silica sand was determined by ANSI/ASAE Standard S319.3 (ASABE-Standards, 1997) using a sieve shaker (CSC Scientific, Fairfax, Va.). To determine bulk density, the silica sand was poured into a container of known weight and volume. The container with silica sand was weighed. The bulk density was the ratio of the weight of the silica sand and the volume of the container. The particle size and bulk density of the silica sand were in the range of 106 to 850 μm and 1612 to 1668 kg/m^3, respectively.

2.2.3.2 Chopped switchgrass

Kanlow switchgrass grown at the Oklahoma State University Agronomy Research Station and harvested in the fall of 2009 was used as the biomass feedstock. Switchgrass bales were chopped using a Haybuster tub grinder (H1000, Duratech Industries International, Inc., Jamestown, N.D.) with a screen size of 25 mm. Properties of the chopped switchgrass are shown in Table 2.1. Proximate analysis (moisture, volatile matter, fixed carbon, and ash percentages on weight basis) was performed using ASTM D-3172 and ASAE Standard S358.2 (ASABE-Standards, 2008). Proximate analysis was performed using three representative samples of switchgrass. Moisture content was obtained by placing the samples in an oven at 104°C for 24 h. The ash content was obtained by heating the dry sample in a furnace at 750°C for 4 h, while the volatile content was obtained by heating the sample at 950°C for 7 min. Ultimate analysis was performed by Midwest Microlab, LLC (Indianapolis, Ind.). A bomb calorimeter (model

A1290DDEB, Parr Instrument Co., Moline, Ill.) was used to determine calorific value of the biomass. The average bulk density of chopped switchgrass was measured to be 138 kg/m^3. ANSI/ASAE Standard S424.1 (ASABE-Standards, 2007) was used to calculate the geometric mean length and standard deviation by mass of the chopped switchgrass particles.

Table 2.1. Chopped switchgrass properties

Proximate Analysis[a]		Ultimate Analysis	
Moisture (%, w.b.)	9.70	Carbon	46.62%
Volatile matter (% d.b.)	80.36	Hydrogen	5.74%
Ash (% d.b.)	4.62	Oxygen	42.27%
Fixed carbon (% d.b.)	15.02	Nitrogen	0.18%
HHV of biomass (MJ/kg, d.b.)	18.83	Sulfur	<0.3%

[a] w.b. = wet basis, d.b. = dry basis, and HHV = higher heating value

2.2.4 Gasification test runs

2.2.4.1 Startup

Initially, a silica sand bed of a 102 mm height was prepared above the distributor plate inside the gasifier reactor. Hot air was supplied below the distributor plate for preheating the sand bed up to 400°C. Chopped switchgrass was then fed into the reactor bed using the screw feeder to initiate the gasification process. The air preheater was shut off after the reactor bed temperature stabilized above 700°C. In general, it took approximately 20 to 30 min for temperature to stabilize since the start of biomass feeding. Operating parameters such as biomass feed rate and airflow rate were then adjusted to desired levels.

2.2.4.2 Measurements and calculations

All measurements were made after gasifier operation stabilized with a uniform gasifier temperature profile. ERs of 0.20 to 0.45 were obtained by varying the air and biomass flow rates. At each ER level, two numbers of test runs were conducted. The reactor temperature and flow rates of air and biomass were recorded using a LabVIEW system (National Instruments, Austin, Tex.). An average of the data during the test run was reported for each ER. The airflow rate and dry biomass feed rate corresponding to the selected ERs are shown in Table 2.2. Airflow rates and dry biomass feed rates were in the range of 4.5 to 10 kg/h and 2.9 to 4.2 kg/h, respectively. Each test run was of 2 to 3 h in duration.

Table 2.2. Flow rates of air and biomass into the gasifier

Equivalence ratio	Airflow rate (kg/h)	Dry biomass feed rate (kg/h)
0.20	4.5	3.9
0.29	6.8	4.2
0.32	6.5	3.4
0.40	6.4	2.9
0.45	10	3.7

The reactor temperature profile, gas temperatures at the gasifier exit and orifice plate, gas flame temperature, pressure drops across the gasifier and orifice plate, and flow rates of air and biomass were closely monitored and logged using a LabVIEW system. For each ER, three gas samples were collected to determine the gas composition. Gas samples were taken at every 30 min interval. The producer gas composition (percentages of H_2, N_2, CH_4, CO, CO_2, C_2H_2, C_2H_4, and C_2H_6) was measured with a gas chromatograph (model CP3800, Varian, Inc., Cal.) containing a packed column (HayeSep DB-100/120, Alltech Associates, Inc., Deefield, Ill.) and a thermal

conductivity detector (TCD). Calibration of the gas chromatograph was performed using two standard gas mixtures (Superior Specialty Gas, Inc., Tulsa, Okla.): one consisting of 11.71% H_2, 29.5% N_2, 3.9% CH_4, 23.39% CO, 14.76% CO_2, 2.08% He, 4.78% C_2H_2, 4.98% C_2H_4, and 4.9% C_2H_6 and the other consisting of 5% H_2, 60.01% N_2, 20.01% CO, and 14.98% CO_2. The gas yield from the gasifier was calculated by balancing the mass of nitrogen and was also verified using a calibrated orifice plate. The orifice plate was connected in line of the gas flow path to measure the producer gas flow rate. The orifice plate was calibrated using flowmeter (model 8059MPNH, Eldridge Products, Inc., Monterey, Cal.). A graph of the pressure drop across the orifice plate versus the airflow rate was plotted to obtain the calibration equation. The pressure drop across the orifice plate was continuously recorded during each test run.

For measuring tar and particulates, a sample of producer gas was passed through an isokinetic sampling probe. One end of the probe was curved at angle of 90° for sampling tar and particulates from the main gas stream. The other end of the probe contained a thimble filter (34 mm o.d. × 100 mm long) to remove particulates from the producer gas. The thimble filter was made of ceramic material (fused alumina oxide). The sampling probe and downstream pipeline were heated to 250°C to prevent condensation of tar vapor. The producer gas from the sampling probe was passed through six impinger bottles containing acetone and immersed in an ethylene glycol solution maintained at -5°C. A vacuum pump and a rotameter were fitted in-line following the impinger bottles for suction of the gas and for measuring the flow rate of the gas, respectively. The tar concentration of the acetone solution, collected from the impinger bottles, was measured gravimetrically with a rotary evaporator. The same procedure was

replicated three times to obtain the average tar content of the producer gas. The thimble was dried before and after gas sampling. Initial and final weights of the dried thimble filter were measured to determine particulate content in the producer gas.

The ER was calculated using equation 1 (Patil et al., 2008) as follows:

$$ER = \frac{AIR}{(DBIR \times STADB)} \quad \text{Eq.(1)}$$

where AIR = air input (Nm^3/h)

DBIR = dry biomass input (kg/h)

STADB = stoichiometric air requirement for dry biomass (Nm^3/kg).

The HHV of the producer gas was calculated using following equation (Waldheim and Nilsson, 2001):

$$HHV = (13.6 \times H_2\%) + (13.4 \times CO\%) + (42.3 \times CH_4\%) + (61.7 \times C_2H_2\%) + (67 \times C_2H_4\%) + (74.1 \times C_2H_6\%)$$

where H_2%, CO%, CH_4%, C_2H_2%, C_2H_4%, and C_2H_6% represent the volumetric percentages of H_2, CO, CH_4, C_2H_2, C_2H_4, and C_2H_6, respectively.

Cold gas, hot gas, and carbon conversion efficiencies of the gasifier system were calculated using equations 2, 3 (Patil et al., 2008) and 4, respectively:

$$CGE = \left[\frac{PCE}{(DBE + ASE)}\right] \times 100 \quad \text{Eq.(2)}$$

where CGE = cold gas efficiency (%)

PCE = chemical energy in dry producer gas (MJ/Nm^3)

DBE = dry biomass energy (MJ/kg)

ASE = hot air sensible energy (MJ/m^3).

$$HGE = \left[\frac{(PCE + PSE)}{(DBE + ASE)}\right] \times 100 \quad \text{Eq.(3)}$$

where HGE = hot gas efficiency (%)

PSE = sensible energy in dry producer gas (MJ/m^3).

$$CCE = \left[\left(12 \times Y_{dry\ gas}\right) \times \left(CO\% + CO_2\% + CH_4\% + 2C_2H_2\% + 2C_2H_4\% + 2C_2H_6\%\right)\right] \div (C\% \times 22.4) \quad \text{Eq.(4)}$$

where CCE = carbon conversion efficiency (%)

$Y_{dry\ gas}$ = yield of dry gas per kg of dry biomass (Nm^3/kg).

CO_2% represents the volumetric percentage of CO_2 and C% is the percentage of carbon in the dry biomass, determined through ultimate analysis of switchgrass. Equation 5 (Ju et al., 2010) was used to calculate the yield of dry gas (Nm^3/kg of biomass):

$$Y_{dry\ gas} = \frac{(Q_{air} \times 0.79)}{(m_b \times N_2\%)} \quad \text{Eq.(5)}$$

where Q_{air} = flow rate of air(Nm^3/h)

m_b = feed rate of dry biomass (kg/h)

N_2% = volumetric percentage of N_2 in the producer gas.

2.3 Results and discussion

The effects of ER on performance of the lab-scale fluidized bed gasifier were analyzed. Feedstock characteristics and the effects of ER on gasifier performance parameters such as gas yield, gas composition, gas heating value, gasifier bed temperature and gasifier efficiencies are discussed in the subsequent sections.

2.3.1 Feedstock characteristics

The properties of Kanlow switchgrass are given in Table 2.1. Proximate analysis of Kanlow switchgrass showed a fixed carbon content of 15.02% (d.b.), which was higher than the fixed carbon content of Kentucky bluegrass straw (13.51% d.b.) and almost similar to the fixed carbon content of hemlock wood (14.8% d.b.). The volatile matter content of Kanlow switchgrass was 80.36% (d.b.), which was very close to the volatile matter content of Kentucky bluegrass straw (81% d.b.) but lower than the volatile matter content of hemlock wood (84.8% d.b.). The ultimate analysis showed 46.62% carbon content (d.b.) of Kanlow switchgrass, which was less than the carbon content of Kentucky bluegrass straw (48.96% d.b.) and hemlock wood (51.8% d.b.). The heating value of Kanlow switchgrass was determined to be 18.83 MJ/kg (d.b.), which was very close to the heating value of Kentucky bluegrass straw (17.46 MJ/kg, d.b.) and lower than the heating value of hemlock wood (20.3 MJ/kg, d.b.) (Boateng et al., 2007; Doherty et al., 2009). The geometric mean length and standard deviation by mass of the chopped switchgrass particles were calculated to be 10.27 mm and 1.73, respectively.

2.3.2 Performance characteristics of the fluidized bed gasifier

2.3.2.1 Gas yield

The gas yields (amount of gas produced per kg of biomass) at different values of ER are given in Table 2.3. It can be seen that the gas yield was in direct correlation with ER. Gas yield continuously increased with an increase in ER because of two main reasons. First, with an increase in ER, a larger quantity of O_2 entered the gasifier, which increased the degree of oxidation of biomass and available carbon. These resulted in increased temperature and conversion of biomass into gaseous forms (also evident from

CCE in Fig. 2.4). Second, with an increase in ER, a larger quantity of N_2 injected into the gasifier also contributed to the increase in gas yield. Mansaray et al. (1999) studied fluidized-bed air gasification of rice husk and reported a similar trend (Mansaray et al., 1999). In this study, the maximum gas production of 2.5 Nm^3 per kg of dry switchgrass was observed at an ER of 0.45.

Table 2.3. Process parameters and gas yields with change in ER

Parameter	Equivalence ratio				
	0.20	0.29	0.32	0.40	0.45
Reactor bed temperature (°C)	801 ± 78	809 ± 77	825 ± 72	893 ± 53	907 ± 57
Exit gas temperature (°C)	137 ± 7	126 ± 8	161 ± 12	181 ± 20	177 ± 5
Gasifier pressure drop (mm H_2O)	80	150	130	240	130
Gas production rate (Nm^3/h)	4.6	7.2	7.0	6.4	9.2
Gas yield (Nm^3/kg d.b.)	1.2 ± 0.1	1.7 ± 0.03	2 ± 0.1	2.2 ± 0.02	2.5 ± 0.03

2.3.2.2 Gas composition

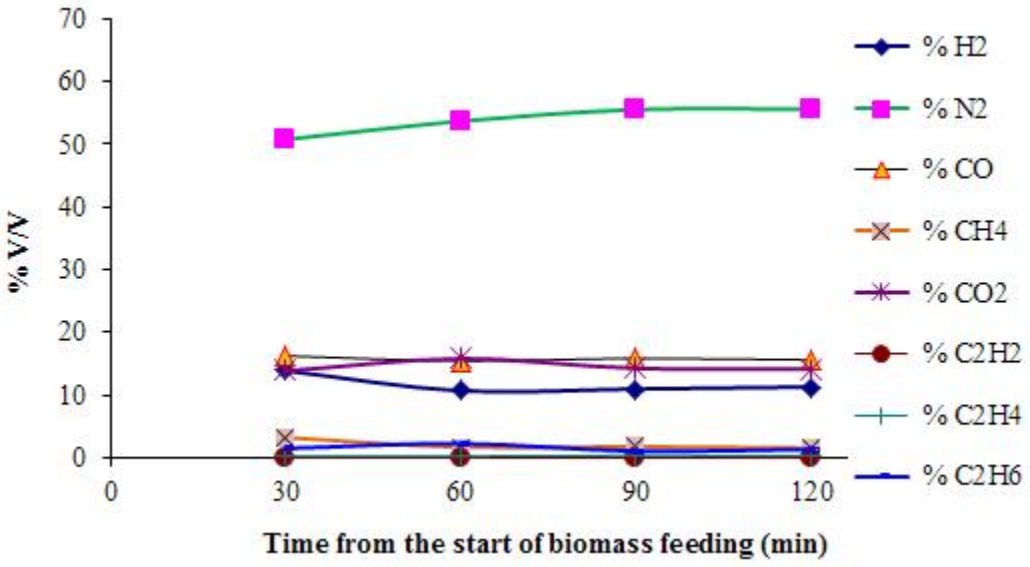

Fig. 2.2. Variation in gas composition with time (ER = 0.32)

The variation in producer gas composition with time from the start of biomass feeding is shown in Fig. 2.2 for one experimental condition. As shown in Fig. 2.2, the

quality of producer gas remained consistent throughout the gasifier run. This could be due to a uniform and stable gasifier bed temperature at a constant ER of 0.32. The composition of producer gas with varying ER is given in Table 2.4. With an increase in ER from 0.20 to 0.32, CO and H_2 concentrations increased. These concentrations decreased with further increase in ER from 0.32 to 0.45. A similar trend of increase and decrease in CO and H_2 concentrations with the maximum at an ER of 0.35 for fluidized-bed air gasification of hemlock wood was reported by Doherty et al. (2009) (Doherty et al., 2009). This increase and decrease of CO and H_2 concentrations could be explained by the gasification reactions shown in Table 2.5, which are dependent upon the gasifier temperature and the concentration of reactants.

Table 2.4. Gas composition and heating value with change in ER

Gas composition (% V/V, d.b.)	Equivalence ratio				
	0.20	0.29	0.32	0.40	0.45
H_2	5.9 ± 2	9.2 ± 1.8	9.3 ± 0.8	7.3 ± 1	2 ± 0.1
N_2	60.1 ± 1.8	57.4 ± 0.7	56.7 ± 1.1	60.7 ± 1.4	65.9 ± 0.7
CO	15.2 ± 2.1	16 ± 1.8	16.5 ± 1.1	14.9 ± 0.9	12.4 ± 1
CH_4	2.5 ± 0.4	1.9 ± 0.5	2.2 ± 0.7	1.8 ± 0.3	2.1 ± 0.2
CO_2	14.3 ± 0.4	13.1 ± 0.6	12.2 ± 1.2	12.8 ± 2	16.8 ± 0.2
C_2H_2	0.1 ± 0.1	0.5 ± 0.1	0.3 ± 0.2	0.3 ± 0.3	0.04 ± 0.04
C_2H_4	0.8 ± 0.3	1 ± 0.01	0.6 ± 0.4	0.8 ± 0.4	0.7 ± 0.1
C_2H_6	1.1 ± 0.9	1.3 ± 0.1	2.1 ± 1	1.4 ± 0.3	0.1 ± 0.02
HHV of dry gas (MJ/Nm^3)	5.3 ± 0.8	6.2 ± 0.3	6.6 ± 0.2	5.5 ± 0.5	3.4 ± 0.1

As explained earlier, with an increase in ER, the quantity of O_2 entering the gasifier increased, which resulted in a continuous increase in the gasifier temperature due to enhanced oxidation of available char. In this study, with an increase in ER from 0.20 to 0.32, the increase in the gasifier temperature from 801°C to 825°C may have favored the endothermic reactions, as shown by equations 6 to 8 in Table 2.5. As a result of these

reactions, the CO and H_2 concentrations increased until there was enough char available in the gasifier. Rapagna and Latif (1997) also reported an increase in CO and H_2 concentrations of producer gas with the initial increase in gasifier temperature (Rapagnà and Latif, 1997). As shown in Table 2.3, with further increase in ER from 0.32 to 0.45, the gasifier temperature continued to increase from 825°C to 907°C because of the increased degree of oxidation. The higher oxidation may also have contributed to the increase in CO_2 and decrease in CO in the producer gas through the reactions shown in equations 9 and 12 in Table 2.5. The H_2 concentration decreased with an increase in ER from 0.32 to 0.45. One of the reasons for the decrease in H_2 concentration may be that less char was available in the gasifier at higher ERs to produce H_2 through a water gas reaction (eq. 7 in Table 2.5). The N_2 concentration decreased with an increase in ER from 0.20 to 0.32 and increased with a further increase in ER from 0.32 to 0.45. The quantity of N_2 in the air supplied and in the producer gas generally remains same during these conditions, so the nitrogen concentration primarily depends on nitrogen supplied in the air and gas yield from biomass. With the initial increase in ER, gas yield from the biomass predominated the increase in N_2, which resulted in decreased N_2 concentration. However, with further increase in ER, the increase in N_2 may have predominated the gas yield, resulting in increased N_2 concentration. The maximum concentration of CO (16.5 ± 1.1%) and H_2 (9.3 ± 0.8%) was found at ER of 0.32. Patil et al. (2008) reported CO and H_2 concentrations of 19.2 ± 1.6% and 9.8 ± 1.2%, respectively, at an ER of 0.23 for switchgrass gasification in a downdraft gasifier. The difference in optimum ER (0.32 vs. 0.23) can be explained by the different reactor conditions due to different designs of the gasifiers (fluidized bed vs. downdraft).

In this study, the amount of tar and particulate contents were found to be 4.28 g/Nm^3 (w.b.) and 0.13 g/Nm^3 (d.b.), respectively, at the ER of 0.32, which were lower than those reported by both Patil et al. (2008) and Cateni (2008). Patil et al. (2008) reported tar and particulate contents of 18 g/Nm^3 (w.b.) and 2.5 g/Nm^3 (d.b.), respectively (Patil et al., 2008). Cateni (2008) reported tar and particulate contents of 5 to 12 g/Nm^3 and 0.4 to 0.45 g/Nm^3, respectively in a fluidized bed gasification of wood pallet (Cateni, 2007).

Table 2.5. Gasification reactions

Boudouard	$C + CO_2$	$\leftrightarrow$ $2CO$	(ΔH = +172.6 kJ/mol)	Eq. 6
Water gas	$C + H_2O$	$\leftrightarrow$ $CO + H_2$	(ΔH = +131 kJ/mol)	Eq. 7
Methane reforming	$CH_4 + H_2O$	$\leftrightarrow$ $CO + 3H_2$	(ΔH = +206 kJ/mol)	Eq. 8
Complete combustion of char	$C + O_2$	= CO_2	(ΔH = -394.4 kJ/mol)	Eq. 9
Water gas shift	$CO + H_2O$	$\leftrightarrow$ $CO_2 + H_2$	(ΔH = -41.2 kJ/mol)	Eq. 10
Partial combustion of char	$C + 0.5O_2$	= CO	(ΔH = -111 kJ/mol)	Eq. 11
Partial combustion of CO	$CO + 0.5O_2$	= CO_2	(ΔH = -283 kJ/mol)	Eq. 12
Partial combustion of H_2	$H_2 + 0.5O_2$	= H_2O	(ΔH = -242 kJ/mol)	Eq. 13

As air is available free of cost, air gasification of biomass for generating producer gas is one of the most economical options for producing heat, power, and fuels when the nitrogen content of the producer gas does not adversely affect the process. The producer gas quality obtained in this study could be suitable for direct combustion in a boiler for generating steam and can replace conventional fuels. Additionally, the producer gas can be used for equipment such as furnaces, kilns, and ceramic dryers for heating processes where the non-combustible gases (N_2 and CO_2) in the producer gas do not have any adverse effect on the process or processing equipment. After removal of tar and particulates, the producer gas can be used in internal combustion engines and gas turbines if the contaminants and energy content are acceptable (Ståhl et al., 2004). The producer

gas can also be converted into alcohols fuels through microbial fermentation or to produce hydrocarbon fuels through chemical catalytic conversion. However, the producer gas may not be suitable where the non-combustibles gases will have adverse effect on the process.

2.3.2.3 Gas heating value

Table 2.4 shows the HHV of dry producer gas with varying ER. With an increase in ER from 0.20 to 0.32, the reactor bed temperature increased which may have accelerated the endothermic reactions (eqs. 6 to 8 in Table 2.5) and yielded more CO and H_2, the main combustible components of the producer gas. As a result, HHV of dry gas increased from 5.3 MJ/Nm^3 to a maximum of 6.6 MJ/Nm^3. With an additional increase in ER from 0.32 to 0.45, the higher oxygen throughput into the gasifier may have caused partial oxidation of CO, H_2 and char (eqs. 11 through 13 in Table 2.5). As a result, the concentrations of CO and H_2 decreased, so the HHV decreased from 6.6 to 3.4 MJ/Nm^3. This can be evidenced by the increased percentage of CO_2 and decreased percentages of CO and H_2 for ER above 0.32.

2.3.2.4 Gasifier temperature

Fig. 2.3 shows the gasifier bed temperature, 76.2 mm above the distributor plate, from the start of biomass feeding. After an initial 30 to 40 min of gasifier run, the reactor bed temperature stabilized between 700°C and 950°C and showed relatively smooth and consistent gasifier performance with a reactor bed temperature of 825°C ±72°C, and exit gas temperature of 161 ±12°C, respectively. Table 2.3 shows the variation in the gasifier bed temperature with increasing ER from 0.20 to 0.45. As explained earlier, the reactor bed temperature increased continuously with increase in ER due to the higher degree of

oxidation. The average and maximum reactor temperatures were observed to be in the ranges of 801°C to 907°C and 851°C to 963°C, respectively. Generally, a bed temperature above 900°C is not suitable for gasification as it results in choking of the gasifier bed due to agglomeration of bed materials. Ergudenler and Ghaly (1993) observed agglomeration of silica sand in the form of hard brittle solids in a fluidized bed gasification of wheat straw at 850°C (Ergudenler and Ghaly, 1993). Fryda et al. (2008) tested two bed materials (quartz and olivine) in a lab-scale fluidized bed gasifier using olive bagasse and observed agglomeration of quartz and olivine at 830°C and above 850°C, respectively (Fryda et al., 2008). In this study, after 2 h of smooth gasifier operation at 907°C for ER of 0.45, the pressured drop across the gasifier gradually increased from 130 to 400 mm H_2O. The increase in pressure drop was due to agglomeration of silica sand in the gasifier bed. A clinker (hard solids) was observed in the bed during cleaning of the gasifier. A fresh bed of silica sand was then prepared for the next test run. No noticeable amount of agglomerates was found during gasification with ER below 0.45.

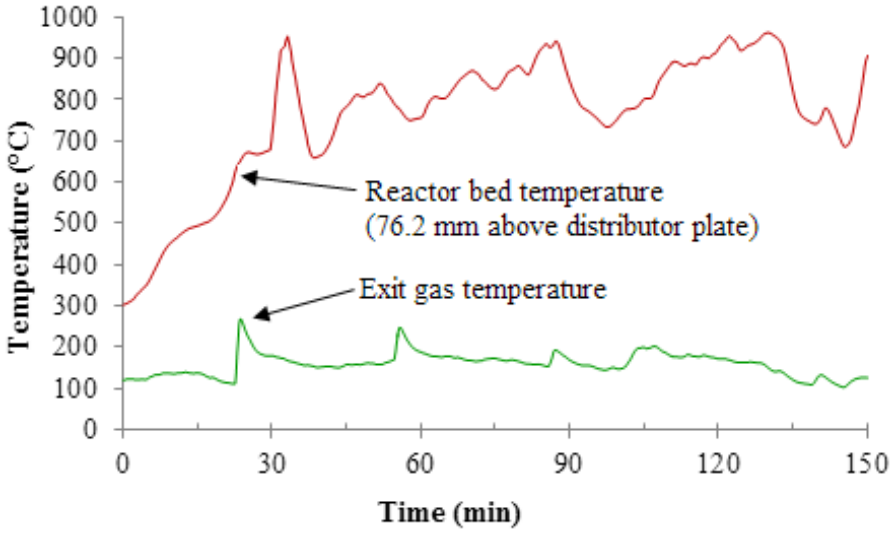

Fig. 2.3. Variation in temperatures with time (ER = 0.32)

2.3.2.5 Gasifier efficiencies

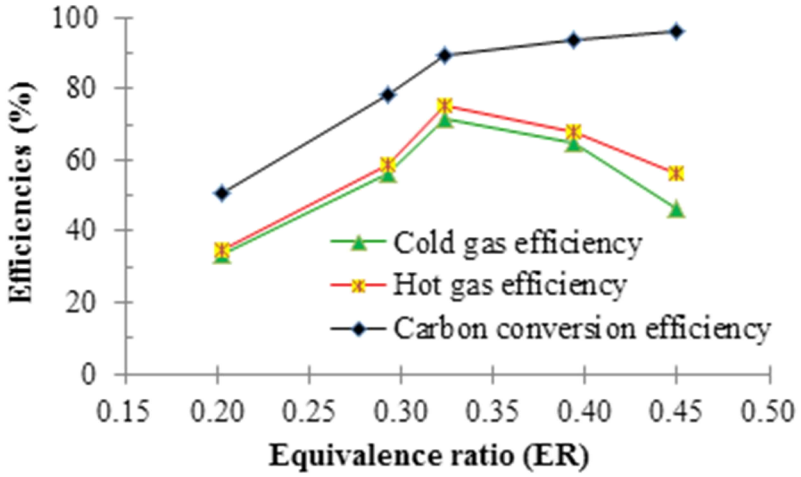

Fig. 2.4. Variation in gasifier efficiencies with change in ER

The variations in CGE, HGE, and CCE with varying ER are shown in Fig. 2.4. The CGE and HGE were directly related to the HHV of the producer gas, which depends on the concentrations of the main combustible gases (CO and H_2). As shown earlier, the CO and H_2 concentrations initially increased with increasing ER from 0.20 to 0.32, and so did the HHV. As a result both CGE and HGE increased. With a further increase in ER from 0.32 to 0.45, the CO and H_2 concentrations decreased, and so did the HHV. This resulted in decreases in CGE and HGE. The maximum values of CGE and HGE were 71% and 75%, respectively, at an ER of 0.32. Campoy et al. (2009) reported CGE of 59% for wood pallet gasification in a bubbling fluidized bed gasifier at an ER of 0.35 (Campoy et al., 2009). Patil et al. (2008) observed CGE and HGE of 72% and 82%, respectively, at an ER of 0.22 for switchgrass gasification in a downdraft gasifier (Patil et al., 2008).

The CCE indicates the percentage of carbonaceous biomass that is converted into gaseous forms. The increase in bed temperature with increase in ER accelerated the

conversion of biomass carbon into gaseous forms. As a result, the CCE continued to increase with an increase in ER from 0.20 to 0.45. The maximum value of CCE was found to be 96% at the maximum ER. The CCE at an ER of 0.32 was 89%. Campoy et al. (2009) reported a maximum CCE of 93% (Campoy et al., 2009).

2.4 Conclusions

The performance of a laboratory-scale FBBG was evaluated using Kanlow switchgrass. The performance parameters such as gas yield, gas composition, gas heating value, gasifier bed temperature, and gasifier energy efficiencies were studied by varying the ER from 0.20 to 0.45. The HHV of the producer gas increased and then decreased as ER increased from 0.20 To 0.45, with a maximum value of 6.6 MJ/Nm^3 (d.b.) at an ER of 0.32 (airflow rate of 6.5 kg/h and dry biomass feed rate of 3.4 kg/h). Hot and cold gas efficiencies followed a similar trend as ER varied, with maximum values of 71% and 75%, respectively, at an ER of 0.32. However, gas yield and carbon conversion efficiency continued to increase as ER increased from 0.20 to 0.45. The optimum ER of 0.32 resulted in carbon conversion efficiency of 89% and average gas yield of 2 ± 0.1 Nm^3 per kg of dry biomass.

Acknowledgements

This work was supported in part by the Oklahoma State Regents for Higher Education (NSF-EPSCoR Award EPS-0814361) and the Director of the Oklahoma Agricultural Experiment Station. The authors highly appreciate assistance from the workshop team of the Department of Biosystems and Agriculture Engineering: Wayne R. Kiner (laboratory manager), Robert J. Harrington (research equipment specialist), Mike Veldman (senior research equipment specialist), and Jason Walker (instrument specialist)

for fabrication of the gasifier and its components. We also convey our sincere thanks to graduate students Bipul Chandra, Siddharth Patil, Balaji Dhamodharan, and Vamsee Pasangulapati for their assistance in conducting the experiments.

2.5 References

ASABE-Standards. 1997. ANSI/ASAE S319. 3 JUL97: Method of determining and expressing fineness of feed materials by sieving. in: *ASAE standards*.

ASABE-Standards. 2007. ANSI/ASAE S424.1 MAR 1992 (R2007): Method of determining and expressing particle size of chopped forage materials by screening, Standard.

ASABE-Standards. 2008. ASAE S358. 2 DEC1998 (R2008): Moisture measurement–forages, ASABE Standards, 608, American Society of Agricultural and Biological Engineers, St. in: *Joseph, MI*.

Boateng, A., Walawender, W., Fan, L., Chee, C. 1992. Fluidized-bed steam gasification of rice hull. *Bioresource Technology*, **40**(3), 235-239.

Boateng, A.A., Banowetz, G.M., Steiner, J.J., Barton, T.F., Taylor, D.G., Hicks, K.B., El-Nashaar, H., Sethi, V.K. 2007. Gasification of Kentucky bluegrass (*Poa pratensis l.*) straw in a farm-scale reactor. *Biomass & Bioenergy*, **31**(2-3), 153-161.

Brown, M., Baker, E., Mudge, L. 1986. Environmental design considerations for thermochemical biomass energy. *Biomass*, **11**(4), 255-270.

Buragohain, B., Mahanta, P., Moholkar, V. 2010. Biomass gasification for decentralized power generation: The Indian perspective. *Renewable and Sustainable Energy Reviews*, **14**(1), 73-92.

Campoy, M., Gómez-Barea, A., Vidal, F., Ollero, P. 2009. Air-steam gasification of biomass in a fluidised bed: Process optimisation by enriched air. *Fuel Processing Technology*, **90**(5), 677-685.

Cateni, B.G. 2008. Effects of feed composition and gasification parameters on product gas from a pilot scale fluidized bed gasifier. Ph. D. Thesis, Oklahoma State University, Department of Biosystems and Agricultural Engineering. Stillwater, Oklahoma.

Dai, J., Grace, J.R. 2008a. Biomass screw feeding with tapered and extended sections. *Powder Technology*, **186**(1), 56-64.

Dai, J., Grace, J.R. 2008b. A model for biomass screw feeding. *Powder Technology*, **186**(1), 40-55.

Doherty, W., Reynolds, A., Kennedy, D. 2009. The effect of air preheating in a biomass CFB gasifier using ASPEN Plus simulation. *Biomass and Bioenergy*, **33**(9), 1158-1167.

Ergudenler, A., Ghaly, A.E. 1993. Agglomeration of silica sand in a fluidized bed gasifier operating on wheat straw. *Biomass and Bioenergy*, **4**(2), 135-147.

Fryda, L., Panopoulos, K., Kakaras, E. 2008. Agglomeration in fluidised bed gasification of biomass. *Powder Technology*, **181**(3), 307-320.

Gabra, M., Nordin, A., Öhman, M., Kjellström, B. 2001. Alkali retention/separation during bagasse gasification: a comparison between a fluidised bed and a cyclone gasifier. *Biomass and Bioenergy*, **21**(6), 461-476.

Ju, F., Chen, H., Yang, H., Wang, X., Zhang, S., Liu, D. 2010. Experimental study of a commercial circulated fluidized bed coal gasifier. *Fuel Processing Technology*, **91**(8), 818-822.

Kurkela, E., Ståhlberg, P. 1992. Air gasification of peat, wood and brown coal in a pressurized fluidized-bed reactor. I. Carbon conversion, gas yields and tar formation. *Fuel Processing Technology*, **31**(1), 1-21.

Li, X., Grace, J., Lim, C., Watkinson, A., Chen, H., Kim, J. 2004. Biomass gasification in a circulating fluidized bed. *Biomass and Bioenergy*, **26**(2), 171-193.

Mansaray, K.G., Ghaly, A.E., Al-Taweel, A.M., Hamdullahpur, F., Ugursal, V.I. 1999. Air gasification of rice husk in a dual distributor type fluidized bed gasifier. *Biomass & Bioenergy*, **17**(4), 315-332.

Miller, R. W. 1996. *Flow Measurement Engineering Handbook*. 3rd ed. New York, N.Y.: McGraw-Hill.

Natarajan, E., Nordin, A., Rao, A.N. 1998. Overview of combustion and gasification of rice husk in fluidized bed reactors. *Biomass and Bioenergy*, **14**(5-6), 533-546.

Overend, R. 2004. Thermochemical conversion of biomass. Renewable energy sources charged with energy from the sun and originated from earth-moon interaction. *In Encyclopedia of Life Support Systems (EOLSS).* Developed under the auspices of the UNESCO. Oxford, U.K.: EOLSS Publishers.

Parnell, C., Guzman, F. 1982. Cyclone design methodology for agricultural processing [Air pollution control]. ASAE Paper No. 823582. St. Joseph, Mich.: ASAE.

Patil, K., Bowser, T., Bellmer, D., Huhnke, R. 2005. Fluidization characteristics of sand and chopped switchgrass-sand mixtures. *Agricultural Engineering International the CIGR Ejournal*, **7**: article EE 4(005).

Patil, K.N., Huhnke, R.L., Bellmer, D.D. 2008. Gasification of Switchgrass Using a Unique Downdraft Reactor. ASABE Paper No. 084415. St. Joseph, Mich.: ASABE.

Perlack, R.D., Wright, L.L., Turhollow, A.F., Graham, R.L., Stokes, B.J., Erbach, D.C., Oak Ridge National Lab, T.N. 2005. Biomass as feedstock for a bioenergy and bioproducts industry: the technical feasibility of a billion-ton annual supply. Report No. ORNL/TM-2005/66. Oak Ridge, Tenn.: Oak Ridge National Laboratory.

Priestley, J.J. 1973. *Industrial Gas Heating: Design and Application*. London, U.K.: Ernest Benn, Ltd.

Rapagnà, S., Latif, A. 1997. Steam gasification of almond shells in a fluidised bed reactor: The influence of temperature and particle size on product yield and distribution. *Biomass and Bioenergy*, **12**(4), 281-288.

Ståhl, K., Waldheim, L., Morris, M., Johnsson, U., Gårdmark, L. 2004. Biomass IGCC at Värnamo, Sweden: Past and future, GCEP Energy Workshop, April 27. KS Ducente AB, Limhamn, Sweden.

van den Enden, P.J., Lora, E.S. 2004. Design approach for a biomass fed fluidized bed gasifier using the simulation software CSFB. *Biomass and Bioenergy*, **26**(3), 281-287.

Waldheim, L., Nilsson, T. 2001. Heating value of gases from biomass gasification. Report prepared for IEA Bioenergy Agreement: Task 20 - Thermal gasification of biomass. Report No. TPS-01/16. TPS Termiska Processer AB, Nyköping, Sweden.

Wang, L., Weller, C., Jones, D., Hanna, M. 2008. Contemporary issues in thermal gasification of biomass and its application to electricity and fuel production. *Biomass and Bioenergy*, **32**(7), 573-581.

CHAPTER III

FLUIDIZATION CHARACTERISTICS OF A MIXTURE OF GASIFIER SOLID RESIDUES, SWITCHGRASS AND INERT MATERIAL

This research paper was published as "Sharma, A.M., Kumar, A., Patil, K.N., Huhnke, R.L. 2013. Fluidization characteristics of a mixture of gasifier solid residues, switchgrass and inert material. *Powder Technology,* **235**, 661-8."

Abstract

Effective fluidization of materials present in the reactor bed is critical for optimizing reaction conditions in a fluidized-bed gasifier. An improper fluidization leads to inefficient conversion due to many reasons such as low heat and mass transfers, ineffective gas-solid phase reactions, and uneven reactor temperature in autothermal gasification. The objective of this study was to investigate effect of reactor bed composition, i.e. a mixture of gasifier solid residues (GSR), switchgrass, and inert material, on fluidization using a 0.25 m i.d. transparent column. In this cold-flow study, the amount of inert material, i.e. silica sand, in the bed was held at 20 kg. The switchgrass in the mixture ranged from 0.17 to 5% of the sand quantity while the GSR ranged from 5 to 35% of the switchgrass. The particle geometric sizes by mass of sand, GSR and switchgrass were 348±1.6 μm, 80±2.6 μm, and 10.3±1.7 mm, respectively. For all conditions, with an increase in gas superficial velocity, i.e. ratio of volumetric gas flow and bed cross-sectional area, the pressure drop across the bed increased reaching a maximum level at the minimum fluidization condition. Results showed that when the bed consisted of only GSR and sand, with an increase in the GSR from 5% to 35%, the gas superficial velocity at minimum fluidization condition, called minimum fluidization velocity (U_{mf}), decreased significantly ($p < 0.05$); however, corresponding bed pressure drop (dP_{mf}) remained constant. When the bed consisted of GSR, switchgrass and sand, there were significant effects ($p < 0.001$) of GSR, switchgrass and their interaction (GSR*Switchgrass) on U_{mf} and dP_{mf}. Fluidization improved with an increase in GSR up to 35% in the mixture. Overall, both U_{mf} and dP_{mf} increased with an increase in levels of GSR (5 to 35%) and switchgrass (0.17 to 3%) in the mixture. Fluidization characteristics

were found to be strongly dependent upon mixture's effective properties, which were determined using properties of all mixture components. Correlations available in literature were used to predict U_{mf} using effective properties of tertiary mixture with GSR, switchgrass and sand. Prediction of U_{mf} from all selected correlations did not match well with the experimental data for the entire range of tertiary mixture compositions. Fluidization of bed materials sustained up to 3% level of switchgrass. However, segregation of bed materials and in-bed channelization caused ineffective fluidization at 5% level of switchgrass in the mixture.

Keywords: Fluidized-bed gasifier; fluidization velocity; bed pressure drop; solid residues; switchgrass; sand

3.1 Introduction

Effective fluidization of materials present in the reactor bed is essential for optimizing reaction conditions in a fluidized-bed gasifier. Gasifier bed normally consists of gasifier solid residues (GSR), such as char and ash, biomass and inert material such as silica sand. An improper fluidization of bed materials can results in low heat and mass transfers (Daleffe et al., 2008), ineffective gas-solid phase reactions, and inability to maintain a uniform reactor temperature in autothermal gasification. Such conditions can also cause an in-bed accumulation of GSR and biomass, further resulting in choking of the gasifier bed and can ultimately stop the gasification process. Therefore, a thorough understanding of fluidization characteristics of all participating solids during gasification is essential for reactor design (Patil et al., 2005) and optimizing reaction conditions of the gasifier.

A typical fluidized bed gasifier is a cylindrical reactor that consists of a bed of inert material, such as sand, or a mixture of sand and catalyst. A distributor plate is used to support a bed material inside the gasifier. For gasification, initially, the bed is preheated by an external heat source. Thereafter the bed is fluidized by supplying an oxidizing agent, such as air, through the distributor plate. Finally, a biomass feedstock is injected into a fluidized-bed using a screw feeder. Biomass particles then pass upward through the bubbling fluidized-bed, undergo a series of gasification reactions, and finally convert into gaseous products (McKendry, 2002). Both fluidization of bed materials and gasification of biomass are occurred simultaneously during gasification. Several parameters such as flowrates and types of oxidizing agent and biomass, properties of oxidizing agent, biomass and bed material, and operating temperature and pressure have

influence of fluidization characteristics of materials that are normally present in the gasifier bed. These, in turn, play key roles in the gasification process and influence gasifier performance in terms of gas composition and yield, gas impurities and gasifier efficiencies (Sharma et al., 2011).

The flow rate of oxidizing agent supplied to the fluidized-bed gasifier is a key parameter to maintain effective fluidization of bed materials. The fluidization condition is usually described using a gas superficial velocity which is the ratio of volumetric gas flowrate and bed cross-sectional area. The gas superficial velocity, at which the drag force on the bed materials equals the gravitational force, is defined as the minimum fluidization velocity (U_{mf}) of the bed materials. At minimum fluidization condition, the bed materials lift upward and remain in suspension; bed pressure drop (dP_{mf}) reaches to a maximum and remains constant with further increase in the gas superficial velocity. Fluidization characteristics, such as U_{mf} and dP_{mf}, depend upon the particle size and composition of the bed materials (Jena et al., 2008). U_{mf} and dP_{mf} are also influenced by segregation and mixing behaviors of bed materials. Segregation is a process during which a bed material with higher particle density, such as sand, moves downwards in the bed while a material with lower particle density, such as biomass, floats upwards (Formisani & Girimonte, 2003; Noda et al., 1986). This, in turn, causes separation of biomass from sand and results in a localized accumulation of biomass particles as smaller and/or bigger sized lumps throughout the bed. These lumps further lead to channel formation, called in-bed channelization, that give rise to larger void space and a shorter path to the gas flow (Rao & Reddy, 2010). As a result, the gas easily escapes through in-bed channels, which affect bubble formation, and thus turbulence level in the bed resulting in ineffective

fluidization. Segregation occurs due to differences in densities or sizes of the bed materials such as a sand and biomass (Chiba et al., 1979; Chok et al., 2010a; Chok et al., 2010b; Noda et al., 1986; Werther, 2000; Wu & Baeyens, 1998; Zhang et al., 2010). Further, segregation tendency increases with an increase in the biomass weight fraction in a mixture (Chok et al., 2010a). Thus, the quantity of biomass in the mixture plays a crucial role in segregation behavior of bed materials. Also, a bed consisting of a material, such as particulate matters, that has adhesive or cohesive properties may enhance segregation tendency and suppress fluidization (Daleffe et al., 2008). In case of segregation or channelization, comparatively a higher gas superficial velocity than U_{mf} is needed for fluidization of bed materials (Chok et al., 2010a). This is because at higher gas velocity, formation and collapsing of bubbles become predominant leading to high turbulence in the bed. The high turbulence breakdowns segregated lumps and removes in-bed channels. Hence, higher gas velocity eradicates segregation of bed materials resulting in a better particle mixing. As opposed to segregation, mixing prevents separation of bed materials resulting in a uniform distribution of mixture particles in the bed. Mixing enhances particle-particle interactions, and thus improves heat and mass transfers in fluidized bed. Chok et al. (Chok et al., 2010b) indicated improved mixing with decrease in the particle size ratio from 30 to 20 of palm shell and sand mixture. The author also reported that segregation and channelization were predominant at higher particle size ratio, and biomass weight fraction (10% and 15%) in the mixture. Correlations to determine U_{mf} and bed expansion of coal particles were suggested for coal gasification (Babu et al., 1978). Equations to determine U_{mf} for a mixture of sand and biomass, such as sawdust, rice husk and groundnut shell, have been developed (Rao & Reddy, 2010;

Rao & Bheemarasetti, 2001). However, fluidization behavior and correlations for determining U_{mf} for a tertiary mixture of GSR, switchgrass, and silica sand have not been reported. The specific objective of this study was to investigate the fluidization characteristics of a mixture of switchgrass, GSR, and silica sand for determining the optimum operating conditions in terms of fluidization velocity and bed pressure drop.

3.2 Materials and methods

3.2.1 Bed materials

GSR, biomass and silica sand were used as bed materials, shown in Fig. 3.1, for fluidization experiments. GSR was obtained by gasification of switchgrass in a 0.25 m i.d. pilot-scale bubbling fluidized-bed gasifier with constant switchgrass and air flow rates of 12 kg/h and 17 m^3/h (i.e. 0.096 m/s superficial velocity), respectively. The gasifier was connected to three cyclone separators in series for removing the GSR from the producer gas. The GSR in the cyclone separators were collected, weighed, and analyzed for its properties. On an average the GSR production rate was 0.5 kg/h, which contained 64% ash and 36% char. A Kanlow switchgrass, a perennial grass, was used as a biomass material in this study. It was grown at the Agronomy Research Station of Oklahoma State University and harvested in the fall of 2010. A Haybuster tub grinder (H1000, Duratech Industries International, Inc. Jamestown, ND) with a screen size of 25 mm was used to grind the switchgrass. Moisture and ash contents of the switchgrass, determined through proximate analyses, were 12.76% and 4.72%, respectively. A silica sand is the most commonly used inert bed material for fluidized-bed gasifier. In this study, silica sand, supplied by Oglebay Norton Industrial Sands, Inc. (Brady, TX), was used as an inert bed material.

Fig. 3.1. Bed materials

3.2.2 Density of bed materials

Bulk densities of bed materials were determined by using a container of 0.001 m^3 volume. To measure bulk density of GSR, weights of the empty container and container filled with GSR were measured. Bulk density was calculated by dividing the mass of the GSR in the container with the volume of the container. A similar method was used to determine bulk densities of ground switchgrass and silica sand. Particle densities of silica sand and switchgrass were obtained from the supplier and literature (Lam et al., 2008), respectively. A 3 g GSR pellet was prepared to measure particle density of GSR, which was determined by dividing the mass with the volume (3.22 cm^3) of the GSR pellet. Table 3.1 shows the bulk and particle densities of GSR, ground switchgrass, and silica sand.

Table 3.1. Densities of bed material

Bed material	GSR	Ground switchgrass	Sand
Bulk density [a], kg/m^3	205 ± 5.6	111 ± 6.2	1602 ± 11.1
Particle density, kg/m^3	932	400	2650

[a] Average of six replications

3.2.3 Particle size distribution of bed materials

Particle size distributions of GSR and silica sand samples were determined following ANSI/ASAE standard S319.3 JUL97 (ASAE, 2000) using a sieve shaker (CSC Scientific, Fairfax, VA). The sieve shaker consisted of seven screens, a lid, and a pan. The screen size ranged from 850 to 106 μm. Initially, the empty screens and pan were weighed and arranged in a descending order of screen sizes in the sieve shaker. The pan was placed below the lowest screen. A 50 g representative sample was kept in the first screen (850 μm), and the screen was closed with the lid. The sieve shaker was set to sieve the sample for 10 minutes. After each sieving test, the mass of the sample in each screen and pan was measured. A total of six samples were used to determine its particle size distribution. An average of the data was used to calculate a percentage mass distribution of GSR on each screen and on the pan. Six representative samples (500 g each) of silica sand were analyzed using the sieve shaker. Particle size distribution (length and width) of ground switchgrass was measured manually with a digital vernier caliper (Digimatic, Mitutoyo, Japan) having a resolution of 0.1 mm. The geometric mean sizes by mass of bed materials were determined using ANSI/ASAE standard S424.1 (ASABE, 2007). The particle size ratio of GSR, silica sand and switchgrass (i.e. GSR/silica sand/switchgrass) was calculated using geometric mean sizes by mass of GSR, silica sand and switchgrass particles.

3.2.4 Test setup and instrumentation

The fluidization test setup, shown in Fig. 3.2, consisted of a cylindrical column (0.25 m i.d. × 2 m height) made of a transparent acrylic glass to facilitate visual observation during the experiment. A distributor plate (0.28 m o.d.) located at the bottom

of the column supported the bed materials and also helped to ensure a uniform distribution of inlet air supply. The distributor plate was made of a 6.4 mm-thick acrylic glass sheet with 145 equally-spaced 1.6 mm i.d. holes. To prevent bed materials from falling through the distributor plate, a wire screen (40 mesh size) was placed on top of the distributor plate. Air was supplied into the test setup by an air compressor (TS10K10 model, Ingersoll Rand, Davidson, NC)connected to a mass flowmeter (8059MPNH model, Eldridge Products, Inc., Monterey, CA), a flow control valve, and a pressure regulator . A water tube manometer was installed across the bed of the column for measuring the pressure drop across the bed. Rubber packings were used between the flanges to make the whole unit air-tight. A silicone gel (Type 650 RED RTV, Versachem, Riviera Beach, FL) was applied between rubber packings and flanges to prevent any air leak.

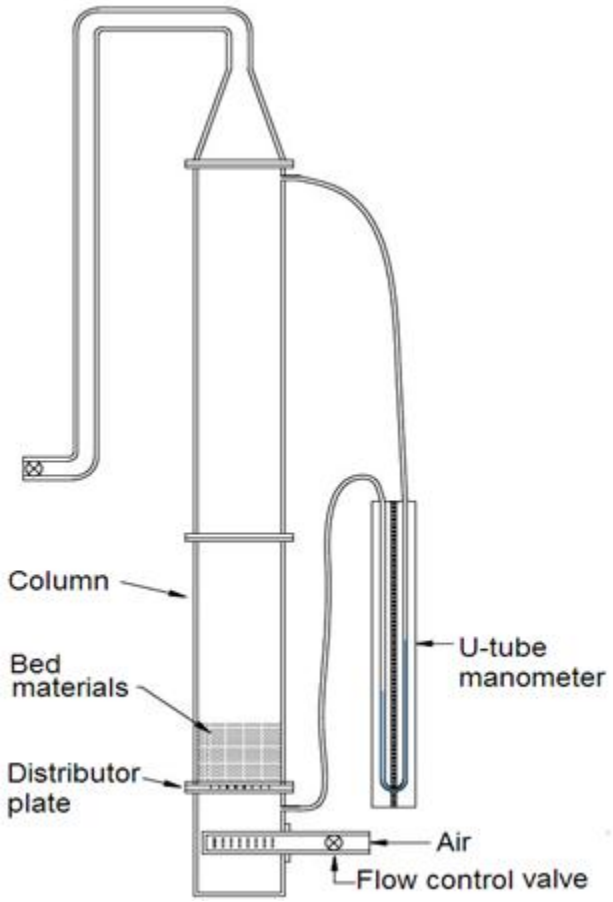

Fig. 3.2. Fluidization test setup

3.2.5 Experimental design and mixture preparation

Quantities of GSR and switchgrass were varied while holding quantity of sand constant 20 kg (i.e. 0.25 m bed height). A 4 x 5 full factorial design (four levels of GSR, i.e. 5%, 15%, 25% and 35% of switchgrass levels in the mixture, and five levels of switchgrass, i.e. 0%, 0.17%, 1%, 3% and 5% of sand quantity in the mixture) with two replications (40 experiments) was used. The levels of GSR and switchgrass were selected based on bed composition observed in our pilot-scale fluidized bed gasifier. Experiments were completely randomized and the data were analyzed using a general linear model (GLM) procedure. Bed was prepared by mixing predetermined quantities of GSR, switchgrass, and silica sand as shown in Table 3.2.

Table 3.2. Bed compositions

Sand, kg	Switchgrass, kg	GSR, kg			
		5%	15%	25%	35%
20	0	0.01[a]	0.03 [a]	0.05 [a]	0.07 [a]
20	0.035	0.002	0.005	0.009	0.012
20	0.2	0.01	0.03	0.05	0.07
20	0.6	0.03	0.09	0.15	0.21
20	1	0.05	0.15	0.25	0.35

[a] GSR levels were based on 1% level of the switchgrass

3.2.6 Test and maintenance procedures

For each experiment, mixture was placed above the distributor plate (Fig. 3.2). The air flow rate was increased from 0 to a maximum of 34 m^3/h (i.e. 0.19 m/s superficial velocity) to facilitate fluidization, and then decreased from the maximum to 0, to facilitate defluidization. The pressure drop across the bed was continuously monitored during fluidization and defluidization. Also, visual observations, such as bubble formation, initial and complete fluidization of the bed, and height of fluidized bed, were recorded during each experiment. After each experiment, the bed material was removed and the test setup was dismantled for cleaning. Prior to the next experiment, a leakage test was performed on the test setup to ensure no air leakage.

3.2.7 Determination of minimum fluidization velocity, U_{mf}

Several correlations are available to determine U_{mf} of a bed consisting of a single material or a binary mixture such as sand and biomass (Babu et al., 1978; Bourgeois & Grenier, 1968; Coltters & Rivas, 2004; Cui & Grace, 2007; Kunii & Levenspiel, 1991; Leva, 1965; Lucas et al., 1986; Rao & Reddy, 2010; Rao & Bheemarasetti, 2001; Sau et al., 2008; Saxena & Vogel, 1977; Si & Guo, 2008; Wen & Yu, 1966; Yudong & Zhiqiang, 2010; Zhong et al., 2008). In present work, U_{mf} was determined using

experimental and theoretical approaches. Experimental U_{mf} was determined using graphical method. The bed pressure drop against gas superficial velocity was plotted, and the U_{mf} was determined to be the gas superficial velocity at the intersection of the inclined line representing a fixed bed pressure drop before minimum fluidization and the horizontal line representing a constant bed pressure drop after minimum fluidization (shown in Fig. 3.3). The fluidization region during which the bed pressure drop linearly followed the gas superficial velocity till the minimum fluidization condition reached is known as the fixed bed zone (Daleffe et al., 2008; Formisani & Girimonte, 2003) shown in Fig. 3.3. At the minimum fluidization condition, the bed pressure drop reached a maximum level and remained constant with further increase in the gas superficial velocity.

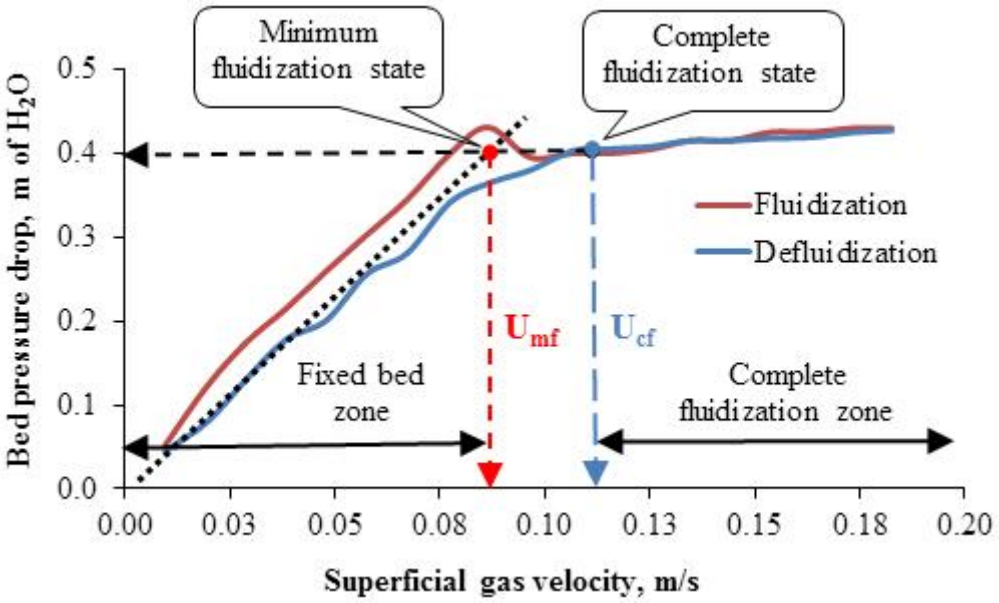

Fig. 3.3. Fluidization characteristics of sand

Table 3.3. Correlations to determine U_{mf}

Correlation	Reference
$Re_{mf} = (25.25^2 + 0.0651Ar)^{0.5} - 25.25$	(Babu et al., 1978)
$U_{mf} = d_{peff}^2 (\rho_{eff} - \rho_g) g /1650\mu_g$	(Rao & Bheemarasetti, 2001)
$Re_{mf} = (25.46^2 + 0.0384Ar)^{0.5} - 25.46$	(Bourgeois & Grenier, 1968)
$Re_{mf} = (28.7^2 + 0.0494Ar)^{0.5} - 28.7$	(Kunii & Levenspiel, 1991)
$U_{mf} = 0.00094 [(\rho_s - \rho_g) g]^{0.934} d_p^{1.8} / \mu_g^{0.87} \rho_g^{0.066}$	(Leva, 1965)
$Re_{mf} = [(42.857C_1 /C_2)^2 + Ar /1.75C_1]^{0.5} - (42.857C_1 /C_2)$ where, $C_1 = (1 /\Phi^3 \varepsilon_{mf})$ and $C_2 = (1 - \varepsilon_{mf}) /\Phi^2 \varepsilon_{mf}^3$	(Lucas et al., 1986)
$Re_{mf} = (25.28^2 + 0.0571Ar)^{0.5} - 25.28$	(Saxena & Vogel, 1977)
$Re_{mf} = (33.7^2 + 0.0408Ar)^{0.5} - 33.7$	(Wen & Yu, 1966)
$U_{mf} = 0.000701(\rho_s - \rho_g) g d_p^2 / \mu_g$	(Si & Guo, 2008)

Where, $Re_{mf} = d_{peff} U_{mf} \rho_g /\mu_g$ and $Ar = d_{peff}^3 \rho_g (\rho_{eff} - \rho_g) g /\mu_g^2$

U_{mf} was calculated, theoretically, using available correlations shown in Table 3.3. Effective properties such as effective density (ρ_{eff}) and effective particle diameter (d_{peff}) of the tertiary mixture were needed to determine U_{mf} theoretically. Effective density and effective particle diameter of a binary mixture can be calculated using following equations 1 and 2 (Rao & Bheemarasetti, 2001):

$$\rho_{eff} = (w_1\rho_1 + w_2\rho_2) / (w_1 + w_2) \quad \text{Eq.(1)}$$

$$d_{peff}^2 = k' \{ d_{p1} [(\rho_1 / \rho_2) (d_{p2} / d_{p1})]^{(w2 / w1)} \}^2, \text{ where } k' = (20d_{p1} + 0.36) \quad \text{Eq.(2)}$$

where w_1 and w_2, ρ_1 and ρ_2, and d_{p1} and d_{p2} were the masses, particle densities and particle diameters, respectively, of the two components in a binary mixture.

To determine effective properties of a tertiary mixture consisting of three bed materials such as GSR, switchgrass and sand, first, effective density (ρ_{eff}') and effective particle diameter (d_{peff}') for a binary mixture of switchgrass and GSR were obtained using following equations 3 and 4:

$$\rho_{eff}' = (w_2\rho_2 + w_3\rho_3) / (w_2 + w_3) \quad \text{Eq.(3)}$$

$$d_{peff}' = k_2\, d_{p2}\, [(\rho_2 / \rho_3)\, (d_{p3} / d_{p2})]^{(w3 / w2)}, \text{ where } k_2 = (20d_{p2} + 0.36)^{0.5} \quad \text{Eq.(4)}$$

where w_2, ρ_2 and d_{p2} were the mass, particle density and particle diameter, respectively, of the switchgrass. Similarly, w_3, ρ_3 and d_{p3} were the mass, particle density and particle diameter, respectively, of the GSR.

Next, effective properties of the tertiary mixture were obtained using effective properties of binary mixture of switchgrass and GSR (ρ_{eff}' and d_{peff}') and sand as follows in equations 5 and 6:

$$\rho_{eff} = (w_1\,\rho_1 + w_2\,\rho_2 + w_3\,\rho_3) / (w_1 + w_2 + w_3) \quad \text{Eq.(5)}$$

$$d_{peff} = k_1\, d_{p1}\, \{\, k_2\, [\, (\rho_1\, d_{p2}\, w_2 + \rho_1\, d_{p2}\, w_3) / (\rho_2\, d_{p1}\, w_2 + \rho_3\, d_{p1}\, w_3)\,]$$
$$(\rho_2\, d_{p3}\, /\rho_3\, d_{p2})^{(w3 / w2)}\, \}^{(w2 + w3)/ w1} \quad \text{Eq.(6)}$$

where $k_1 = (20d_{p1} + 0.36)^{0.5}$ and $k_2 = (20d_{p2} + 0.36)^{0.5}$ and w_1, ρ_1 and d_{p1} were the mass, particle density and particle diameter, respectively, of the sand in tertiary mixture of sand, switchgrass and GSR.

Effective bed void space at the minimum fluidization conditions (ε_{mfeff}) was calculated using effective properties of the tertiary mixture in equation 7 (Broadhurst & Becker, 1975) as follows:

$$\varepsilon_{mfeff} = (0.586 / \psi^{0.72})\, \{\mu_g^{\,2} / [\rho_g\, (\rho_{eff} - \rho_g)\, g\, d_{peff}^{\,3}]\}^{0.029}\, (\rho_g/\rho_{eff})^{0.021} \quad \text{Eq.(7)}$$

Another fluidization parameter called complete fluidization velocity (U_{cf}) was determined experimentally using graphical approach. U_{cf} was defined as the gas superficial velocity where the bed pressure drop begins to decrease from the constant bed pressure line during defluidization (Chok et al., 2010a). The fluidization state at U_{cf} is

known as complete fluidization state. Experimentally, U_{cf} was determined by gradually decreasing the gas flowrate (defluidization) immediately after reaching maximum gas flowrate during fluidization.

3.3 Results and discussion

3.3.1 Particle size distribution of bed materials

Particle geometric diameters by mass of GSR and sand were 80±2.6 μm and 348±1.6 μm, respectively (shown in Table 3.4). The geometric diameter by mass of sand particles was more than four times larger than that of GSR particles. About 64% of the GSR particles were below 125 μm in size while 88% of the sand particles were between 212 to 600 μm sizes. Particle length of more than 88% of the switchgrass was between 2 to 30 mm (shown in Table 3.5). The geometric mean length by mass of switchgrass particles was 10.3±1.7 mm. Width of the switchgrass particle ranged from 0.3 to 3.1 mm.

Table 3.4. Particle size distribution of GSR and sand

Sieve size (μm)	GSR		Sand	
	Mass on sieve (g)	% of total mass on sieve	Mass on sieve (g)	% of total mass on sieve
> 850	0.7 ± 0.2	1.4	0	0
600 - 850	0.5 ± 0.2	1.1	1.7 ± 0.8	0.3
300 - 600	3.8 ± 1.7	7.7	367.3 ± 6.3	73.9
212 - 300	2.1 ± 0.7	4.2	70.9 ± 1.9	14.3
150 - 212	5.0 ± 0.4	10.3	34.4 ± 0.8	6.9
125 - 150	5.5 ± 0.4	11.1	13.4 ± 2.1	2.7
106 - 125	7.8 ± 1.0	16.0	6.9 ± 1.3	1.4
<106	23.8 ± 1.6	48.4	2.5 ± 1.6	0.5

Table 3.5. Particle size distribution of ground switchgrass

Particle size (mm)	Mass (g)	% of total mass
60 - 70	0.09	2.7
50 - 60	0	0
40 - 50	0.01	0.2
30 - 40	0.15	4.4
20 - 30	0.43	13.1
10 - 20	1.25	37.6
5 - 10	0.91	27.6
2- 5	0.32	9.7
< 2	0.16	4.7

3.3.2 Fluidization characteristics of bed materials

3.3.2.1 Bed containing only sand

Fig. 3.3 shows typical fluidization characteristics of bed containing only sand. The bed pressure drop increased linearly within the fixed bed zone and reached maximum at the minimum fluidization state. U_{mf} and dP_{mf} were 0.093 m/s and 0.42 m of H_2O, respectively. Beyond the minimum fluidization state, formation of bubbles was steady and predominant throughout the bed. As a result, a continuous internal-circulation of bed particles from the bottom to the top and vice-versa was observed showing a good mixing among bed particles. Further increases in gas superficial velocity above U_{mf}, i.e. beyond minimum fluidization state, exhibited a large-sized bubble formation with rapid internal-circulation of bed particles. As a result, a rigorous mixing of sand particles with a considerable bed expansion was observed at U_{cf} of 0.12 m/s.

3.3.2.2 Bed containing GSR and sand

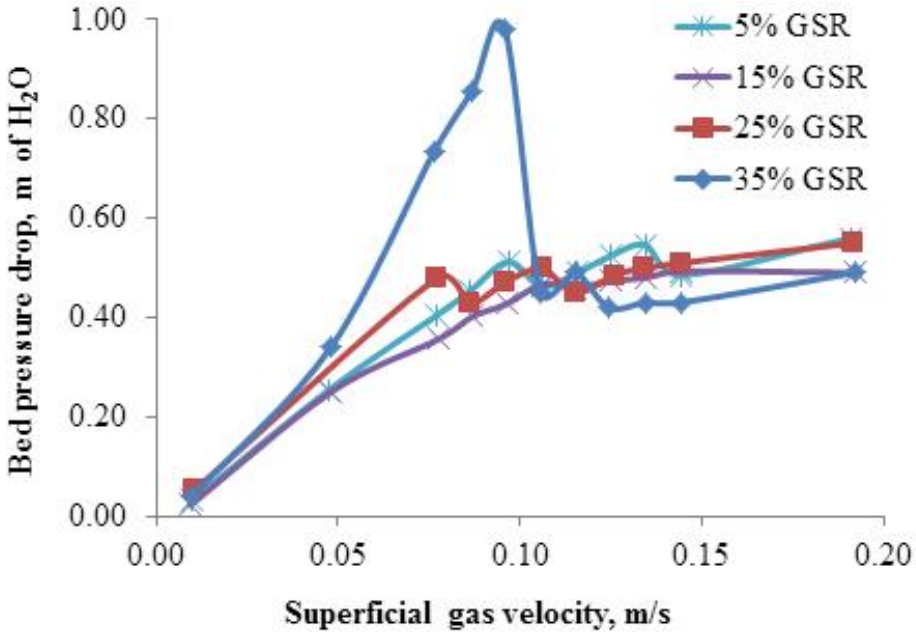

Fig. 3.4. Fluidization characteristics of bed containing GSR and sand

Bed containing different levels of GSR, i.e. 5%, 15%, 25% and 35% of the switchgrass level in the mixture of GSR and sand, were studied to determine fluidization characteristics. Since no switchgrass was used in these cases, quantities of GSR in the mixture were based on 1% level of switchgrass. A sudden increase in the bed pressure drop within the fixed bed zone was observed before collapse of the first bubble (Fig. 3.4). This sudden rise in the bed pressure drop can be due to the presence of comparatively smaller sized GSR particles than the sand particles, which precipitated in-between the sand particles, thus, reduced the total void space in the bed. This decrease in the void space may have resulted in a higher static resistance to the gas flow till the first bubble collapsed before the minimum fluidization state. With an increase in the quantity of GSR in the mixture, U_{mf} decreased significantly (p-values < 0.05) from 0.099 to 0.083 m/s. This can be attributed due to decrease in bed mean particle size with increase in GSR.

The GSR particles were 4.2 times smaller than the sand particles. As a result, the effective mean particle diameter of the bed material continuously decreased with an increase in the quantity of GSR in the mixture. Rao and Reddy (Rao & Reddy, 2010) reported decrease in U_{mf} with decreasing mean particle diameter of the sand when a binary mixture of biomass and sand was used for fluidization. However, other fluidization parameters, such as dP_{mf} and U_{cf}, remained constant with change in GSR levels at 0.45 m of H_2O and 0.18 m/s, respectively.

3.3.2.3 Bed containing GSR, switchgrass and sand

When the bed consisted of GSR, switchgrass and sand, there was a sudden rise in the bed pressure drop with an increase in gas superficial velocity within the fixed bed zone. A poorly mixed under-fluidization was observed due to irregular bubble formation and limited internal-circulation of the bed materials. Beyond the minimum fluidization state, fluidization was observed to be normal with improved mixing of bed materials in terms of a continuous bubble formation and frequent internal-circulations. The U_{mf} and dP_{mf} with varying bed composition are shown in Figs. 4.5 and 4.6, respectively. Statistical results showed that quantities of GSR and switchgrass had significant (p-value < 0.001) influence on fluidization. The main effects of GSR, switchgrass and their interaction (GSR*Switchgrass) on U_{mf}, dP_{mf} and U_{cf} were significant. Overall, both U_{mf} and dP_{mf} increased with an increase in levels of GSR and switchgrass.

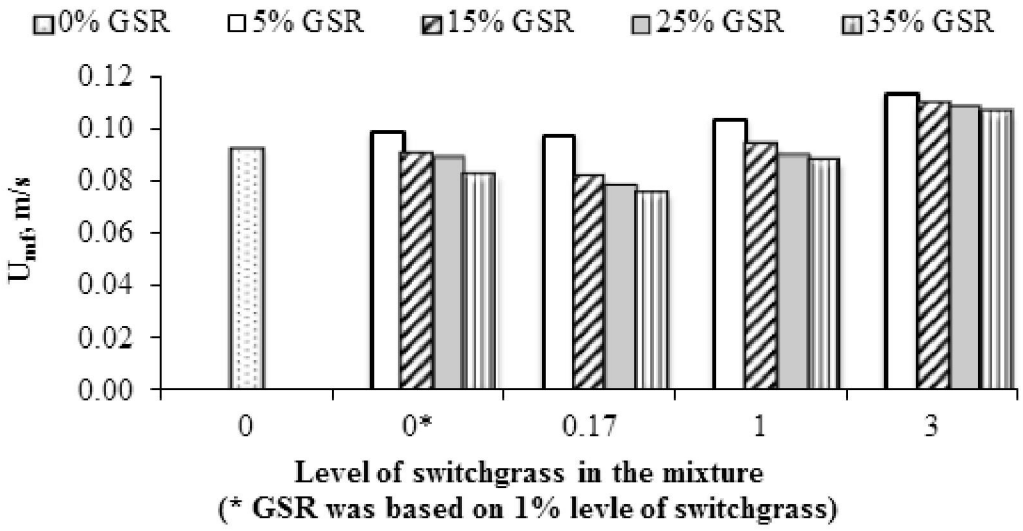

Fig. 3.5. U_{mf} with varying bed composition

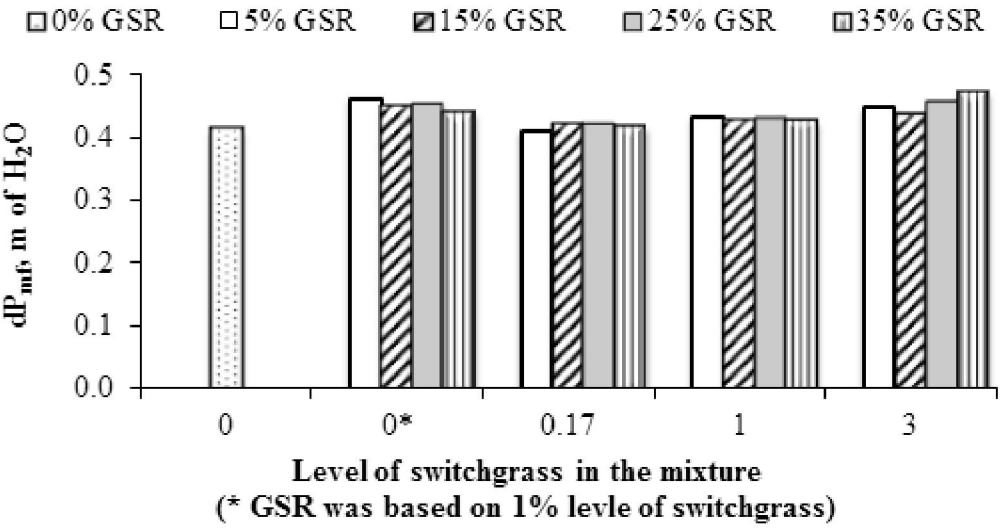

Fig. 3.6. Bed pressure drop with varying bed composition

3.3.3 Theoretical and experimental U_{mf}

Table 3.6 shows the experimental and theoretical (determined using available correlations) values of U_{mf} for different bed compositions. The correlation reported by Babu et al. (Babu et al., 1978) predicted U_{mf} within ± 7% error for only six out of seventeen mixture compositions investigated under this study while it showed higher deviation (± 10% error) for remaining mixture compositions. Similarly, the correlation

reported by Saxena and Vogel (Saxena & Vogel, 1977) predicted U_{mf} within ± 9% for only one out of seventeen mixture compositions while it showed more than ± 12% error for remaining mixture compositions. Also, correlations reported by Rao and Bheemarasetti (Rao & Bheemarasetti, 2001), Wen and Yu (Wen & Yu, 1966) and Leva (Leva, 1965) predicted U_{mf} for only one out of seventeen mixture composition within ± 10%, ± 7% and ± 3% errors, respectively. Overall, results indicated that none of the available correlations (Babu et al., 1978; Bourgeois & Grenier, 1968; Kunii & Levenspiel, 1991; Leva, 1965; Lucas et al., 1986; Rao & Bheemarasetti, 2001; Saxena & Vogel, 1977; Si & Guo, 2008; Wen & Yu, 1966) fit well for the entire range of mixture compositions investigated under this study. The large error deviation between theoretical and experimental U_{mf} can be because these correlations were based on a single material or a mixture of two materials while the present study involved a mixture of three bed materials. Several factors that influence U_{mf} are density, size and shape of bed materials, gas-solid and solid-solid interactions, collision property of particles, friction between particles, wall effect, and effective properties of a mixture (Cui & Grace, 2007; Gupta et al., 2009; Si & Guo, 2008). All of these factors were not considered in correlations shown in Table 3.5. Formisani and Girimonte (Formisani & Girimonte, 2003) reported that fluidization velocity for a binary mixture primarily depends upon density-ratio / size-ratio of bed materials, bed composition, and initial distribution (before fluidization) of bed particles. In this study, the bed materials used had higher particle size ratio (GSR/sand/switchgrass = 1:4:129) and particle density ratio (GSR/sand/switchgrass = 1:2.8:0.4) that could have resulted in the deviation between experimental and theoretical U_{mf}.

Table 3.6. Experimental and theoretical values of U_{mf} for different bed compositions

	Bed composition																
Switchgrass (%)	0	0	0	0	0	0.17	0.17	0.17	0.17	1	1	1	1	3	3	3	3
GSR (%)	0	5	15	25	35	5	15	25	35	5	15	25	35	5	15	25	35
Correlation	Minimum fluidization velocity, U_{mf} (m/s)																
Lucas et al. (1986)	0.038	0.012	0.012	0.012	0.012	0.013	0.013	0.012	0.012	0.014	0.014	0.013	0.013	0.017	0.016	0.016	0.015
Rao and Bheemarasetti (2001)	0.102	0.037	0.037	0.037	0.037	0.038	0.038	0.038	0.038	0.041	0.041	0.040	0.040	0.049	0.048	0.047	0.045
Wen and Yu (1966)	0.099	0.037	0.037	0.037	0.037	0.038	0.038	0.038	0.037	0.040	0.040	0.040	0.039	0.048	0.047	0.046	0.045
Leva (1965)	0.095	0.039	0.039	0.039	0.039	0.039	0.039	0.039	0.039	0.042	0.042	0.041	0.041	0.049	0.048	0.047	0.046
Si and Guo (2008)	0.118	0.043	0.043	0.043	0.043	0.044	0.044	0.044	0.044	0.047	0.047	0.046	0.046	0.056	0.055	0.054	0.052
Bourgeois and Grenier (1968)	0.120	0.046	0.046	0.046	0.046	0.047	0.047	0.047	0.046	0.050	0.050	0.049	0.049	0.060	0.058	0.057	0.055
Kunni and Levenspiel (1991)	0.137	0.052	0.052	0.052	0.052	0.053	0.053	0.053	0.053	0.057	0.057	0.056	0.056	0.068	0.067	0.065	0.063
This study	0.093	0.099	0.091	0.090	0.083	0.098	0.082	0.079	0.076	0.104	0.095	0.091	0.088	0.114	0.110	0.109	0.107
Saxena and Vogel (1977)	0.176	0.068	0.068	0.068	0.068	0.069	0.069	0.069	0.069	0.075	0.074	0.073	0.073	0.089	0.087	0.085	0.082
Babu et al. (1978)	0.199	0.078	0.078	0.078	0.077	0.079	0.079	0.079	0.079	0.085	0.084	0.084	0.083	0.101	0.099	0.096	0.093

3.3.4 Segregation and in-bed channelization

Fig. 3.7. Segregation of bed materials at 5% level of switchgrass in the mixture

In present study, segregation of bed materials was predominant at 5% level of switchgrass (Fig. 3.7) and no fluidization was observed at 5% level of switchgrass in the bed. This can be due to large differences in the particle size ratio (GSR/silica sand/switchgrass = 1:4:129) and particle density ratio (GSR/silica sand/switchgrass = 1:2.8:0.4). In this study, the switchgrass particles were about 31 times larger than the silica sand particles. Also, switchgrass is characterized as a low density and irregularly shaped loose material. Consequently, at higher switchgrass weight fraction in the bed, there can be a higher proclivity between switchgrass particles to join together to form a bigger particle, leading to lump and channel formation in the bed (Chok et al., 2010a; Pattipati & Wen, 1982). In the present study, at 5% switchgrass level in the mixture, there was formation of lumps and channels in the bed. As a result, the air easily escaped through in-bed channels resulted in a segregation of bed materials, and hence no fluidization was observed at 5% level of switchgrass in the mixture. Furthermore, the

adhesive forces of GSR particles may also have contributed to segregation. Abdullah et al. (Abdullah et al., 2003) indicated that higher bed bulk density supports fluidization whereas higher bed void space suppresses fluidization. In the present study, increase in quantity of switchgrass in the mixture decreased the bulk density with subsequent increase in the bed void space. This can be another factor to suppress fluidization at 5% level of switchgrass in the mixture. Overall, the results indicated that fluidization sustained up to 3% level of switchgrass. However, in-bed channelization caused ineffective fluidization at 5% level of switchgrass in the mixture.

3.4 Conclusions

Fluidization characteristics of a mixture of GSR, switchgrass and silica sand were studied. GSR and switchgrass present in the mixture had significant (p-value < 0.001) influence on fluidization. For the binary mixture of GSR and sand, with an increase in the GSR from 5% to 35%, the minimum fluidization velocity decreased significantly ($p < 0.05$). When the bed consisted of GSR, switchgrass and sand, with an increase in GSR and switchgrass from 5 to 35% and 0.17 to 3%, respectively, both minimum fluidization velocity and bed pressure drop increased. Fluidization of bed materials sustained up to 3% level of switchgrass. However, segregation of bed materials and in-bed channelization caused ineffective fluidization when the bed consisted of 5% level of switchgrass, 20 kg of sand and GSR between 5 to 35% in the mixture. For a mixture consisting of three different materials, the fluidization characteristics were found to be strongly dependent upon mixture's effective properties, which were determined using properties of all mixture components. Minimum fluidization velocity determined using effective properties of a tertiary mixture of GSR, switchgrass and sand showed that

prediction of U_{mf} from all selected correlations did not match well with the experimental data for the entire range of mixture compositions investigated under this study.

Nomenclature

Latin letters

Ar	Archimedes number
dP_{mf}	Bed pressure drop at minimum fluidization condition
d_p	Particle diameter, μm
d_{p1}, d_{p2}, d_{p3}	Mean diameters of sand, switchgrass and GSR particles, respectively, m
d_{peff}	Effective particle diameter of a mixture, m
k_1, k_2	Constants (Eq.(2))
Re_{mf}	Reynolds number at minimum fluidization condition
u_0	Fluid superficial velocity, m/s
U_{mf}	Minimum fluidization velocity, m/s
U_s	Minimum fluidization velocity of smaller particles, m/s
U_B	Minimum fluidization velocity of bigger particles, m/s
w_1, w_2, w_3	Masses of sand, switchgrass and GSR particles, respectively, kg
x_B	Weight fraction of bigger particles in the mixture

Greek letters

ρ_g	Fluid density, kg/m^3
ρ_1, ρ_2, ρ_3	Particle densities of sand, switchgrass and GSR, respectively, kg/m^3
ρ_{eff}	Effective density of a mixture of sand, switchgrass and GSR, kg/m^3
μ_g	Fluid viscosity, kg/m s
ε_{mf}, ε_{mfeff}	Effective void space of the bed at minimum fluidization condition

Φ, ψ Shape factor of particle

Acknowledgements

This material is based upon work supported, in part, by the National Science Foundation under Grant No. EPS-0814361 and the Director of the Oklahoma Agricultural Experiment Station. The authors highly appreciate support from graduate students Nitesh Rentam, Bipul Chandra, Karthikragunath Mariyappan and Shaswat Dixit for the experimental work. We convey our sincere thanks to Dr. Daiho Uhm for his guidance in statistical analysis.

3.5 References

Abdullah, M.Z., Husain, Z., Yin Pong, S.L. 2003. Analysis of cold flow fluidization test results for various biomass fuels. *Biomass and Bioenergy*, **24**(6), 487-494.

Babu, S., Shah, B., Talwalkar, A. 1978. Fluidization correlations for coal gasification materials-minimum fluidization velocity and fluidized bed expansion ratio. *AIChE symp Ser*. pp. 176-186.

Bourgeois, P., Grenier, P. 1968. The ratio of terminal velocity to minimum fluidising velocity for spherical particles. *The Canadian Journal of Chemical Engineering*, **46**(5), 325-328.

Broadhurst, T.E., Becker, H.A. 1975. Onset of fluidization and slugging in beds of uniform particles. *Aiche Journal*, **21**(2), 238-247.

Chiba, S., Chiba, T., Nienow, A., Kobayashi, H. 1979. The minimum fluidisation velocity, bed expansion and pressure-drop profile of binary particle mixtures. *Powder Technology*, **22**(2), 255-269.

Chok, V., Gorin, A., Chua, H. 2010a. Minimum and complete fluidization velocity for sand-palm shell mixtures, Part I: fluidization behavior and characteristic velocities. *American Journal of Applied Sciences*, **7**(6), 763-772.

Chok, V., Gorin, A., Chua, H. 2010b. Minimum and complete fluidization velocity for sand-palm shell mixtures, Part II: characteristic velocity profiles, critical loading and binary correlations. *American Journal of Applied Sciences*, **7**(6), 773-779.

Coltters, R., Rivas, A. 2004. Minimum fluidation velocity correlations in particulate systems. *Powder technology*, **147**(1-3), 34-48.

Cui, H., Grace, J.R. 2007. Fluidization of biomass particles: A review of experimental multiphase flow aspects. *Chemical Engineering Science*, **62**(1), 45-55.

Daleffe, R.V., Ferreira, M.C., Freire, J.T. 2008. Effects of binary particle size distribution on the fluid dynamic behavior of fluidized, vibrated and vibrofluidized beds. *Brazilian Journal of Chemical Engineering*, **25**, 83-94.

Formisani, B., Girimonte, R. 2003. Experimental analysis of the fluidization process of binary mixtures of solids. *Kona*, **21**, 66-75.

Gupta, S., Agarwal, V., Singh, S., Seshadri, V., Mills, D., Singh, J., Prakash, C. 2009. Prediction of minimum fluidization velocity for fine tailings materials. *Powder Technology*, **196**(3), 263-271.

Jena, H.M., Roy, G.K., Biswal, K.C. 2008. Studies on pressure drop and minimum fluidization velocity of gas-solid fluidization of homogeneous well-mixed ternary mixtures in un-promoted and promoted square bed. *Chemical Engineering Journal*, **145**(1), 16-24.

Kunii, D., Levenspiel, O. 1991. *Fluidization engineering*. Butterworth-Heinemann Boston.

Lam, P.S., Sokhansanj, S., Bi, X., Lim, C.J., Naimi, L.J., Hoque, M., Mani, S., Womac, A.R., Narayan, S., Ye, X.P. 2008. Bulk density of wet and dry wheat straw and switchgrass particles *Applied Engineering in Agriculture*, **24**(3), 351-358.

Leva, M. 1965. *Fluidization*. New York: McGraw Hill Press.

Lucas, A., Arnaldos, J., Casal, J., Puigjaner, L. 1986. Improved equation for the calculation of minimum fluidization velocity. *Industrial & Engineering Chemistry Process Design and Development*, **25**(2), 426-429.

McKendry, P. 2002. Energy production from biomass (part 3): gasification technologies. *Bioresource Technology*, **83**(1), 55-63.

Noda, K., Uchida, S., Makino, T., Kamo, H. 1986. Minimum fluidization velocity of binary mixture of particles with large size ratio. *Powder Technology*, **46**(2-3), 149-154.

Patil, K., Bowser, T., Bellmer, D., Huhnke, R. 2005. Fluidization characteristics of sand and chopped switchgrass-sand mixtures. *Agricultural Engineering International the CIGR Ejournal*, **7**.

Pattipati, R., Wen, C. 1982. Response to comments on" Minimum fluidization velocity at high temperatures". *Industrial & Engineering Chemistry Process Design and Development*, **21**(4), 785-786.

Rao, K.V.N.S., Reddy, G.V. 2010. Cold Flow Studies of Rice Husk, Saw Dust, and Groundnut Shell Fuels in a Fluidized Bed. *Energy Sources, Part A: Recovery, Utilization, and Environmental Effects*, **32**(18), 1701 - 1711.

Rao, T.R., Bheemarasetti, J.V.R. 2001. Minimum fluidization velocities of mixtures of biomass and sands. *Energy*, **26**(6), 633-644.

Sau, D., Mohanty, S., Biswal, K. 2008. Correlations for critical fluidization velocity and maximum bed pressure drop for heterogeneous binary mixture of irregular particles in gas-solid tapered fluidized beds. *Chemical Engineering and Processing: Process Intensification*, **47**(12), 2386-2390.

Saxena, S., Vogel, G. 1977. The measurement of incipient fluidisation velocities in a bed of coarse dolomite at temperature and pressure. *Chemical Engineering Research and Design*, **55**(a), 184-189.

Sharma, A.M., Kumar, A., Patil, K.N., Huhmke, R.L. 2011. Performance evaluation of a lab-scale fluidized bed gasifier using switchgrass as feedstock. *Transactions of the ASABE*, **56**(6), 2259-66.

Si, C., Guo, Q. 2008. Fluidization Characteristics of Binary Mixtures of Biomass and Quartz Sand in an Acoustic Fluidized Bed. *Industrial & Engineering Chemistry Research*, **47**(23), 9773-9782.

Wen, C., Yu, Y. 1966. A generalized method for predicting the minimum fluidization velocity. *AIChE Journal*, **12**(3), 610-612.

Werther, J. 2000. Fluidized-Bed Reactors. in: *Ullmann's Encyclopedia of Industrial Chemistry*, Wiley-VCH Verlag GmbH & Co. KGaA.

Wu, S., Baeyens, J. 1998. Segregation by size difference in gas fluidized beds. *Powder Technology*, **98**(2), 139-150.

Yudong, Z., Zhiqiang, L. 2010. The text study on the fluid characteristics of sawdust and rice straw. *Advances in Energy Engineering (ICAEE), 2010 International Conference on*, 19-20 June 2010. pp. 256-259.

Zhang, Y., Jin, B.S., Zhong, W.Q. 2010. Fluidization Characteristics of Stalk-Shaped Biomass in Binary Particle System. in: *Proceedings of the 20th International Conference on Fluidized Bed Combustion*, (Eds.) G. Yue, H. Zhang, C. Zhao, Z. Luo, Springer Berlin Heidelberg, pp. 311-316.

Zhong, W., Jin, B., Zhang, Y., Wang, X., Xiao, R. 2008. Fluidization of Biomass Particles in a Gas−Solid Fluidized Bed. *Energy & Fuels*, **22**(6), 4170-4176.

CHAPTER IV

EFFECT OF STEAM INJECTION LOCATION ON SYNGAS OBTAINED FROM AN AIR-STEAM GASIFIER

This research paper was published as "Sharma, A.M., Kumar, A., Huhnke, R.L. 2014. Effect of steam injection location on syngas obtained from an air-steam gasifier. *Fuel,* **116**, 388-394."

Abstract

For a fluidized-bed gasifier, reaction conditions vary along the height of the reactor. Hence, the steam injection location may have a considerable on the syngas quality. The objective of this study was to investigate the effects of steam injection location and steam-to-biomass ratio (SBR) on the syngas quality generated from an air-steam gasification of switchgrass in a 5 kg/h autothermal fluidized-bed gasifier. Steam injection locations of 51, 152, and 254 mm above the distributor plate and SBRs of 0.1, 0.2, and 0.3 were selected. Results showed that the syngas H_2 and CO yields were significantly influenced by the steam injection location ($p < 0.01$) and SBR ($p < 0.05$). The steam injection location also significantly influenced hot and cold gas, as well as carbon conversion efficiencies. The best syngas yields (0.018 kg H_2/kg biomass and 0.513 kg CO/kg biomass) and gasifier efficiencies (cold gas efficiency of 67%, hot gas efficiency of 72%, and carbon conversion efficiency of 96%) were at the steam injection location of 254 mm and SBR of 0.2.

Keywords: Fluidized-bed gasifier; biomass; steam port location; syngas

4.1 Introduction

Dependence on fuels and chemicals derived from petroleum resources has created a major challenge to meet world's demands on a sustainable basis. Biomass is a sustainable and renewable energy resource, which has the potential to reduce a significant portion of world's dependency on petroleum resources with subsequent reduction in global warming due to greenhouse gas emissions (Kumar et al., 2009b; Lv et al., 2004; Schuster et al., 2001). Biomass gasification, a thermochemical conversion technology, is one of the promising routes for producing fuels and chemicals using biomass-derived syngas. However, synthesis of liquid fuels and chemicals using various conversion processes typically requires a syngas with a wide range of H_2/CO ratio, i.e. between 0.4 and 4 (Hamelinck & Faaij, 2002; Jess et al., 1999; Klasson et al., 1993; Spath & Dayton, 2003; Wender, 1996), as well as concentrations of H_2 and CO and CO_2 (Wender, 1996; Zhang, 2010).

Syngas quality generated from biomass depends on several parameters such as biomass properties, gasifier design, gasifier operating conditions, and type of oxidizing agent (Kumar et al., 2009b). Different gasifier designs such as downdraft, updraft, and fluidized-bed have been optimized to produce syngas having high H_2 and CO contents. Biomass properties such as size, shape, moisture content, and chemical compositions, also significantly influence syngas quality in terms of gas composition and impurities. H_2 concentration of the syngas can also be increased by optimizing the design and operating conditions of the gasifier (Cox et al., 1995). Gasifier operating conditions such as biomass feed rate, gasification temperature, and flow rate of oxidizing agent have influence on syngas quality (Kumar et al., 2009b). The biomass feed rate into the gasifier

must be optimized to yield high heating value syngas with maximum energy efficiency (Kumar et al., 2009b). Gasification temperature controls reactions occurring inside the reactor. A gasification temperature above 800°C is desired to obtain high gas yield and H_2 and CO contents (Kumar et al., 2009b).

The type of oxidizing agent such as air, oxygen, and steam, used in biomass gasification also significantly effects quality and yield of syngas. Using air as an oxidizing agent results in a syngas highly-diluted with nitrogen (up to 65%) with low heating value (Delgado et al., 1997; Seo et al., 2010). Using oxygen as an oxidizing agent results in syngas with high CO and H_2 concentrations (Zhou et al., 2009). Using steam as an oxidizing agent results in syngas with high H_2 content (Bridgwater, 2006; Weerachanchai et al., 2009). Overall, air gasification yields a low-calorific syngas containing much less H_2 than that obtained through air-steam or steam-only gasification (Baratieri et al., 2008; Delgado et al., 1997; Lv et al., 2003; Ross et al., 2007). Air-steam gasification using fluidized bed gasifier at equivalence ratio (ER) of 0.22, steam-to-biomass ratio (SBR) of 2.7 and gasifier temperature of 900°C resulted in syngas with a high H_2 yield (71 g/kg of biomass, wet basis) (Lv et al., 2003) . Air-steam gasification of rice hull in a fluidized bed gasifier at 800°C showed high H_2 content (40%) in the syngas (Boateng et al., 1992). Kumar et al. (2009) studied air-steam gasification in a fluidized-bed gasifier and reported significant increase from 4% to 15% in syngas H_2 content with an increase in temperature from 650 to 850°C (Kumar et al., 2009a). Overall, air-steam gasification studies (Kumar et al., 2009a; Lv et al., 2003; Lv et al., 2004) showed that both steam injection and higher gasification temperatures (above 800°C) resulted in a H_2

rich syngas, making it more suitable for further conversion into liquid fuels and chemicals.

In air-steam gasification, major reactions contributing to the high H_2 yield are water-gas and water-gas shift reactions Eqs. (1)-(3) (Lv et al., 2003; Wang et al., 2007). The methane steam reforming reaction (Eq. (4)) also contributes to the H_2 content of the gas (Sharma et al., 2011).

$C+H_2O \rightarrow CO+H_2$ (water-gas reaction, $\Delta H = 131.3$ kJ/mol) Eq.(1)

$C+2H_2O \rightarrow CO_2+2H_2$ (water-gas reaction, $\Delta H = 89.7$ kJ/mol) Eq.(2)

$CO+H_2O \rightarrow CO_2+H_2$ (water-gas shift reaction, $\Delta H = -41.2$ kJ/mol) Eq.(3)

$CH_4+H_2O \rightarrow CO+3H_2$ (methane steam reforming reaction, $\Delta H = 206$ kJ/mol) Eq.(4)

An important consideration in maximizing efficiency and H_2 production in air-steam gasification is the location of steam injection, which can significantly affect the reaction conditions inside the gasifier. Injection of steam into a high temperature zone of the fluidized bed gasifier favors H_2 forming reactions (Eqs. (1)-(2)) and can yield H_2-rich syngas. On the contrary, injecting steam into a low temperature zone can further reduce the gasifier temperature, and thus adversely affect gasification reactions (Eqs. (1)-(3)) leading to low H_2 yield. Additionally, the formation of H_2 depends upon the residence time of reactants involved in gasification reactions. The residence time can also be optimized by changing the location of steam injection, which can further increase the H_2 content of the syngas.

Further, based on the temperature condition and carbon availability, steam injection in the reduction zone of the gasifier can increase H_2 production through

reducing reactions (Eqs. (1)-(3)). In fluidized-bed gasification, drying and devolatilization of biomass occur at the bottom of the fluidized bed, which can be considered as the virtual location of both drying and pyrolysis zones. Oxidation of de-volatized products and char occur next in the middle and top of the bed, which can be considered the virtual oxidation zone. Reduction occurs is the final step of the gasification and involves conversion of pyrolysis products into syngas, and thus, the region above the combustion zone i.e. top of the bed plus the freeboard region can be considered as the virtual reduction zone. Injection of steam into the reduction zone at the top of bed and in freeboard regions may lead to high H_2 yield through reducing reactions (Eqs. (1)-(3)).

Reaction conditions vary along the height of the reactor in especially autothermal fluidized-bed gasifiers. This study is based on the hypothesis that the location of steam injection has a significant effect on syngas quality. The objective of present study was to investigate the effect of steam injection location on the quality of syngas generated from an air-steam gasification in a 5 kg/h autothermal lab-scale fluidized-bed gasifier.

4.2 Materials and methods

4.2.1 Biomass feedstock and bed material

All experiments were performed using Kanlow switchgrass which was grown at the Agronomy Research Station of Oklahoma State University and harvested in the fall of 2010. Proximate and ultimate analyses of switchgrass were performed by Hazen Research, Inc. (Golden, CO). A bomb calorimeter (model A1290DDEB, Parr Instrument Co., Moline, IL) was used to determine higher heating value of switchgrass (18.83 MJ per kg dry biomass). Switchgrass bales were chopped using a 25 mm screen in a

Haybuster tub grinder (Model: H1000, Duratech Industries International, Inc. Jamestown, ND). Silica sand, supplied by Oglebay Norton Industrial Sands, Inc. (Brady, TX), was used as inert bed material. Bulk densities of switchgrass and silica sand were measured using a 0.0001 m^3 container. Switchgrass was poured into the container from 100 mm above the container and mass of the switchgrass in the container was determined. The bulk density was determined by dividing the mass of the switchgrass in the container with the container volume. The bulk density of silica sand was measured using the similar procedure. A digital vernier caliper (Digimatic, Mitutoyo, Japan) with 0.1 mm resolution was used to measure the particle length of switchgrass while a sieve shaker (CSC Scientific, Fairfax, VA) was used to perform particle size distribution of silica sand. The geometric mean sizes by mass of switchgrass and silica sand were determined using ANSI/ASAE Standard S319.3-February 2008 (ASABE Standards, 1997).

4.2.2 Test setup and instrumentation

Fig. 4.1 shows the gasifier test setup. Details of the gasifier system are described elsewhere (Sharma et al., 2011). A fluidized-bed gasifier test setup with a biomass throughput of 5 kg/h was used for this study. The test setup consisted of a fluidized-bed gasifier (0.1 m i.d. × 1.1 m height), a hopper, a double dump valve, a screw feeder, two cyclone separators, a producer gas burner, an air supply unit, a heat torch, and a steam boiler. The inside wall of the gasifier was thermally insulated with 1 inch refractory lining of conventional castable (Resco Products Inc., Pittsburgh, PA) while the outside wall was covered with 1 in. layer of thick cerawool (Kaowool RT Blanket-RCF-24/SW-24, Thermal Ceramics Inc. Augusta, GA). A distributor plate (0.28 m o.d. × 5 mm thickness) was located at the bottom of the gasifier to uniformly distribute the inlet air,

and to support a bed of silica sand. A 30 × 30 mesh size wire screen was placed on the top of the distributor plate to prevent the silica sand from falling down through the distributor plate. The biomass hopper was fitted with a stirrer to prevent bridging of the biomass feedstock and a screw coupled with a 90 V DC motor (Model: 2M168D, Dayton Electric Mfg. Co., Niles, IL) at the bottom for discharging biomass to the gasifier screw feeder. A DC speed regulator (Model: 4Z829B, Dayton Electric Mfg. Co., Niles, IL) was used with the gasifier screw motor to control the biomass flow rate into the gasifier. A double dump valve (Fig. 4.1) between the hopper exit and screw feeder was used to isolate the hopper from the gasifier and thus prevented backflow of hot gases into the biomass hopper. Two cyclone separators were connected in series to remove particulates from the gas at the gasifier exit. A burner at the end of the gas pipe lines was used to combust the exiting gas.

Air was supplied using an air compressor (Model: TS10K10, Ingersoll Rand, Davidson, NC). An air control valve, mass flow meter (Model: 8059MPNH, Eldridge Products, Inc., Monterey, CA), and pressure regulator (Model: 4Zk96, Grainger, Inc., Oklahoma City, OK) were fitted in-line with the air supply line. A heat torch (Model: HT200, Farnam Custom Products, CA) was used to heat air for preheating the sand bed inside the gasifier. A steam boiler (Model: MBA12, Sussman Electric Boilers, NY) was used to inject the steam into the gasifier. A stainless steel tube coil (8 mm i.d.) wrapped with a heat tape (Model: SRT051-040, Omega Engineering, Inc., Stamford, CT) was used to superheat the steam. A mass flow meter (Model: 1/2-73-R-101-HR-ESK, RCM Industries, Inc., CA) and flow control ball valve were used at the boiler outlet to monitor and control the steam flow rate. A U-tube water manometer and a differential pressure

transducer (Model: PX154-025DI, Omega Engineering, Inc., Stamford, CT) were used to measure pressure drop across the gasifier. Sampling ports were available in the gas pipe line for taking samples of syngas, tar and particulates. Gas pipe lines were wrapped with heat tapes for maintaining pipe line temperature above 300°C to prevent condensation of tars and water vapor. Gasifier operation was monitored using a LabVIEW system (National Instruments, Austin, TX).

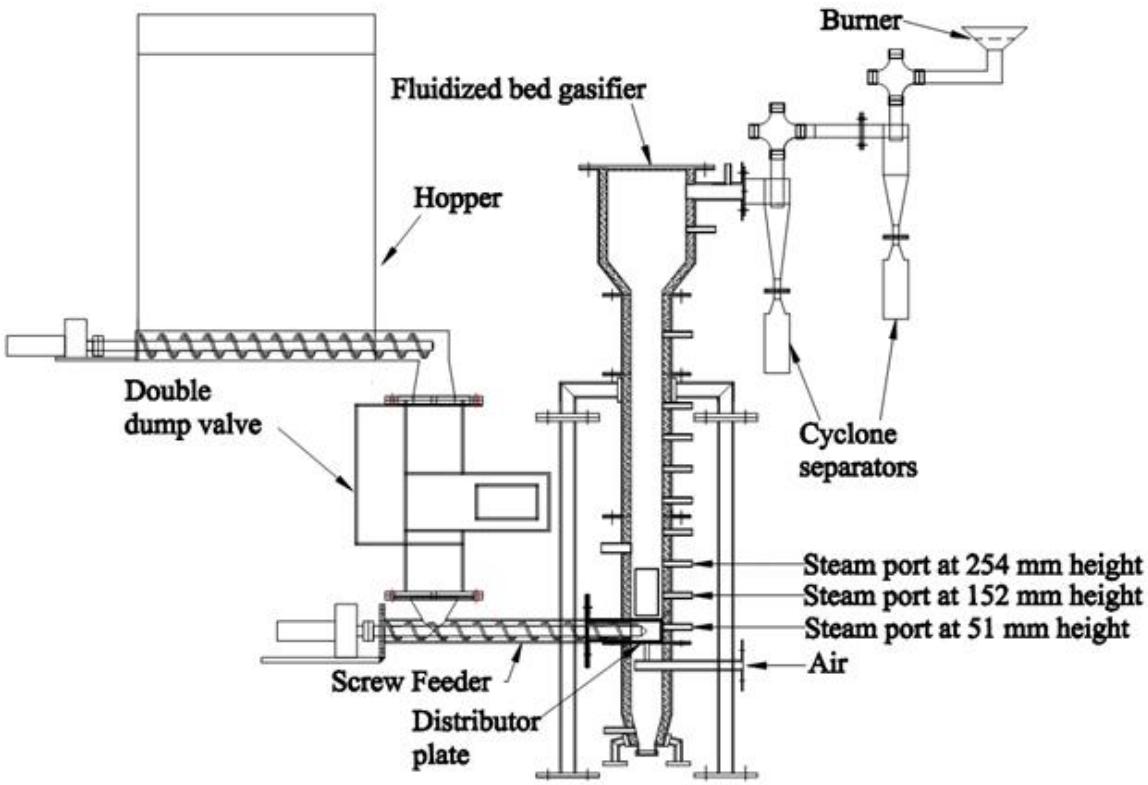

Fig. 4.1. Gasification test setup

4.2.3 Experimental design

A total of 18 gasification experiments (3 locations × 3 SBRs × 2 replications) were performed at ER of 0.32. The ER of 0.32 was selected for this study based on our earlier study with the 5 kg/h autothermal lab-scale fluidized bed gasifier that concluded that ER of 0.32 was optimum to obtain the best syngas composition, gas heating value,

and gasifier energy efficiency (Sharma et al., 2011). The gasifier reactor temperature varied along the height of the reactor at the ER of 0.32, (shown in Table 4.1). Based on the gasifier temperature, three gasifier locations at the heights of 51 mm, 152 mm, and 254 mm above the distributor plate were selected for steam injection. SBR was selected between 0.1 and 0.3 (maximum) based on our preliminary experiments to maintain autothermal requirements of the gasifier reactor.

Table 4.1. Reactor temperature along the height of the gasifier at ER = 0.32

Location above distributor plate (mm)	Average temperature (°C)
51	880
152	755
254	524
Above 356	≤ 340

4.2.4 Test procedure and system maintenance

A small inspection window (102 mm × 152 mm) with an airtight door was provided on the gasifier wall above the distributor plate for loading the sand in the gasifier and for maintenance work. 1.5 kg of sand was placed on the distributor plate through the inspection window and then the window was properly sealed. A thin cerawool packing and a high temperature RED RTV silicone gel (Type 650, Versachem, Riviera Beach, FL) were used to make metal flanges air-tight. Initially, the sand bed was preheated to 400°C by supplying hot air using the heat torch. The bed temperature was further raised to 700°C by feeding a low quantity of biomass into the gasifier. Typically, 20-40 min after the preheating, the gasifier temperature profile became uniform and the gas burner showed consistent flame from the exiting gas. The heat torch was then extinguished, and the gasification conditions such as flow rates of air and biomass were

adjusted to desired levels as per experimental design. Steam was then injected into the gasifier at the specified location. Duration of each test run was between 2 and 3 h.

System maintenance was performed the following day after each test run. During maintenance, the entire gasifier reactor, gas pipe lines, cyclone separators, and the burner were properly cleaned to remove any remaining tars and particulates. Used sand was removed using a vacuum cleaner through inspection window located at the gasifier bottom. After cleaning, the setup was prepared for the next test run. Unused biomass was also removed from the hopper, and the hopper was filled with a fresh biomass for the next test run.

4.2.5 Measurements and calculations

All data measurements were recorded when the gasifier temperature profile was stable, and the exiting gas was flammable. Flow rates of air, biomass, and steam; temperature of gasifier; gas-exit; gas-flame and steam; and pressure drop across the gasifier were continuously monitored. LabVIEW software was used for continuous recording of temperatures, pressure drop and air flow rate. Air and biomass flow rates were controlled using the LabVIEW program. To determine biomass flow rate, a calibration was performed between biomass flow rate and motor speed. The steam flow rate was measured using the steam mass flow meter. Equipment details and measurement techniques used for sampling gas, tar, and particulates, and gas and tar analyses are described elsewhere (Sharma et al., 2011). Equations to determine gas yield, gas heating value and gasifier efficiencies, i.e. cold gas, hot gas, and carbon conversion efficiencies, were used from literature (Sharma et al., 2011). Statistical analysis was performed using statistical software SAS (Release 9.3, SAS, Cary, NC, USA). Analysis of variance

(ANOVA) method with generalized linear model (GLM) procedure was used to study effects of steam injection port location and SBR (independent variables) on syngas yield, concentrations and impurities, gasification temperature, and gasifier efficiencies (dependent variables). The alpha (level of significance) for the statistical analysis was held constant at 0.05.

4.3 Results and discussion

Air-steam gasification of switchgrass was performed using the lab-scale fluidized-bed gasifier to study the effects of steam injection port location and SBR on the gasifier performance. Biomass properties, gas composition and heating value, tar and particulate contents, as well as gasifier efficiencies, are discussed in the following subsections.

4.3.1 Biomass Characteristics

Proximate and ultimate analyses of the Kanlow switchgrass are shown in Table 4.2. Bulk densities of chopped switchgrass and silica sand ranged from 105 to 117 kg/m^3 and 1592 to 1612 kg/m^3, respectively. Particle geometric mean size by mass of chopped switchgrass and silica sand were calculated to be 10 ± 1.7 mm and 336 ± 2 μm, respectively.

Table 4.2. Material properties

Proximate Analysis (wt.%, d.b.) [a]		Ultimate Analysis (wt.%, daf) [b]	
Moisture content	14.63	Carbon	52.74
Ash content	4.72	Hydrogen	5.91
Fixed carbon	13.69	Oxygen	41.05
Volatile matter	81.59	Nitrogen	0.24
		Sulfur	0.06

[a] Dry basis.
[b] Dry ash-free.

4.3.2 Gasifier temperature

The effect of SBR on the gasification temperature at the three steam injection port locations, i.e. 51, 152 and 254 mm, is shown in Fig. 4.2. The average temperature of steam at injection was 201°C, which was lower than the normal operating temperature of the gasifier bed (Table 4.1). Therefore, the steam injection into the gasifier caused quenching of the temperature environment at all injection locations leading to decreases in gasification temperature. Additionally, the quantity of steam injected into the gasifier increased with SBR, which directly influenced the gasifier temperature, resulting in further decreases in the temperature of the reactor bed. As a consequence, the gasifier temperature decreased with an increase in the SBR from 0.0 to 0.3 as shown in Fig. 4.2. The gasifier temperature decreased with increase in SBR at all steam injection port locations. At steam injection port location of 51 mm, with an increase in SBR, the gasifier temperature decreased from 713°C at SBR of 0.1 to 419°C at SBR of 0.2, and 367°C at SBR of 0.3. Similarly, at steam injection port location of 152 mm, the gasifier temperature decreased from 549°C at SBR of 0.1 to 437°C at SBR of 0.2, and 482°C at SBR of 0.3. At steam injection port location of 254 mm, with an increase in SBR, the gasifier temperature decreased from 664°C at SBR of 0.1 to 636°C at SBR of 0.2, and 587°C at SBR of 0.3. At steam injection port locations of 51 and 152 mm, the increase in the SBR from 0.1 to 0.3 significantly decreased ($p < 0.05$) the gasification temperature by 104^{o}C to 449°C (Fig. 4.2). This is primarily attributed to the quenching of the dense phase of bed materials at the lowest and middle, steam injection port, positions. At steam injection port location of 254 mm, with an increase in SBR, the gasifier temperature

decreased from 664°C at SBR of 0.1 to 636°C at SBR of 0.2, and 587°C at SBR of 0.3. The 254 mm steam injection port was located at the top of the bed that included a lean phase of the bed materials. As a result, the increase in the SBR from 0.1 to 0.3 did not show a significant influence on the gasification temperatures at 254 mm steam injection port location (shown in Fig. 4.2).

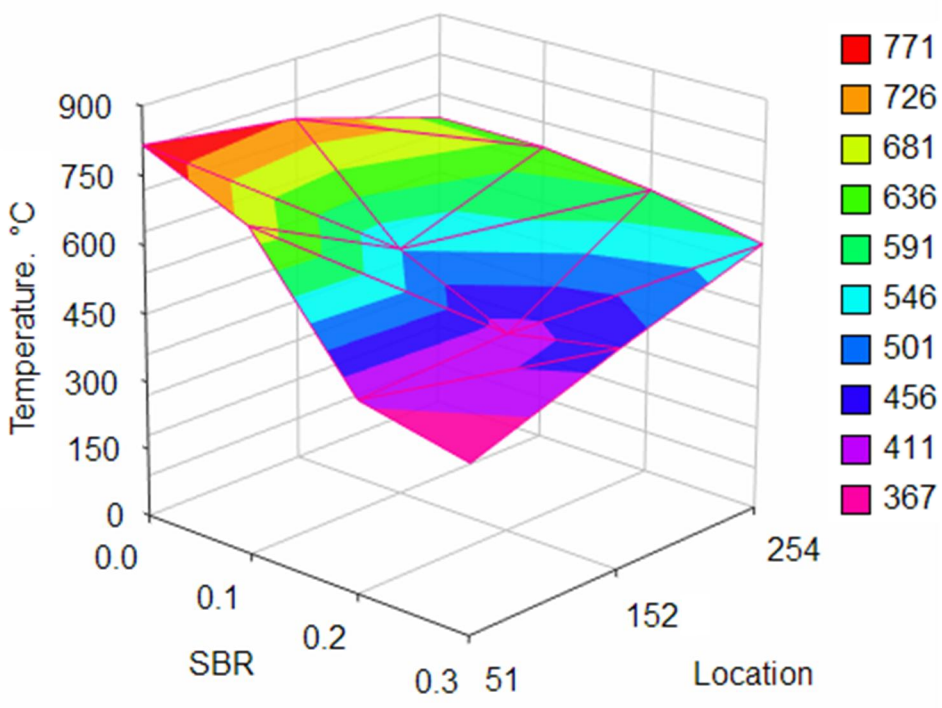

Fig. 4.2. Gasifier temperature with varying steam injection port location and SBR

4.3.3 Gas composition

CO and H_2 yields in syngas are influenced by the gasification temperature and the availability of limited reactant (H_2O). The water-gas reaction (Eq. (1)) that yields both H_2 and CO is an endothermic reaction, i.e. $\Delta H > 0$, and is considerably influenced by the gasification temperature (Franco et al., 2003). Thermodynamically, higher gasification temperatures favor endothermic gasification reactions such as Eq. (1) resulting in more H_2 and CO. Also, in addition to gasification temperatures, the quantity of limiting

reactant, i.e. H_2O, considerably influences the production of H_2 and CO through water gas reaction (Eq. (1)). This is because at higher levels of limiting reactant (H_2O), more H_2O reacts with the available carbon to form H_2, CO, and CO_2 through reactions (Eqs. (1) and (2)).

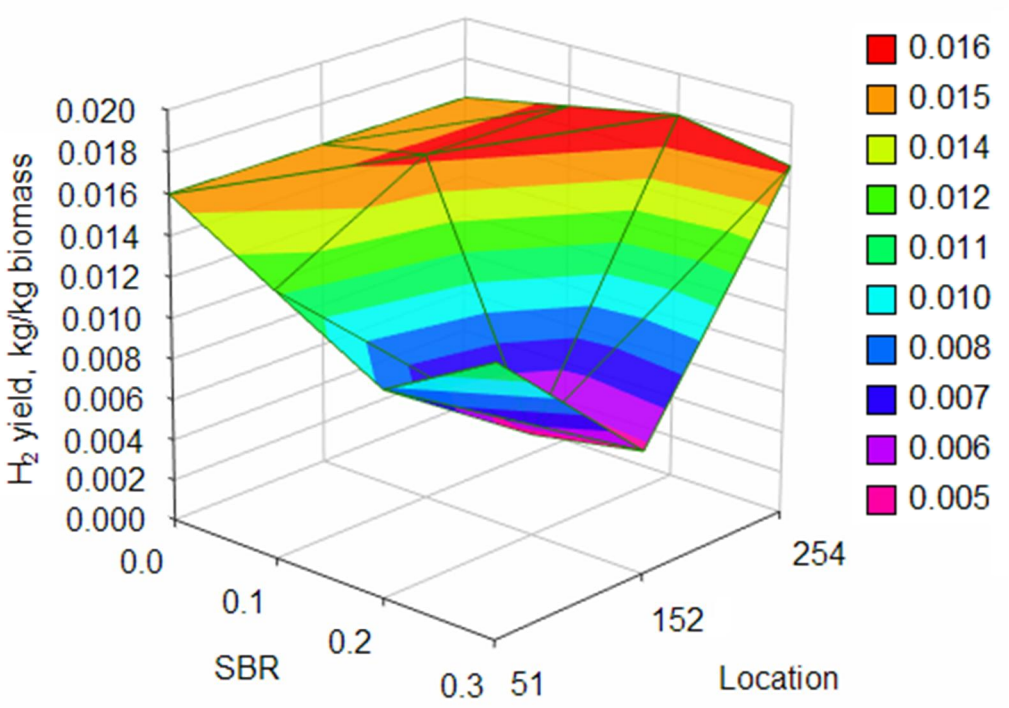

Fig. 4.3. Syngas hydrogen yield with varying steam injection port location and SBR

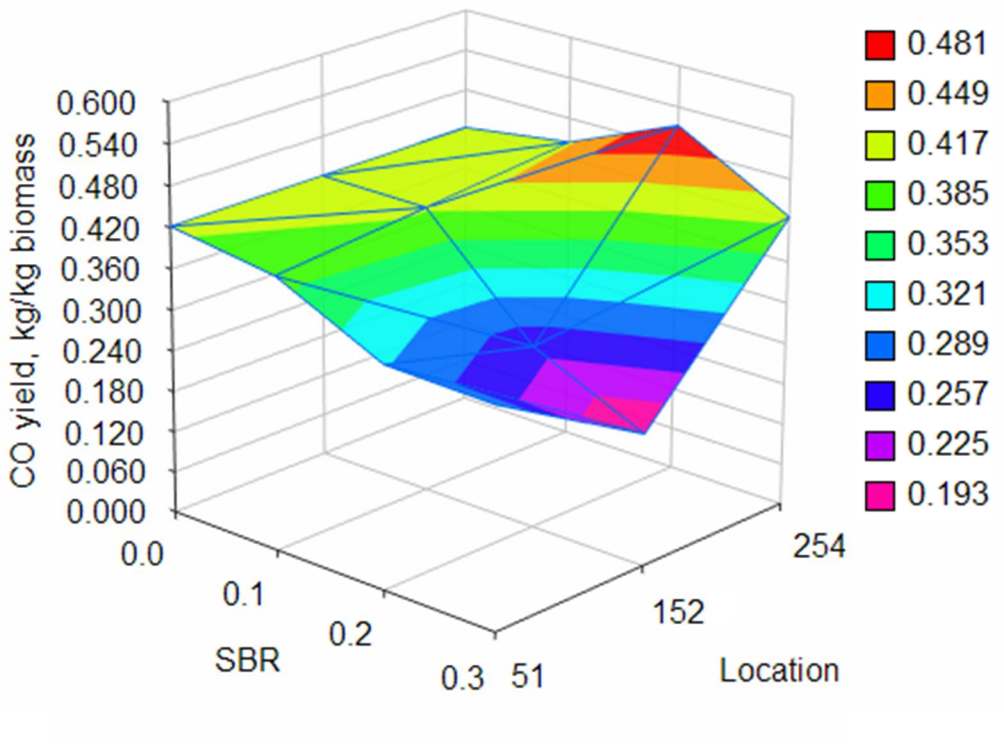

Fig. 4.4. Syngas carbon monoxide yield with varying steam injection port location and SBR

In the present study, the maximum H_2O was available at SBR of 0.3. Hence, it was anticipated that the SBR of 0.3 would result maximum H_2 and CO yields through reaction Eq. (1). However, as explained above, due to a significant decrease in the gasification temperature at the 51 and 152 mm steam injection port locations , the SBR of 0.3 resulted in lower H_2 (Fig. 4.3) and CO (Fig. 4.4) yields. Also, the decrease in the gasification temperature caused reduction in the gas volumetric flowrate (due to cooling effect) through the bed materials resulting in decrease of overall bed-expansion and turbulence level in the fluidized-bed (Daleffe et al., 2008; Sharma et al., 2013). Such a decrease in the bed expansion and in-bed turbulence level may have further reduced the overall heat and mass transfer in the gasifier bed, resulting in the lower H_2 and CO yields at steam injection port locations of 51 and 152 mm.

At the 254 mm steam injection port location, maximum CO and H_2 yields were observed at SBR of 0.2. The SBR of 0.3 showed 4% and 17% lower H_2 and CO yields, respectively, than at SBR of 0.2. Such observations can be explained by the decrease in the gasification temperature (Fig. 4.2) caused by the higher steam injection at SBR of 0.3. Also, at 254 mm steam injection port location, the SBR of 0.1 resulted in 5% and 13% lower H_2 and CO yields, respectively, than those at SBR of 0.2. No steam injection (SBR of 0.0) also resulted in lower CO and H_2 yields than those obtained at SBR of 0.2. It can be inferred from these results that SBR of 0.2 at steam injection of 254 mm provided the best combination of bed temperature and H_2O to maximize CO and H_2 yields. Results show that steam injection at the 254 mm port (located in the reduction zone of the gasifier) led to high H_2 yield. The high H_2 yield can be attributed to reducing reactions (Eqs. (1)-(3)), as discussed earlier.

Water-gas shift reaction (Eq. (3)) is also an important gasification reaction that produces H_2. However, this reaction also increases CO_2 yield. High CO_2 yields at steam injection port location of 254 mm (Fig. 4.5) can be attributed to the water-gas shift reaction (Eq. (3)) that also contributed to the high H_2 yield. Alternatively, the high CO_2 yields can be attributed to the reaction (Eq. (2)) leading to the consumption of injected H_2O (steam), producing H_2 as well as CO_2. The endothermic methane steam reforming reaction (Eq. (4)) could also have contributed to the high H_2 and CO yields at the steam injection port location of 254 mm. This was because at high gasification temperatures, as observed at this location and in the presence of H_2O, methane is less thermodynamically stable and could have converted to more stable gaseous products, i.e. H_2 and CO.

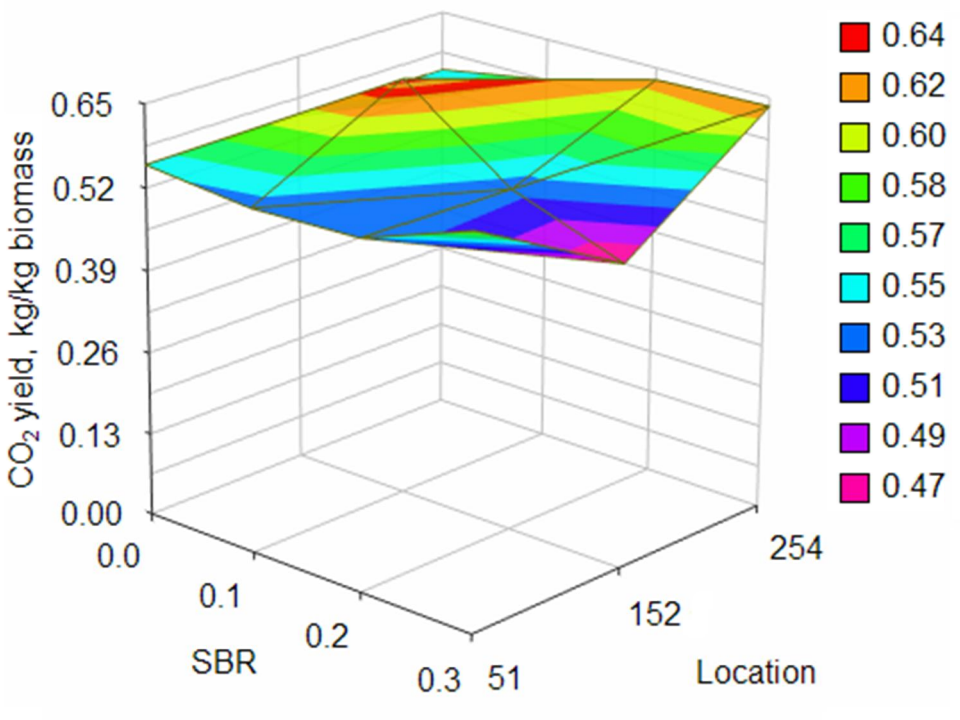

Fig. 4.5. Syngas carbon dioxide yield with varying steam injection port location and SBR

Statistical results showed that both steam injection port location ($p < 0.01$) and SBR ($p < 0.05$) had highly significant effects on H_2 and CO yields. Also, the interaction between steam injection port location and SBR was significant ($p < 0.05$). The effect of steam injection port location and SBR on the syngas CO_2 yield was, however, not significant. Overall, the SBR of 0.2 and steam injection port location of 254 mm resulted in 12% and 18% higher syngas H_2 and CO yields, respectively, than H_2 and CO yields obtained without any steam injection.

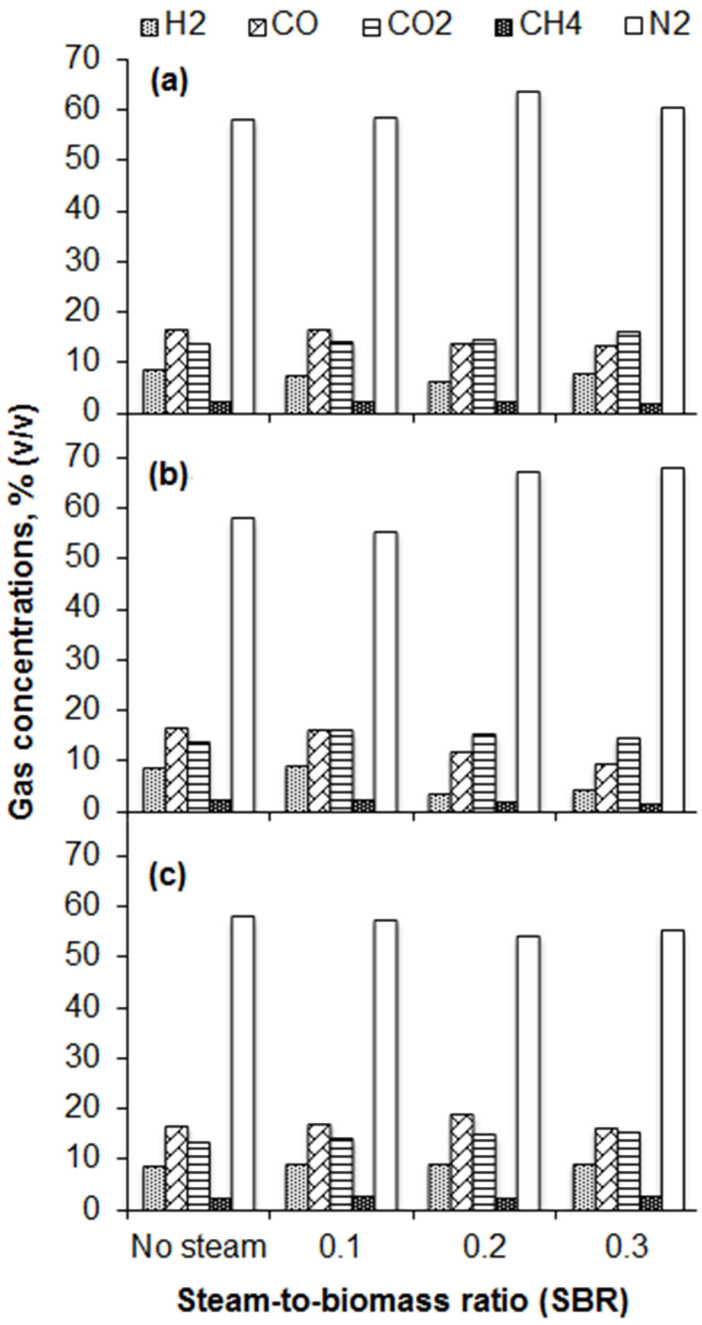

Fig. 4.6. Concentrations of syngas with varying SBR at different steam injection port locations. (a) 51 mm, (b) 152 mm, and (c) 254 mm

Concentrations of CO, H_2, CO_2, CH_4 and N_2 in syngas depend on several factors such as gasification temperature and quantities of limiting reactants (H_2O and O_2). In the present study, concentrations of H_2, CO, CO_2, CH_4 and N_2 with no steam injection (at

SBR of 0.0) were 8.4%, 16.4%, 13.7%, 2.3% and 57.8%, respectively. Steam injection at 51 mm port location decreased H_2, CO and CH_4 concentrations as shown in Fig. 4.6(a). The reduction in H_2, CO and CH_4 concentrations was mainly due to decrease in gasification temperature with steam injection at the 51 mm port. However, with the steam injection, CO_2 content was found to increase (by 2-17%). The N_2 content was mainly dependent on the quantity of air supplied to the gasifier. Since ER in the present study was held constant at 0.32, the syngas N_2 concentration followed an opposite trend with the cumulative concentrations of H_2, CO, CO_2 and CH_4. The N_2 concentration increased (by 1-10%) with an increase in SBR.

At steam port location of 152 mm, syngas H_2 concentration increased by 6 % at SBR of 0.1 as compared to that with no steam injection. However, with further increase in steam injection at SBR of 0.2 and 0.3, H2 concentration considerably decreased by 52-62%. With increase in SBR, CO and CH_4 concentrations continue to decrease by 3-43% and 20-47%, respectively, as compared to those obtained with no steam injection. On the contrary, CO_2 concentration increased by 6-15% with an increase in SBR. The N_2 concentration decreased slightly (4%) at SBR of 0.1 as compared to that with no steam injection and then increased (16-17%) at SBRs above 0.1.

At steam port location of 254 mm, the gasification temperature was not significantly affected by SBR. Further 254 mm steam injection port location and at SBR of 0.2 showed the maximum H_2 (9.0%) and CO (18.7%) concentrations. This implies that the 254 mm port location and the SBR of 0.2 provided the best combination of bed temperature and H_2O to produce CO and H_2. H_2 concentration increased by 4-7% with an increase in SBR compared to that with no steam injection. CO concentration also

increased by 2-14% with an increase in SBR from 0.1 to 0.2 while it decreased by 3% with further increase in SBR from 0.2 to 0.3 (Fig. 4.6(c)). The CH_4 concentration remained constant at SBRs of 0.1 and 0.3; however, it decreased by 7% at SBR of 0.2 as compared to that obtained with no steam injection. The decrease in the CH_4 and increase in CO and H_2 concentrations indicate that methane steam reforming reaction (Eq. (4)) may have occurred. The CO_2 concentration increased by 3 to 10% with an increase in SBR as compared to that obtained with no steam injection. The N_2 concentration decreased by 1 to 7% with an increase in SBR as compared to that obtained with no steam injection. The decrease in N_2 concentration was mainly due to the increase in CO, H_2 and CO_2 concentrations as discussed above. Statistical analysis showed that syngas CO and H_2 concentrations were significantly influenced by the steam injection port location ($p < 0.01$) and SBR ($p < 0.05$). However, the interaction effect of steam injection port location and SBR on the syngas CO_2 concentration was not significant.

4.3.4 Syngas yield, heating value and impurities

Syngas yield, which is the quantity of gas produced (Nm^3) per kg of dry biomass, depends primarily on gasification temperature and quantities of reacting species, i.e. biomass, air, and steam supplied to the gasifier. Since quantities of biomass and air were held constant, gasification temperature and SBR were the variables that influenced the syngas yield. With an increase in SBR from 0.1 to 0.3, higher gasification temperatures were observed at the 254 mm steam injection port location (Fig. 4.2). Further, the maximum quantity of steam injected into the gasifier was at SBR of 0.3; however, SBR of 0.3 resulted in a decrease in the gasification temperature at 254 mm steam injection port location, and thus, showed lower syngas yield (2.14 Nm^3 per kg of dry biomass).

The maximum syngas yield of 2.19 Nm^3 per kg of dry biomass was observed at SBR of 0.2 at the 254 mm steam injection port location.

Syngas heating value depends upon concentrations of primary combustible products, i.e. H_2 and CO. The other minor constituents of the syngas were the lighter hydrocarbons, i.e. CH_4, C_2H_2, C_2H_4 and C_2H_6 that also contain considerable amounts of energy and have influence on the syngas heating value. In the present study for all gasification conditions, the syngas heating value ranged between 3.3 and 5.4 MJ/Nm^3. The 254 mm steam injection port location and SBR of 0.2 resulted in the highest syngas H_2 (9.0%) and CO (18.7%) contents leading to the maximum syngas heating of 5.4 MJ/Nm^3.

Tar and particulate contents are the major impurities in the syngas. Tar, a condensable organic compound, is composed of several hydrocarbons heavier than benzene and its quantity in syngas mainly depends on biomass properties, and gasification conditions such as temperature and residence time. Steam injection can reform tar leading to an overall reduction in tar. In the present study, the maximum tar content of 29.5 g/Nm^3 was observed at the 152 mm steam injection port and SBR of 0.3. At 152 mm steam injection port, the tar content increased from 18.8 to 29.5 g/Nm^3 with an increase in SBR from 0.1 to 0.3. The increase in tar content with increased SBR can be attributed to quenching of devolatilized products within the gasifier bed by the low temperature steam, as explained earlier. However, steam injections at 51 and 254 mm port locations showed low syngas tar contents (1.9-8.1 and 4.1-18.5 g/Nm^3, respectively) implying that the injected steam participated in tar-reforming reactions leading to decrease in the overall tar content. The maximum particulate content of 12 g/Nm^3 was

observed at the 152 mm steam injection port location and the SBR of 0.3. Statistical results showed that both tar and particulate contents were not significantly influenced by either the steam injection port location or SBR.

4.3.5 Gasifier efficiencies

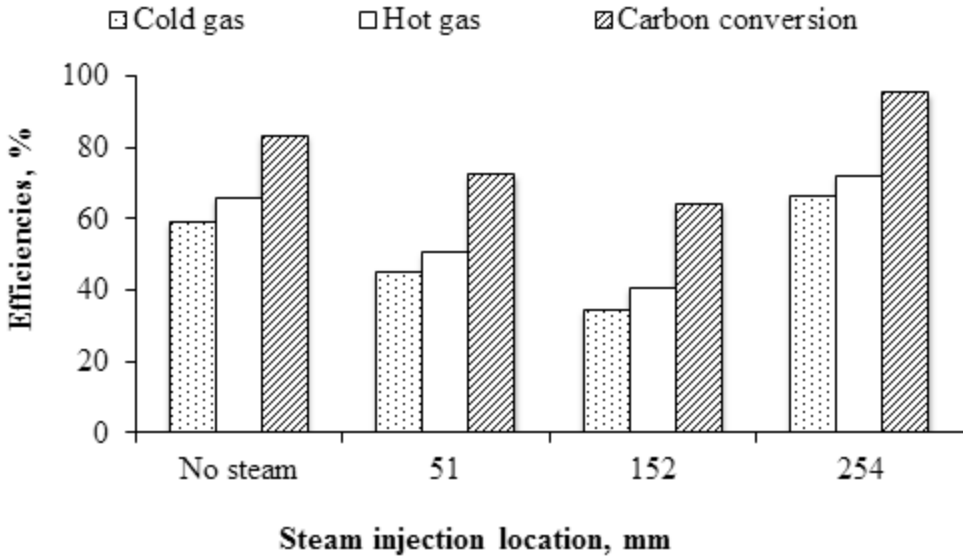

Fig. 4.7. Gasifier efficiencies at three steam injection port locations at SBR of 0.2

The gasifier cold gas and hot gas efficiencies depend on the syngas heating value and yield. The hot gas efficiency also depends on sensible energy content of the syngas, which is directly proportional to the syngas exit temperature. Statistical analysis showed that the steam injection port location had a significant effect on the cold gas and hot gas efficiencies ($p < 0.05$) while SBR showed a significant effect ($p < 0.05$) on only the hot gas efficiency of the gasifier. As explained earlier, the decrease in the gasification temperature at the steam injection port locations of 51 and 152 mm resulted in the lower syngas exit temperature, which in turn decreased the hot gas efficiency at steam injection port locations below 254 mm. The 254 mm steam injection port location and SBR of 0.2 resulted in the maximum cold gas (67%) and hot gas (72%) efficiencies (Fig. 4.7).

Carbon conversion efficiency of the gasifier depends on the concentrations of carbon containing gaseous products of the syngas such as CO, CO_2 and other lighter hydrocarbons. The maximum carbon conversion efficiency of 96% was observed at the 254 mm steam injection port location and SBR of 0.2. Statistical results showed that the steam injection port location had a highly significant influence ($p < 0.01$) on the carbon conversion efficiency. The interaction between steam injection port location and SBR (location*SBR) had significant influence ($p < 0.05$) on the carbon conversion efficiency. However, the effect of SBR alone on the carbon conversion efficiency was not significant.

4.4 Conclusions

Air-steam gasification of switchgrass was performed using an autothermal lab-scale fluidized-bed gasifier to investigate the effects of steam injection port location and steam-to-biomass ratio (SBR) on syngas composition, yield and impurities, as well as, gasifier efficiencies. Statistical results showed that the syngas H_2 and CO yields were significantly influenced by the steam injection port location ($p < 0.01$) and SBR ($p < 0.05$). The steam injection port location had also significant effect ($p < 0.05$) on the gasifier cold gas and hot gas efficiencies. However, SBR had significant effect on the hot gas efficiency but not on the cold gas efficiency. The carbon conversion efficiency was significantly influenced ($p < 0.01$) by the steam injection port location but not by the SBR. The 254 mm steam injection port location and SBR of 0.2 resulted in the maximum syngas H_2 (0.018 kg/dry kg biomass) and CO (0.513 kg/dry kg biomass) yields, cold gas (67%), hot gas (72%) and carbon conversion (96%) efficiencies.

Acknowledgements

This work was supported in part by NSF-EPSCoR award EPS-0814361and the Director of the Oklahoma Agricultural Experiment Station. The authors also acknowledge the support from Graduate students Karthikragunath Mariyappan, Nitesh Rentam and Mohit Dobhal for assisting with the experimental work.

4.5 References

ASABE-Standards. 1997. ANSI/ASAE S319. 3 February2008: Method of determining and expressing fineness of feed materials by sieving. in: *ASABE*. St. Joseph, Mich.

Baratieri, M., Baggio, P., Fiori, L., Grigiante, M. 2008. Biomass as an energy source: Thermodynamic constraints on the performance of the conversion process. *Bioresource Technology*, **99**(15), 7063-7073.

Boateng, A., Walawender, W., Fan, L., Chee, C. 1992. Fluidized-bed steam gasification of rice hull. *Bioresource Technology*, **40**(3), 235-239.

Bridgwater, T. 2006. Biomass for energy. *Journal of the Science of Food and Agriculture*, **86**(12), 1755-1768.

Cox, J.L., Tonkovich, A.Y., Elliott, D.C., Baker, E.G., Hoffman, E.J. 1995. Second Biomass Conference of the Americans: Energy, Environment, Agriculture, and Industry Proceeding; National Renewable Energy Laboratory, Golden, CO 657−674.

Daleffe, R.V., Ferreira, M.C., Freire, J.T. 2008. Effects of binary particle size distribution on the fluid dynamic behavior of fluidized, vibrated and vibrofluidized beds. *Brazilian Journal of Chemical Engineering*, **25**, 83-94.

Delgado, J., Aznar, M.P., Corella, J. 1997. Biomass gasification with steam in fluidized bed: Effectiveness of CaO, MgO, and CaO-MgO for hot raw gas cleaning. *Industrial & Engineering Chemistry Research*, **36**(5), 1535-1543.

Franco, C., Pinto, F., Gulyurtlu, I., Cabrita, I. 2003. The study of reactions influencing the biomass steam gasification process. *Fuel*, **82**(7), 835-842.

Hamelinck, C.N., Faaij, A.P.C. 2002. Future prospects for production of methanol and hydrogen from biomass. *Journal of Power Sources*, **111**(1), 1-22.

Jess, A., Popp, R., Hedden, K. 1999. Fischer-Tropsch-synthesis with nitrogen-rich syngas - Fundamentals and reactor design aspects. *Applied Catalysis a-General*, **186**(1-2), 321-342.

Klasson, K.T., Ackerson, M.D., Clausen, E.C., Gaddy, J.L. 1993. Biological Conversion of Coal and Coal-Derived Synthesis Gas. *Fuel*, **72**(12), 1673-1678.

Kumar, A., Eskridge, K., Jones, D.D., Hanna, M.A. 2009a. Steam-air fluidized bed gasification of distillers grains: Effects of steam to biomass ratio, equivalence ratio and gasification temperature. *Bioresource Technology*, **100**(6), 2062-2068.

Kumar, A., Jones, D.D., Hanna, M.A. 2009b. Thermochemical biomass gasification: A review of the current status of the technology. *Energies*, **2**(3), 556-581.

Lv, P., Chang, J., Xiong, Z., Huang, H., Wu, C., Chen, Y., Zhu, J. 2003. Biomass Air-Steam Gasification in a Fluidized Bed to Produce Hydrogen-Rich Gas. *Energy Fuels*, **17**(3), 677-682.

Lv, P., Xiong, Z., Chang, J., Wu, C., Chen, Y., Zhu, J. 2004. An experimental study on biomass air-steam gasification in a fluidized bed. *Bioresource Technology*, **95**(1), 95-101.

Ross, D., Noda, R., Horio, M., Kosminski, A., Ashman, P., Mullinger, P. 2007. Axial gas profiles in a bubbling fluidised bed biomass gasifier. *Fuel*, **86**(10-11), 1417-1429.

Schuster, G., Löffler, G., Weigl, K., Hofbauer, H. 2001. Biomass steam gasification–an extensive parametric modeling study. *Bioresource Technology*, **77**(1), 71-79.

Seo, M.W., Goo, J.H., Kim, S.D., Lee, S.H., Choi, Y.C. 2010. Gasification Characteristics of Coal/Biomass Blend in a Dual Circulating Fluidized Bed Reactor. *Energy & Fuels*, **24**, 3108-3118.

Sharma, A.M., Kumar, A., Patil, K.N., Huhmke, R.L. 2011. Performance evaluation of a lab-scale fluidized bed gasifier using switchgrass as feedstock. *Transactions of the ASABE*, **56**(6), 2259-66.

Sharma, A.M., Kumar, A., Patil, K.N., Huhnke, R.L. 2013. Fluidization characteristics of a mixture of gasifier solid residues, switchgrass and inert material. *Powder Technology*, **235**, 661-668.

Spath, P.L., Dayton, D.C. 2003. Preliminary screening - technical and economic assessment of synthesis gas to fuels and chemicals with emphasis on the potential for biomass-derived syngas. NREL Report, Contract No. DE-AC36-99-GO10337.

Wang, Y., Yoshikawa, K., Namioka, T., Hashimoto, Y. 2007. Performance optimization of two-staged gasification system for woody biomass. *Fuel Processing Technology*, **88**(3), 243-250.

Weerachanchai, P., Horio, M., Tangsathitkulchai, C. 2009. Effects of gasifying conditions and bed materials on fluidized bed steam gasification of wood biomass. *Bioresource Technology*, **100**(3), 1419-1427.

Wender, I. 1996. Reactions of synthesis gas. *Fuel Processing Technology*, **48**(3), 189-297.

Zhang, W. 2010. Automotive fuels from biomass via gasification. *Fuel Processing Technology*, **91**(8), 866-876.

Zhou, J., Chen, Q., Zhao, H., Cao, X., Mei, Q., Luo, Z., Cen, K. 2009. Biomass–oxygen gasification in a high-temperature entrained-flow gasifier. *Biotechnology Advances*, **27**(5), 606-611.

CHAPTER V

PREDICTION OF BIOMASS-GENERATED SYNGAS USING EXTENTS OF MAJOR REACTIONS IN A CONTINUOUS STIRRED-TANK REACTOR

This research paper was submitted for publication as "Sharma, A.M., Kumar, A., Madihally, S., Whiteley, J.R., Huhnke, R.L. Prediction of biomass-generated syngas using extents of major reactions in a continuous stirred-tank reactor."

Abstract

Syngas, the main gasification product, is a well-known intermediate for making fuels, chemicals and power. Literature shows several gasification models based on the Gibbs equilibrium approach. However, the assumption made in the Gibbs equilibrium model that the gasification reactions reach equilibrium condition does not occur in application due to the short residence time and multiphase reactions. The objective of this study was to develop and validate reaction kinetics-based gasification model using extents of major reactions in a continuous stirred-tank reactor (CSTR) to predict syngas composition and yield. The model was studied by varying biomass and air flowrates from 2.9 to 4.2 dry kg/h and 4.5 to 10 kg/h, respectively, with temperature ranging from 801 to 907°C. Results showed significant improvement in the prediction of syngas composition and yield, and gasification energy efficiencies. The extents of gasification reactions indicated that at equivalence ratio (ER) below 0.29, water gas reaction contributed the most to the syngas CO and H_2 yields while char oxidation reaction contributed to the CO yield. At ER of 0.29 and above, Boudouard and methane oxidation reactions were the most dominating reactions contributing to the CO yield while water gas shift reaction contributed to the H_2 yield.

Keywords: Biomass gasification; syngas; kinetics; Gibbs equilibrium; extent of reaction

5.1 Introduction

Biomass, such as grass, plants and crop residues, is a sustainable and renewable energy feedstock. Many research efforts have been successfully demonstrated for generating energy from biomass (Abelson, 1976; Jenkins & Bhatnagar, 1991; Patel et al., 2006; Quaak et al., 1999). However, biomass is categorized as a low grade energy fuel and has limited uses as a direct feedstock for generating liquid fuels and chemicals. Gasification, a thermochemical conversion process, converts a low grade solid biomass under high temperature into gaseous fuel called syngas. The biomass generated syngas consists mainly of CO, H_2, CO_2, CH_4, N_2 (if air is used as an oxidizing agent), and impurities such as tar, H_2O, NH_3 and H_2S. Syngas is a well-known intermediate for making biofuels, biochemical and biopower through various conversion processes. However, these conversion processes require syngas with different concentrations of H_2, CO, and CO_2 (Wender, 1996) as well as H_2/CO ratios from 0.4 to 4 (Hamelinck & Faaij, 2002; Jess et al., 1999; Klasson et al., 1993; Spath & Dayton, 2003; Wender, 1996). To maximize the product (fuels, chemicals or power) yield, it is necessary that biomass gasification matches the needs of downstream conversions in terms of gas composition, levels of impurities, and yield of the syngas. The biomass-generated syngas quality and yield, on the other hand, rely heavily on several factors such as the properties of biomass, gasifier operating conditions, and complex chemical reactions that occur during the gasification.

With the advent of latest computational techniques and sophisticated simulation tool, such as Aspen™ Plus, the biomass gasification process can be modeled and the syngas composition and yield can be predicted more reliably. Several Aspen™ Plus

gasification modeling studies (Kumar et al., 2009b; Paviet et al., 2009; Puig-Arnavat et al., 2010; Wenyi & Qin, 2010) using Gibbs equilibrium reactor (RGibbs) are available for different biomass feedstocks. However, little information is available on kinetics modeling of biomass gasification using extents of major reactions in a continuous stirred-tank reactor (CSTR).

When using the Gibbs equilibrium reactor modeling approach, one of the primary assumptions many researchers make is that the gasification reactions reach equilibrium, which does not happen due to short residence time. In addition, the gasification involves several homogenous and heterogeneous reactions R(1) to R(7) (Kumar et al., 2009a) and the kinetics of these reactions play a significant role on syngas composition and yield. Equilibrium modeling approaches do not consider the influence of these influential reactions. As a result, large deviations between the predicted and experimental values of the syngas composition have been found while using the equilibrium modeling approach.

Water gas reaction	$C + H_2O$	$\leftrightarrow$ $CO + H_2$	(ΔH = + 131 kJ/mol)	R(1)
Boudouard reaction	$C + CO_2$	$\leftrightarrow$ $2CO$	(ΔH = + 173 kJ/mol)	R(2)
Water gas shift	$CO + H_2O$	$\leftrightarrow$ $CO_2 + H_2$	(ΔH = - 41 kJ/mol)	R(3)
Methane oxidation	$CH_4 + 3/2O_2$	$\rightarrow$ $CO + 2H_2O$	(ΔH = - 519 kJ/mol)	R(4)
Methane reforming	$CH_4 + H_2O$	$\leftrightarrow$ $CO + 3H_2$	(ΔH = + 206 kJ/mol)	R(5)
Char combustion	$C + O_2$	= CO_2	(ΔH = - 394 kJ/mol)	R(6)
Char partial combustion	$C + 1/2O_2$	= CO	(ΔH = - 111 kJ/mol)	R(7)

By including kinetics of the major reactions, the CSTR based reaction kinetics gasification model can more reliably predict the syngas composition for the given biomass feedstock, gasification conditions, and type of oxidizing agent. Nikoo and Mahinpey (2008) developed an Aspen™ Plus gasification model using CSTR reactor

model (RCSTR) for pine sawdust. Simulations were performed assuming reactor temperatures of 700-900 °C. The authors, however, considered only five gasification reactions which may have led to the deviations between experimental and predicted gas compositions. The authors reported mean error deviations of 0.18 - 0.34 for H_2, 0.09 – 0.11 for CO, 0.20 – 0.30 for CO_2 and 0.16 – 0.27 for CH_4 on % volume basis. Authors also assumed that the volatile reactions followed Gibbs equilibrium that is unlikely to happen because of the fast volatile reactions leading to the deviations observed between experimental and simulation data. Moreover, most of the previous biomass gasification models use RYield reactor of Aspen™ Plus to decompose biomass (a non-conventional material) into conventional elemental components such as C, H, O, N, S and ash. This is done because properties of non-conventional materials are not available in Aspen™ Plus database whereas properties of conventional components are. However, the above decomposition of biomass into several elemental components can only occur in extreme reaction conditions far beyond the conditions during gasification. Hence, the currently available models of biomass gasification are inadequate to simulate reaction mechanisms of biomass gasification to reliably predict syngas needed for production of fuels and chemicals.

The novelty of present study lies in the development of a gasification model using a modeling approach based on extents of major gasification reactions and the fundamental design of CSTR. The model incorporated extensive gasification condition, such as seven major gasification reactions, their kinetics parameters, reactor volume and residence time that are not possible in Gibbs equilibrium based gasification model studied by several researchers. Also, the this model incorporates a novel biomass decomposition

approach of converting the biomass into products such as C, H_2O, CO, CO_2, CH_4, H_2 and tar that are feasible during biomass gasification (Pasangulapati et al., 2012). The specific objectives of this study were to develop kinetics-based gasification model using extents of major reactions in a CSTR to predict syngas composition and yield, and to validate model prediction with the experimental results obtained on our fluidized-bed gasifier.

5.2 Materials and methods

5.2.1 Biomass feedstock and gasification conditions

Kanlow switchgrass was gasified in a lab-scale fluidized-bed gasifier with air as an oxidizing agent. The higher heating value of the switchgrass was 18.83 MJ/kg dry biomass. The details of the experimental conditions (Table 5.1) and the experimental results were reported previously (Sharma et al., 2011). Operating pressure of the gasifier was 1.01 MPa. The gasification model was studied by varying the equivalence ratio (ER), which is defined using following Eq.(1).

$$ER = \left(\frac{\textit{Actual air supplied for gasification per unit mass of biomass}}{\textit{Theoretical air required for complete combustion per unit mass of biomass}} \right) \quad \text{Eq.(1)}$$

Table 5.1. Experimental conditions used for simulation of gasification models (Sharma et al., 2011)

ER	0.20	0.29	0.32	0.40	0.45
Dry biomass feed rate, kg/h	3.9	4.2	3.4	2.9	3.7
Air flowrate, kg/h	4.5	6.8	6.5	6.4	10.0
Air temperature, °C	25.2	29.0	29.5	29.0	32.0
Gasification temperature, °C	801	809	825	893	907
Syngas volume flowrate, Nm^3/h	4.61	7.23	6.99	6.43	9.25

5.2.2 Biomass decomposition characteristics

Ultimate and proximate analyses of switchgrass (Table 5.2) were used to calculated chemical formulas of switchgrass ($CH_{1.46}O_{0.68}N_{0.003}S_{0.002}Ash_{0.02}$, dry basis) and its volatile matters ($CH_{2.16}ON_{0.005}S_{0.004}$, dry basis). Based on the proximate analysis properties, switchgrass was decomposed into four major components, i.e. fixed carbon, moisture, ash and volatile matters (Fig. 5.1). Coefficients *a*, *b*, *c* and *d* of the biomass decomposition reaction (Fig. 5.1) were determined based on the fixed carbon, moisture, ash and volatile matters, respectively. The volatile matters were further decomposed into possible devolatization products (i.e. CO, CO_2, CH_4, H_2, tar, NH_3 and S); hence, the overall reaction of biomass decomposition into several species used in the present study was represented by Eq. (1) (Kumar et al., 2009b). In equation 1, coefficients *a*, *b* and *c* were based on Fig. 5.1, while coefficients *e* to *k* were calculated based on the total volatile matters (i.e. *d* VM) obtained based on decomposition scheme shown in Fig. 5.1.

Table 5.2. Switchgrass properties (Sharma et al., 2011)

Proximate Analysis (wt.%, d.b.)[a]		Ultimate Analysis (wt.%, daf)[b]	
Moisture content	14.63	Carbon	52.74
Ash content	4.72	Hydrogen	5.91
Fixed carbon	13.69	Oxygen	41.05
Volatile matter	81.59	Nitrogen	0.24
		Sulfur	0.06

[a] Dry basis
[b] Dry ash-free

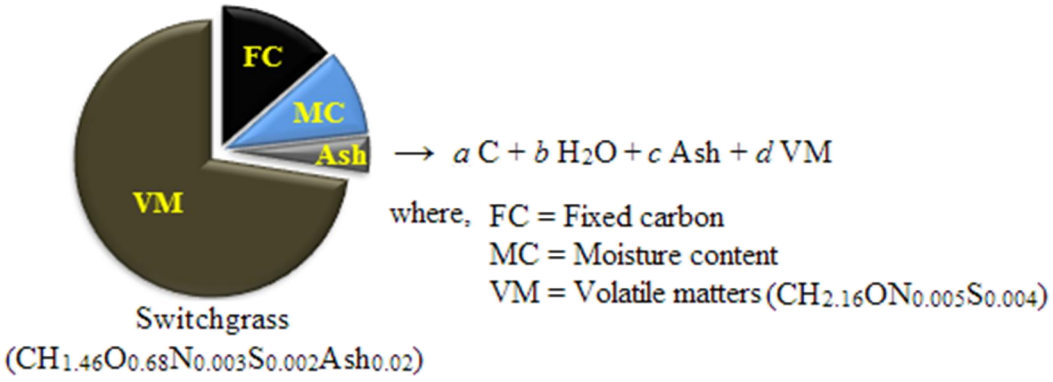

Fig. 5.1. Decomposition of switchgrass into different species

$$CH_{1.46}O_{0.68}N_{0.003}S_{0.002}Ash_{0.02}\ (\text{Switchgrass}) \rightarrow aC + bH_2O + c\text{Ash} + eCO + fCO_2 + gCH_4 + hH_2 + i\text{Tar} + jNH_3 + kS \quad \text{Eq.(2)}$$

Pasangulapati et al. (2012) studied characterization of switchgrass for thermochemical conversion using the Thermogravimetric Analysis (TGA) coupled with Fourier Transform Infrared Spectrometer (FTIR) and reported that CO, CO_2 and CH_4 were the major products generated from switchgrass devolatization. The diatomic molecule such as H_2 was not detected by the FTIR as it has no IR absorption (Pasangulapati et al., 2012). Therefore, CO, CO_2, CH_4 and H_2 plus tar, NH_3 and S (Eq. 2), were assumed to be the possible devolatization products generated from volatile matters of switchgrass.

Mass balance of C, H, O, N and S elements of volatile matters ($CH_{2.16}ON_{0.005}S_{0.004}$) resulted in five equations; however, the overall switchgrass decomposition reaction (Eq. 2) contained a total of seven unknowns (*e* through *k*). Hence two more equations were required to determine all seven unknowns. Kumar et al. (2009) developed Gibbs equilibrium biomass gasification model using Aspen™ Plus. In their model, the authors assumed CO/CO_2 ratio equal to one to determine the seven unknowns

in the biomass decomposition reaction (Eq. 2). It was reported that CO/CO_2 ratio of one did not affect the predicted composition of syngas because the Gibbs equilibrium reactor depends on total energy of final product at the given temperature and accordingly rebalances the syngas composition (Kumar et al., 2009b). Hence, the sixth equation in this study was obtained by considering CO/CO_2 ratio to be one. The seventh equation was obtained by assuming that tar yield is known based on the experimental results. Three possible combinations of devolatization products were evaluated to improve the overall reliability of the gasification models under the present study (Table 5.3).

Because switchgrass contains negligible S content, S yield in the devolatization products was assumed to be negligible in case 1. In case 2, S was considered as one of the devolatization products. As described earlier, in addition to the main constituents of syngas (CO, H_2, CO_2, CH_4 and N_2), the biomass generated syngas may also contain light hydrocarbons, such as C_2H_2, C_2H_4, and C_2H_6 (Sharma et al., 2011) resulting from the biomass volatile matters. Hence, these lighter hydrocarbons were also considered as devolatization products in case 3 (Table 5.3). The yields of C_2H_2, C_2H_4, and C_2H_6 in case 3 were assumed to be known based on the experimental results (Sharma et al., 2011). The three cases were evaluated through preliminary simulation runs to determine the best possible products of biomass devolatization with a goal to improve model predictions.

Table 5.3. Biomass devolatization reactions

Case 1: VM $\rightarrow$ eCO + $f$$CO_2$ + $g$$CH_4$ + $h$$H_2$ + iTar
Case 2: VM $\rightarrow$ eCO + $f$$CO_2$ + $g$$CH_4$ + $h$$H_2$ + iTar + $j$$NH_3$ + kS
Case 3: VM $\rightarrow$ eCO + $f$$CO_2$ + $g$$CH_4$ + $h$$H_2$ + iTar + $j$$NH_3$ + kS + $l$$C_2H_2$ + $m$$C_2H_4$ + $n$$C_2H_6$

5.3 Modeling approach

Two approaches were used for modeling biomass gasification process to predict syngas composition and yield. In the first approach, Aspen™ Plus software was used for modeling biomass gasification using the Gibbs equilibrium reactor model (RGibbs). In the second approach, the kinetics of various gasification reactions and gasification residence time were incorporated using the CSTR, which is the most common reactor to design the chemical processes. RGibbs was used as a baseline to compare the improvement in prediction of the reaction kinetics gasification model. The detailed description of both modeling approaches are described as follows.

5.3.1 Gibbs equilibrium reactor Aspen™ Plus gasification model

The equilibrium gasification model for switchgrass was developed using Gibbs equilibrium reactor (RGibbs) of Aspen™ Plus (Version 7.0, Aspen™ Technology, Inc., MA). The input parameters to the model included biomass properties (ultimate and proximate analyses), flowrates of biomass and air, and gasification temperature and pressure, shown in Fig. 5.2. The model outputs included gas composition and yield.

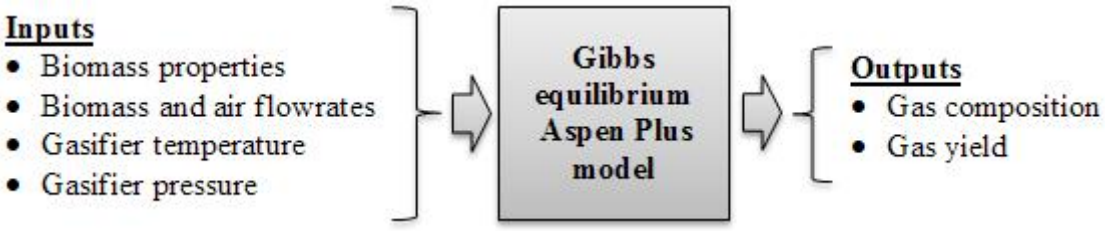

Fig. 5.2. Input and output parameters of Gibbs equilibrium Aspen™ Plus model

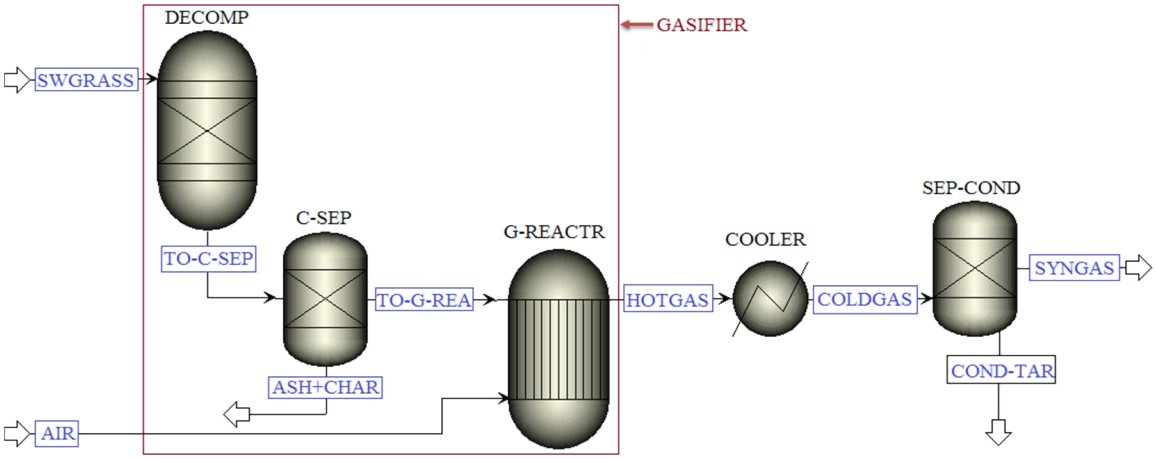

Fig. 5.3. Gibbs equilibrium Aspen™ Plus biomass gasification model

Fig. 5.3 shows the process flow diagram of Gibbs equilibrium Aspen™ Plus biomass gasification model. In Aspen™ Plus model, air, C, S, H_2O, CO, CO_2, H_2, O_2, CH_4 and NH_3 were defined as conventional material components while switchgrass, tar, and ash were defined as the unconventional material components. The Soave-Redlich-Knowg (SRK) property method was used in the Aspen™ Plus biomass gasification model. The entire gasifier system including biomass supply, gasifier reactor and cyclone separator, was modeled using three different blocks, i.e. DECOM, C-SEP and G-REACTR, shown using the rectangular box in Fig. 5.3. DECOM block was used to decompose input material stream (switchgrass) into several output material steams such as solid (C, S and ash), vapor (tar and H_2O) and gaseous (CO, CO_2, H_2, O_2, CH_4 and NH_3) material streams. DECOM block was simulated using RYield reactor model of Aspen™ Plus. In DECOM block, the yields of all outgoing materials (decomposed products) were specified based on the biomass decomposition as described in previous section (Fig. 5.1 and Table 5.3). All decomposed products (TO-C-SEP) from DECOM block were supplied to C-SEP block for separation and removal of ash and unreacted char from the decomposed products. C-SEP block was simulated using SEP (separator) model of Aspen™ Plus. The

ash and unreacted char-free decomposed products (TO-G-REC) from C-SEP block plus air through separate stream (AIR) were fed to G-REACTR for gasification. The N_2 to O_2 molar ratio of 3.76 was used for air. The G-REACTR was simulated using RGibbs reactor model of Aspen™ Plus in which temperature and pressure conditions were defined using the experimental data. G-REACTR block computed concentrations of feasible products (thermodynamically and chemically) based on the minimization of total Gibbs free energy (Kumar et al., 2009b). The output product stream (HOTGAS) from G-REACTR contained only gaseous species (CO, H_2, CO_2, CH_4 and N_2) and impurities (tar, H_2O and NH_3). The impurities of the HOTGAS stream were condensed to 30°C using COOLER block, which was simulated using HEATER (heat exchanger) model of Aspen™ Plus. The condensed stream from COOLER (COLDGAS) was supplied into SEP-COND block for separation and removal of condensed impurities from the COLDGAS stream. The SEP-COND block was simulated using SEP (separator) model of Aspen™ Plus. The outlet stream from SEP-COND block (SYNGAS) contained only gaseous species (CO, H_2, CO_2, CH_4 and N_2).

Following assumptions were made in the Gibbs equilibrium Aspen™ Plus model (Kumar et al., 2009b; Nikoo & Mahinpey, 2008; Paviet et al., 2009; Puig-Arnavat et al., 2010; Wenyi & Qin, 2010).

1. Gasification reactions reached equilibrium condition, and thus, the Gibbs equilibrium reactor calculated the final gas composition based on the minimization of total Gibbs free energy (Kumar et al., 2009b; Nikoo & Mahinpey, 2008).

2. Fluidized-bed reactor is assumed to be a well-mixed and steady state system with uniform temperature throughout the reactor (Fogler, 1999). Therefore, the gasifier (Gibbs reactor) operation was assumed to be an isothermal and steady state process.
3. As described earlier, switchgrass instantly decomposed into possible devolatization products such as C, H_2O, ash, CO, CO_2, CH_4, H_2, tar, NH_3, S, C_2H_2, C_2H_4 and C_2H_6.
4. Carbon conversion efficiency and tar yield were assumed to be known based on the experimental results. The tar, which primarily contained C, H and O, was represented as $CH_{1.55}O_{0.55}$ (Kumar et al., 2009b). Char yield was assumed to be negligible.
5. The operating pressure of the fluidized-bed gasifier previously studied (Sharma et al., 2011) was atmospheric, and the Gibbs equilibrium gasification was assumed to be an isobaric process.
6. The hydrodynamics of fluidized-bed were not incorporated in the gasification model; rather it was assumed that the temperature, and heat and mass transfer conditions within the gasifier were sufficient for gasification reactions (Kumar et al., 2009b).

5.3.2 Reaction kinetic gasification model

If the operating condition of a fluidized-bed gasifier is constant, it can be considered as a continuous and steady state system wherein the bed materials, such as the mixture of biomass and inert sand, are uniformly distributed within the fluidized-bed. Hence, the fluidized-bed gasifier was assumed to be a well-mixed reactor. The fluidized-bed is also under high temperature (above 750 °C) and turbulence conditions; hence, drying, heating and devolatization of biomass, and various gas-solid and gas-gas reactions of gasification can be considered to be completed within the fluidized-bed. Therefore, a continuous type of well-mixed chemical reactor, called CSTR, was used to

develop reaction kinetics gasification model. CSTR is the commonly used reactor in chemical industries to design chemical processes. CSTR is characterized as a perfectly mixed reactor in which all participating species are assumed to be uniformly distributed throughout the volume of reactor (Fogler, 1999). The CSTR is designed based on the kinetics and residence time of various reactions involved. In this study, seven major gasification reactions and their kinetics, plus residence time, were included in the reaction kinetics biomass gasification model to predict the syngas composition. The input parameters to the reaction kinetics gasification model included biomass properties, flowrates of biomass and air, gasification temperature and pressure, seven major gasification reactions and their kinetics (reaction rates and rate constants), and residence time (as shown in Fig. 5.4). The model outputs included gas composition and yield.

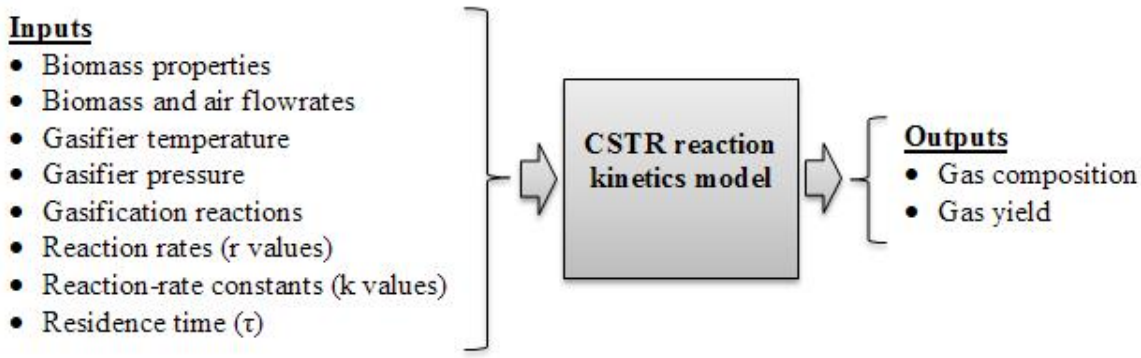

Fig. 5.4. Input and output parameters of CSTR reaction kinetic model

Based on the overall biomass decomposition reaction (Eq. 2) and devolatization reactions shown in Table 5.3, the biomass was decomposed into several possible products. The molar flowrate of each decomposed product were calculated using flowrates of biomass and air from experimental data. The decomposed products with their respective molar flow rates were specified as input feed streams to the CSTR gasification model. Table 5.4 shows the kinetics parameters, i.e. reaction rates and rate

constants, of seven major gasification reactions R(1) to R(7) used in the present study to develop reaction-kinetics gasification model. The inlet gas concentrations of the CSTR were calculated as ratio of molar flowrate of each decomposed product and the volume of the CSTR.

Table 5.4. Kinetic parameters of gasification reactions

Reaction No.	Rate equation[a], r	Reference
R(1)	$r_1 = \frac{2\,k_1\,C_{H2O}\,g(X)}{1 + k_2\,C_{H2O} + k_3\,C_{H2} + k_4\,C_{CO}}$ where, $k_1 = 239\,e^{\left(\frac{-129000}{RT}\right)}$ $k_2 = 0.0316\,e^{\left(\frac{-30100}{RT}\right)}$ $k_3 = 0.00536\,e^{\left(\frac{-59800}{RT}\right)}$ $k_4 = 8.25 * 10^{-5}\,e^{\left(\frac{-96100}{RT}\right)}$ $g(X) = (1 - X)\frac{\rho_{char}}{M_C}$ X = carbon conversion ρ_{char} = char density M_C = carbon molar weight	(Matsui et al., 1985; Petersen & Werther, 2005)
R(2)	$r_2 = \frac{2\,k_5\,C_{CO2}\,g(X)}{1 + k_6\,C_{CO2} + k_7\,C_{CO}}$ where, $k_5 = 4.89 * 10^7\,e^{\left(\frac{-268000}{RT}\right)}$ $k_6 = 0.066$ $k_7 = 0.12\,e^{\left(\frac{-25500}{RT}\right)}$	(Matsui et al., 1987a; Matsui et al., 1987b; Petersen & Werther, 2005)
R(3)	$r_3 = k_8\left(C_{H2O}C_{CO} - \frac{C_{H2}C_{CO2}}{K_{eq}}\right) f$ where, $k_8 = 2.778\,e^{\left(\frac{-12560}{RT}\right)}$ $K_{eq} = 0.022\,e^{\left(\frac{34730}{RT}\right)}$ $f = 0.1$	(Biba et al., 1978; Petersen & Werther, 2005)
R(4)	$r_4 = k_9\,C_{CH4}\,C_{O2}$ where, $k_9 = 5.16 * 10^{13}\,T^{-1}\,e^{\left(\frac{-130}{RT}\right)}$	(Gómez-Barea & Leckner, 2010)
R(5)	$r_5 = k_{10}\left(C_{CH4}C_{H2O} - \frac{C_{CO}C_{H2}^2}{0.0265\,\left(\frac{32900}{T}\right)}\right)$ where, $k_{10} = 3.1005\,e^{\left(\frac{-15000}{T}\right)}$	(Corella & Sanz, 2005; Umeki et al., 2010)
R(6)	$r_6 = k_{11}\,C_C$ where, $k_{11} = 17.67\,R\,T\,e^{\left(\frac{-13600}{T}\right)}$	(Goyal et al., 2010)
R(7)	$r_7 = k_{12}\,C_C\,C_{O2}$ where, $k_{12} = 8710\,e^{\left(\frac{-17967}{T}\right)}$	(Choi et al., 2001; Inayat et al., 2010).

[a] C_{CO}, C_{H2}, C_{H2O}, C_{CO2}, C_{CH4}, C_{O2} and C_C are CSTR inlet concentrations of CO, H_2, H_2O, CO_2, CH_4, O_2 and C, respectively.

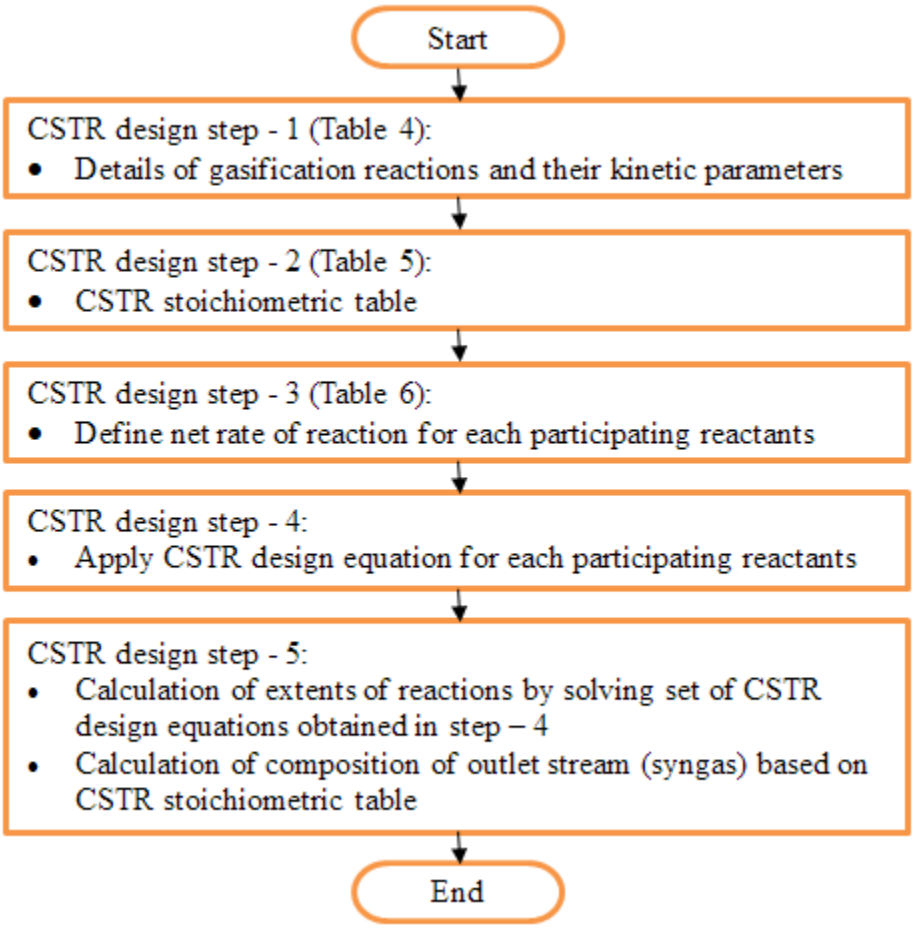

Fig. 5.5. Flow chart showing CSTR design steps

Fundamental design steps to develop CSTR biomass gasification model are illustrated in Fig. 5. In step 1 of the CSTR design, the seven major gasification reactions R(1) to R(7), their rate equations (r_1 to r_7, Table 4), reaction rate constants (k_1 to k_{12} and K_{eq}, Table 4), and extents of gasification reactions (ζ_1 to ζ_7) were specified in a tabulated form (as shown in Table 5). The extent of reaction (ζ) was the fractional conversion of reactant into the product for a given reaction..

In the step 2 of the CSTR design, mass balance of CSTR inlets (decomposed products) and outlets (final products) was performed. The details of CSTR mass balance were shown in the stoichiometric Table 6. The molar flowrates of CSTR inlets were

specified in column 2 using the notation F_0 before each material. For example, the initial molar flowrate of C entering into the CSTR was denoted using notation F_0C. As shown in Table 6, F_0T was the total initial molar flowrate of combined CSTR inlet stream. Based on gasification reactions details (step 1, Table 5), the change in each material within the CSTR was obtained in terms of extents of gasification reactions as shown in column 3, Table 6. The final composition of each CSTR outlet material was obtained by subtracting values in column 3 from respective values in column 2 (shown in column 5, Table 6). Column 4 shows the composition of final CSTR outlet product (syngas) wherein FT denotes the total molar flow of the final product.

In the step 3 of CSTR design, the net rate of reaction for each participating reactant was derived using the gasification reactions given in step 1 of Table 5. The net rates of reactions for all participating reactants are shown in column 2 of Table 7.

In the step 4 of CSTR design, the fundamental design equation of CSTR was solved for each of the seven participating reactants (Table 4) to obtain seven nonlinear equations in terms of extents of gasification reactions. The CSTR design equation for reactant C is given as follows.

$$F_0C \text{ (entering)} - FC \text{ (leaving)} + r_C V_R \text{ (generation)} = 0 \text{ (accumulation)} \qquad \text{Eq.(3)}$$

where, V_R was the volume of CSTR that was calculated using ideal gas law as follows.

$$(P V_R / P_0 V_0) = (FT R T / F_0T R T_0) \qquad \text{Eq.(4)}$$

where, P_0, V_0, F_0T and T_0 were the initial values of pressure, volume, molar flow rate and temperature, respectively, of reactants while P, V_R, FT and T were the final values of pressure, volume, molar flow rate and temperature, respectively, of products. R is the ideal gas constant. Since the gasification temperature and pressure were assumed to

Table 5.5. Step 1 - Gasification reactions details

Reaction No.	Gasification reactions			Reaction rate	Rate constant	Extent of reaction
R(1)	$C + H_2O$	$\leftrightarrow$	$CO + H_2$	r_1	k_1, k_2, k_3, k_4	ζ_1
R(2)	$C + CO_2$	$\leftrightarrow$	$2CO$	r_2	k_5, k_6, k_7	ζ_2
R(3)	$CO + H_2O$	$\leftrightarrow$	$CO_2 + H_2$	r_3	k_8, K_{eq}	ζ_3
R(4)	$CH_4 + 3/2O_2$	$\rightarrow$	$CO + 2H_2O$	r_4	k_9	ζ_4
R(5)	$CH_4 + H_2O$	$\leftrightarrow$	$CO + 3H_2$	r_5	k_{10}	ζ_5
R(6)	$C + O_2$	$=$	CO_2	r_6	k_{11}	ζ_6
R(7)	$C + 1/2O_2$	$=$	CO	r_7	k_{12}	ζ_7

Table 5.6. Step 2 - CSTR stoichiometry table

Material	Material entering CSTR[a] (mol/s)	Material change	Material leaving CSTR (mol/s)
C	F_0C	$-\zeta_1 - \zeta_2 - \zeta_6 - \zeta_7$	$FC = F_0C - \zeta_1 - \zeta_2 - \zeta_6 - \zeta_7$
H_2O	F_0H_2O	$-\zeta_1 - \zeta_3 + 2\zeta_4 - \zeta_5$	$FH_2O = F_0H_2O - \zeta_1 - \zeta_3 + 2\zeta_4 - \zeta_5$
O_2	F_0O_2	$-1.5\zeta_4 - \zeta_6 - 1/2\zeta_7$	$FO_2 = F_0O_2 - 2\zeta_4 - \zeta_6 - 1/2\zeta_7$
CO	F_0CO	$\zeta_1 + 2\zeta_2 - \zeta_3 + \zeta_4 + \zeta_5 + \zeta_7$	$FCO = F0CO + \zeta1 + 2\zeta2 - \zeta3 + \zeta4 + \zeta5 + \zeta7$
H_2	F_0H_2	$\zeta_1 + \zeta_3 + 3\zeta_5$	$FH_2 = F_0H_2 + \zeta_1 + \zeta_3 + 3\zeta_5$
CH_4	F_0CH_4	$-\zeta_4 - \zeta_5$	$FCH_4 = F_0CH_4 - \zeta_4 - \zeta_5$
CO_2	F_0CO_2	$-\zeta_2 + \zeta_3 + \zeta_6$	$FCO_2 = F_0CO_2 - \zeta_2 + \zeta_3 + \zeta_6$
Inert, N_2	F_0N_2	0	$FN2 = F0N2$
Total	$F_0T = F_0C+F_0H_2O+F_0O_2+F_0CO+F_0H_2+F_0CH_4+F_0CO_2+F_0N_2$		$FT = F_0T + 0.5\zeta_4 + 2\zeta_5 - \zeta_6 - 1/2\zeta_7$

[a] F_0C, F_0H_2O, F_0O_2, F_0CO, F_0H_2, F_0CH_4, F_0CO_2 and F_0N_2 were the initial molar flowrates of C, H_2O, O_2, CO, H_2, CH_4, CO_2 and N_2, respectively, entering into the CSTR.

Table 5.7. Step 3 - Net rate of reaction for participating reactants during gasification

Material	Net rate of reaction[a]
C	$r_{C} = - r_1 - r_2 - r_6 - r_7$
H_2O	$r_{H2O} = - r_1 - r_3 + 2r_4 - r_5$
O_2	$r_{O2} = - 1.5r_4 - r_6 - 1/2r_7$
CO	$r_{CO} = r_1 + 2r_2 - r_3 + r_4 + r_5 + r_7$
H_2	$r_{H2} = r_1 + r_3 + 3r_5$
CH_4	$r_{CH4} = - r_4 - r_5$
CO_2	$r_{CO2} = - r_2 + r_3 + r_6$

[a] r_C, r_{H2O}, r_{O2}, r_{CO}, r_{H2}, r_{CH4} and r_{CO2} are the net rate of reactions for C, H_2O, O_2, CO, H_2, CH_4 and CO_2, respectively.

be constant, i.e. $T = T_0$ and $P = P_0$, the equation (4) was further simplified by substituting values of F_0T and FT from stoichiometry Table 6 in the equation (4) as follows

$$V_R = (F_0T + 0.5\zeta_4 + 2\zeta_5 - \zeta_6 - 1/2\zeta_7)\ V_0 / F_0T \qquad \text{Eq.(5)}$$

Next, by substituting values of FC (Table 6) in the equation (5), the CSTR design equation for the reactant C was reduced to following equation (6).

$$(\zeta_1 + \zeta_2 + \zeta_6 + \zeta_7) + r_C\ V_R = 0 \qquad \text{Eq.(6)}$$

Since the volume of the gasifier reactor is constant, by dividing the equation (6) with the volume flowrate (v_0), the CSTR design equation (6) for reactant C was further simplified and expressed in terms of residence time (τ) as follows.

$$(\zeta_1 + \zeta_2 + \zeta_6 + \zeta_7) / v_0 + r_C\ \tau = 0 \qquad \text{Eq.(7)}$$

where, τ was defined as the ratio of V_R to volume flowrate (v_0) of materials through the CSTR. As explained earlier, the τ was calculated as the ratio of the gasifier volume (V_R) and syngas flowrate (v_0) and was used in the present study [17].

Similarly, based on the equations (3) to (7), the CSTR design equation for reactants H_2O, O_2, CO, H_2, CH_4 and CO_2 were deduced as follows.

$$(\zeta_1 + \zeta_3 - 2\zeta_4 + \zeta_5) / v_0 + r_{H2O}\,\tau = 0 \quad \text{Eq.(8)}$$

$$(1.5\zeta_4 + \zeta_6 + 1/2\zeta_7) / v_0 + r_{O2}\,\tau = 0 \quad \text{Eq.(9)}$$

$$(-\zeta_1 - 2\zeta_2 + \zeta_3 - \zeta_4 - \zeta_5 - \zeta_7) / v_0 + r_{CO}\,\tau = 0 \quad \text{Eq.(10)}$$

$$(-\zeta_1 - \zeta_3 - 3\zeta_5) / v_0 + r_{H2}\,\tau = 0 \quad \text{Eq.(11)}$$

$$(\zeta_4 + \zeta_5) / v_0 + r_{CH4}\,\tau = 0 \quad \text{Eq.(12)}$$

$$(\zeta_2 - \zeta_3 - \zeta_6) / v_0 + r_{CO2}\,\tau = 0 \quad \text{Eq.(13)}$$

The seven nonlinear equations (7) to (13) were solved using polymath software to determine extents of reactions ζ_1 to ζ_7. Using the formulas of *FC*, FH_2O, FO_2, *FCO*, FH_2, FCH_4, and FCO_2 (column 4, Table 6), the extents of reactions were used to calculate composition of final products leaving the CSTR.

In addition to assumptions 3 to 6 made in the Gibbs equilibrium gasification model, following assumptions were used to develop CSTR reaction kinetic gasification model.

- CSTR was assumed to be a perfectly mixed reactor [18]; hence the fluidized-bed gasifier was assumed to be a well-mixed reactor.
- Based on the seven possible participating reactants (C, H_2O, O_2, CO, H_2, CH_4 and CO_2) and kinetics of seven major gasification reactions, only seven nonlinear equations were possible; hence concentrations of syngas impurities (NH_3 and H_2S) and lighter hydrocarbons (C_2H_2, C_2H_4 and C_2H_6) were assumed to be negligible.

5.4 Results and Discussion

5.4.1 Extent of gasification reactions

Several reactions occur simultaneously during biomass gasification process; hence, for the given gasification conditions, dominating reactions can be determined using the approach of extent of reaction for seven major gasification reactions R(1) to R(7). The extent of reaction can easily identify the relative importance of the seven major gasification reactions involved during gasification process. High extent of a specific reaction represents high conversion of reacting species into product through the reaction.

Reactions R(1), R(2), R(4), R(5) and R(7) were the five gasification reactions having relative influence on the syngas CO yield. The reaction R(3) can contribute to the syngas CO yield if this equilibrium reaction proceeds in the reverse direction. Among these five reactions, char partial combustion reaction R(7) was the most dominating at ERs of 0.20 and 0.32 as indicated by the highest extent of reaction of 0.011 and 0.006 at ERs of 0.20 and 0.32, respectively (Table 5.8). The extent of 0.011 at ER of 0.20 indicated that only 0.011 mol/s of input carbon supplied into the gasifier reacted through reaction R(7) to form CO. At ER of 0.29, the water gas reaction R(1) was the most dominating reaction contributing to the syngas CO yield indicated by the highest extent of reaction (0.014). At ER of 0.40, both the Boudouard R(2) and methane oxidation R(4) reactions were the most dominating reactions contributing to the syngas CO yield indicated by the highest extents of reaction (0.004). At ER of 0.45, the extent of Boudouard reaction R(2) was the maximum (0.022) indicating higher conversion of available carbon into syngas CO.

Table 5.8. Extent of gasification reactions at different ERs

Reaction No.	Extent of reaction	ER				
		0.20	0.29	0.32	0.40	0.45
R(1)	ζ_1	0.007	0.014	-0.004	-0.003	-0.025
R(2)	ζ_2	-0.009	-0.011	0.002	0.004	0.022
R(3)	ζ_3	-0.003	-0.002	0.006	0.005	0.016
R(4)	ζ_4	0.002	0.007	0.004	0.004	0.003
R(5)	ζ_5	-0.002	-0.004	-0.001	-0.001	0.003
R(6)	ζ_6	0.001	0.001	0.004	0.006	0.016
R(7)	ζ_7	0.011	0.006	0.006	0.002	-0.002

Reactions R(1), R(3) and R(5) were the three gasification reactions having considerable influence on the syngas H_2 yield. Among these three reactions, water gas reaction R(1) was the most dominating at ERs of 0.20 and 0.29 as indicated by the highest extent of reaction of 0.007 and 0.014 at ERs of 0.20 and 0.29, respectively (Table 5.8). At ERs of 0.29 and above, the water gas shift reaction R(3) was the most dominating reaction contributing to the syngas H_2 yield as indicated by the highest extent of reaction, shown in Table 5.8.

Reactions R(3) and R(6) were the two gasification reactions having considerable influence on the syngas CO_2 yield. Result showed that the char combustion reaction R(6) was highly sensitive to the ER as indicated by the continuous increase in its extent of reaction from 0.001 to 0.016 (Table 5.8) with an increase in the ER from 0.20 to 0.45. This resulted in a continuous increase in the syngas CO_2 yield with ER.

Reactions R(4) and R(5) were the two gasification reactions having considerable influence on the syngas CH_4 yield. Among these two reaction, methane oxidation reaction R(4) was the most dominating reaction as indicated by its higher extent of

reactions at all ERs. This resulted in a continuous conversion of CH_4 into CO and H_2O through reaction R(4) with an increase in the ER from 0.20 to 0.45. At all ERs below 0.45, extents of methane steam reforming reaction R(5) were negative, which indicated that the equilibrium reaction R(5) occurred in the reverse direction resulting in formation of CH_4. At ER of 0.45, the reaction R(5) occurred in the forward direction leading to conversion of CH_4 into CO and H_2 as indicated by the positive extent of reaction of 0.003 (Table 5.8). Overall, the extents of reactions approach revealed insight regarding the dominating reactions for increasing CO and H_2 yields in biomass generated syngas. Biomass-generated syngas typically has low H_2/CO ratio, which is a technical challenge in its conversion to hydrocarbon fuels. The modeling approach presented here can be used to maximize the H_2/CO ration in the syngas.

5.4.2 Syngas composition

Composition of biomass generated syngas at different ERs was predicted using the two different models: Gibbs equilibrium biomass gasification model and reaction kinetics biomass gasification model. The predictions of biomass gasification models under present study are compared with experimental data and discussed below in terms of four major syngas constituents i.e. CO, H_2, CO_2 and CH_4.

5.4.2.1 Carbon monoxide

Experimental and predicted syngas CO yields (kg/kg dry biomass) with variation in ER from 0.20 to 0.45 are shown in Table 5.9. At low ER of 0.20, compared to the corresponding experimental result, the Gibbs equilibrium gasification model over-predicted (309% high) syngas CO yield while the reaction kinetics gasification model showed result comparable to the experimental data (53% high) of CO yield. At ER of

0.29, compared to the corresponding experimental result, the Gibbs equilibrium gasification model again over-predicted CO yield (138% high) while, the reaction kinetics gasification model showed a good agreement with the experimental data (1%) of the CO yield. At ER of 0.32, compared to the experimental result, the reaction kinetics gasification model closely predicted syngas CO yield within 15% deviation while a large deviation (80%) was observed in the corresponding predicted result obtained using the Gibbs equilibrium gasification model. At ER of 0.40, compared to the experimental result, the reaction kinetics gasification model comparatively showed a better agreement in the predicted syngas CO yield (within 3%) than the corresponding result (within 78%) obtained using the Gibbs equilibrium gasification model. At ER of 0.45, compared to the experimental result, the reaction kinetics gasification model closely predicted the syngas CO yield within 12% compared to the corresponding predicted result (57% deviation) obtained from the Gibbs equilibrium gasification model. Overall, compared to the experimental results, the reaction kinetics gasification model showed a considerable improvement in the predicted syngas CO yields while the Gibbs equilibrium gasification model showed higher deviations (57 to 309%) in the corresponding predicted results.

The large deviations in the predicted syngas CO yields using the Gibbs equilibrium gasification model were due to the assumption that the gasification reactions reached equilibrium conditions, which does not occur in application due to short residence time. Further, the fluidized-bed gasifier involved fluidization hydrodynamics, which are influenced by the size, shape, and composition of participating materials in the gasifier bed (Sharma et al., 2013). The fluidization hydrodynamics have considerable effect on turbulence level and mixing characteristics of the participating materials which

further influence the overall heat and mass transfers, and thus, kinetics of gasification reactions within the fluidized-bed gasifier. In the present gasification models, the fluidization hydrodynamics were assumed to be negligible. As a result, the reaction kinetics gasification model also showed deviations within 53% in the predicted syngas CO yields compared to the corresponding results obtained thorough experiment.

Table 5.9. Experimental and predicted yields of syngas constituents at various ERs

Syngas constituents	Yield (kg/kg dry biomass)		
	Experimental yield (Sharma et al., 2011)	Gibbs equilibrium model	Reaction kinetics model
	ER = 0.20		
CO	0.203	0.829	0.310
H_2	0.007	0.053	0.014
CO_2	0.301	0.229	0.639
CH_4	0.019	0.001	0.145
	ER = 0.29		
CO	0.312	0.741	0.316
H_2	0.013	0.047	0.018
CO_2	0.402	0.370	0.687
CH_4	0.021	0.000	0.093
	ER = 0.32		
CO	0.384	0.689	0.325
H_2	0.016	0.043	0.018
CO_2	0.448	0.452	0.724
CH_4	0.030	0.000	0.074
	ER = 0.40		
CO	0.368	0.653	0.358
H_2	0.013	0.038	0.017
CO_2	0.499	0.508	0.771
CH_4	0.026	0.000	0.073
	ER = 0.45		
CO	0.359	0.563	0.402
H_2	0.005	0.032	0.021
CO_2	0.768	0.650	0.838
CH_4	0.035	0.000	0.036

5.4.2.2 Hydrogen

Experimental and predicted syngas H_2 yields (kg/kg dry biomass) with variation in ER from 0.20 to 0.45 are shown in Table 5.9. At low ER of 0.20, compared to the experimental result, the Gibbs equilibrium gasification model predicted 648% higher syngas H_2 yield while the reaction kinetics gasification model showed improved prediction of the corresponding result within 93% deviation. At ER of 0.29, the Gibbs equilibrium gasification model showed large deviation (267%) in the predicted syngas H_2 yield whereas the reaction kinetics gasification model predicted comparatively better corresponding result (within 36%). At ER of 0.32, compared to experimental results, the Gibbs equilibrium gasification model showed a large deviation (180%) in the predicted syngas H_2 yield whereas the reaction kinetics gasification model comparatively predicted better syngas H_2 yield (within 17%). At ER of 0.40, compared to experimental result, the Gibbs equilibrium gasification model predicted 194% higher syngas H_2 yield while the reaction kinetics gasification model comparatively predicted better syngas H_2 content within 29%. At ER of 0.45, the Gibbs equilibrium and reaction kinetics gasification models respectively predicted seven and four folds higher syngas H_2 yield than the corresponding experimental result. As explained earlier, due to equilibrium assumption and negligible effect of fluidization hydrodynamics, the Gibbs equilibrium gasification model showed large deviations in the predicted syngas H_2 yields at all ER conditions. The reaction kinetics gasification model predicted comparatively better syngas H_2 yields at ERs of 0.29, 0.32 and 0.40. As described earlier, the fluidization hydrodynamics were not included in the reaction kinetics gasification model, which may have resulted in higher syngas H_2 yields at the minimum and maximum ERs of 0.20 and 0.45, respectively.

5.4.2.3 Carbon dioxide

Experimental and predicted syngas CO_2 yields (kg/kg dry biomass) with variation in ER from 0.20 to 0.45 are shown in Table 5.9. Compared to experimental results, the Gibbs equilibrium gasification model predicted syngas CO_2 yields within 24% at all ER conditions. With an increase in the ER, the predicted syngas CO_2 yield continuously increased. Such increasing trend in the syngas CO_2 yields with ER can be explained using the Le Chatelier's principle (Jenkins, 2008), which states that when the equilibrium state of a given reacting system is disturbed by introducing a change in the system, such as varying the quantity of limiting reactant (i.e. oxidizing agent in the present study), the system oppose this change. Hence, system tries to restore its equilibrium state by favoring conversion of added reactant into possible products. The quantity of oxidizing agent (limiting reactant) used in the present gasification models were in the increasing order with minimum at ER of 0.20 and maximum at ER of 0.45. This increase in the quantity of oxidizing agent accelerated the oxidation of available carbon to form more stable product, such as CO_2, at the equilibrium state. As a result, the Gibbs equilibrium gasification model showed increasing trend in the predicted syngas CO_2 yield with an increase in ER from 0.20 to 0.45. Such increasing trend in the predicted CO_2 yield was also evident from the decreasing trend in the predicted syngas CO yield (Table 5.9), which indicated higher oxidation of available of CO into CO_2.

Compared to the experimental result, the reaction kinetics gasification model closely predicted the syngas CO_2 yield (within 9%) at the maximum ER of 0.45. At ERs below 0.45, the model predicted higher (54 to 112%) syngas CO_2 yields. As stated earlier, the actual gasification temperatures based on the experimental results were used

in the gasification model to perform simulation runs. With an increase in the ER from 0.20 to 0.45, the temperature condition used in the gasification model also increased from 801 to 907°C. This increase in the gasification temperature resulted in higher oxidation of carbonaceous species into CO_2 through char reaction R(6). As a result, the syngas CO_2 yield continuously increased with an increase in the ER from 0.20 to 0.45, shown in Table 5.9.

5.4.2.4 Methane

Experimental and predicted syngas CH_4 yields (kg/kg dry biomass) with variation in ER from 0.20 to 0.45 are shown in Table 5.9. Compared to experimental results, the Gibbs equilibrium gasification model predicted negligible syngas CH_4 yields at all ER conditions. This was due to the assumption of equilibrium at which CH_4 thermodynamically becomes less stable under higher gasification temperatures, i.e. 801 to 907°C used in the present study, and oxidizing agent, resulting in the conversion to more stable products, such as CO, H_2, CO_2 and H_2O (Nikoo & Mahinpey, 2008). The reaction kinetics gasification model showed good agreement with experimental result with CH_4 yield (within 1% deviation) at the maximum ER of 0.45. At ERs below 0.45, the model over-predicted CH_4 yields (between 148 and 645%). Such large deviation in the predicted CH_4 yield was because of two reasons. First, results showed that the selected kinetics parameters had least influence on the reactions involving CH_4 as the reacting species (Table 5.4); hence, this resulted in low CH_4 conversion. Second, initial molar flowrate of CH_4 supplied into the gasification model was high (24 to 35 mol/h) that could have resulted in unconverted CH_4 in the outlet let material stream. Hence, a considerable portion of the CH_4 in the inlet stream supplied into the model remained

unconverted, resulting in a high CH_4 yield. Despite of higher predictions of the syngas CH_4 yields, the deviation in the predicted syngas CH_4 yield continuously decreased from maximum of 645% at ER of 0.20 to minimum of 1% at ER of 0.45. This indicated that the CH_4 conversion into possible products through reactions R(4) and R(5) continuously increased with an increase oxidizing atmosphere (from 0.20 to 0.45 ER). The considerable increase in the CH_4 conversion was primarily due to the increased gasification temperature and oxidizing atmosphere at high ERs. Since the rate of a given reaction increases with an increase in the reaction temperature, the increase in the gasification temperature from 801 to 907°C showed increased conversion of CH_4. Also, the increase in the quantity of oxidizing agent (4.5 to 10 kg/h) with increase in ER could have accelerated the CH_4 oxidation, and thus, CH_4 conversion increased with an increase in the ER from 0.20 to 0.45.

5.4.3 Syngas yield

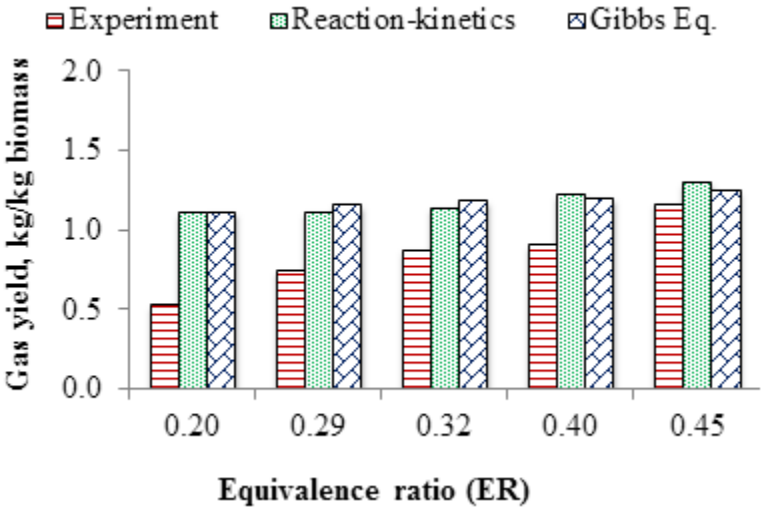

Fig. 5.6. Experimental and predicted syngas yields with varying ER

The comparison between experimental and predicted syngas yields with ER varying from 0.20 to 0.45 is shown in Fig. 5.6. With an increase in the ER, both of the

present gasification models predicted similar syngas yields. As described earlier that the Gibbs equilibrium gasification model predicted considerably higher syngas CO (Table 5.9) and H_2 (Table 5.9) yields at all ER conditions. As results, the Gibbs equilibrium gasification model over-predicted syngas yields compared to the experimental results at all ERs. The deviation in the predicted syngas yield continuously decreased from a maximum of 109% at ER of 0.20 to a minimum of 7% at ER of 0.45. The reaction kinetics gasification model also over-predicted syngas yields compared to experimental results at all ER conditions. The deviation in the predicted syngas yield continuously decreased from maximum of 109% at ER of 0.20 to minimum of 11% at ER of 0.45. As described earlier, the reaction kinetics gasification model predicted CH_4 yields (Table 5.9) higher than the corresponding experimental results at all ER conditions; this contributed to the over prediction of the syngas yield. The gasification models showed increasing trend in the syngas yield with an increase in the ER, which was in agreement with the experimental trend of the syngas yield.

5.4.4 Energy efficiency

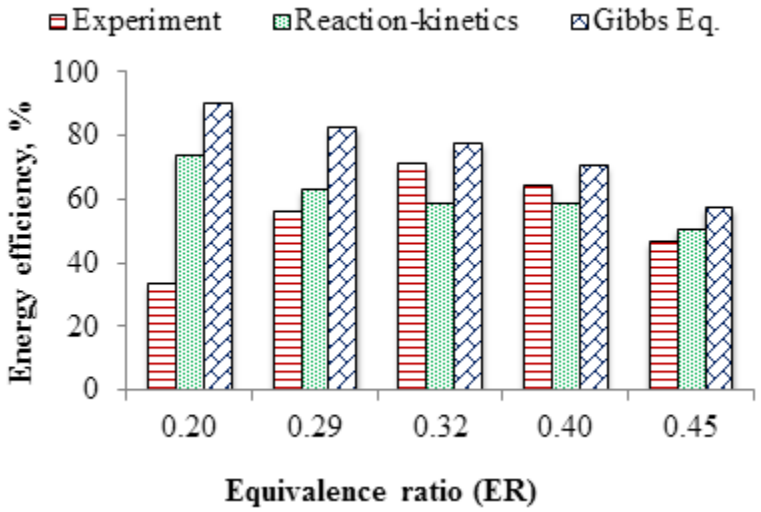

Fig. 5.7. Experimental and predicted energy efficiencies with varying ER

Variation in experimental and predicted gasification energy (cold gas) efficiencies with an increase in ER from 0.20 to 0.45 is shown in Fig. 5.7. Using Gibbs equilibrium gasification model, the predicted gasification energy efficiency continuously decreased with an increase in ER from 0.20 to 0.45. The deviation between the predicted and the experimental gasification energy efficiency also continuously decreased from 171% at ER of 0.20 to 23% at ER of 0.45. As discussed earlier, the Gibbs equilibrium gasification model over-predicted CO (Table 5.9) and H_2 (Table 5.9) yields at all ER conditions. As results, the model also over-predicted gasification energy efficiency. However, the reaction kinetics gasification model closely predicted the gasification energy efficiency within 18% deviation at ERs above 0.20. However, at low ER of 0.20, the model showed large deviation (122%) in the predicted gasification energy efficiency as compared to corresponding experimental result. As explained earlier, at low ER of 0.20, the reaction kinetics gasification model predicted the maximum CH_4 yield (Table 5.9) and the energy content of CH_4 is more than three times higher than that of CO and H_2 gases. Therefore, the reaction kinetics gasification model showed a large deviation in the predicted gasification energy efficiency at low ER of 0.20.

5.5 Conclusions

Gasification models were developed to predict composition and yield of biomass generated syngas using two different modeling approaches: Gibbs equilibrium gasification model and reaction kinetics gasification model using CSTR. The predictions from both gasification models were compared and validated using experimental results on lab-scale fluidized-bed gasifier. The Gibbs equilibrium gasification model showed large deviations in the predicted syngas composition (CO, H_2, CO_2 and CH_4) and yield,

and gasification energy efficiency compared to the corresponding experimental results. These deviations were primarily due to assumption of equilibrium used in the Gibbs equilibrium gasification model. The reaction kinetics gasification model showed much better prediction of syngas composition (CO, H_2, CO_2 and CH_4) and yield, and gasification energy efficiency as compared to the predictions from Gibbs equilibrium gasification model. The selected kinetics of seven major gasification reactions showed considerable influence on the predictions of reaction kinetics gasification model. The extents of gasification reactions indicated that at ER below 0.29, water gas reaction R(1) contributed the most to syngas CO and H_2 yields. The char partial combustion reaction R(7) was also the dominating reaction contributing to CO yield at ERs below 0.29. At ER of 0.29 and above, the Boudouard R(2) and methane oxidation R(4) reactions were the most dominating reactions contributing to CO yield while the water gas shift reaction R(3) was the most dominating reaction contributing to H_2 yield. Small deviations in the predicted syngas composition and yield compared to the experimental results can be attributed to the fluidization hydrodynamics that was not considered in this reaction kinetics gasification model.

Nomenclature

Latin letters

C_C, C_{CH4}, C_{CO}, C_{CO2},	
C_{H2}, C_{H2O}, C_{O2}	Concentrations of C, CH_4, CO, CO_2, H_2, H_2O, O_2, respectively, in the inlet material stream, mol/m^3
f	Dampering factor
F_0C, F_0CH_4, F_0CO,	

F_0CO_2, F_0H_2, F_0H_2O,	
F_0N_2, F_0O_2	Initial molar flowrates of C, CH_4, CO, CO_2, H_2, H_2O, N_2 and O_2, respectively, entering into the CSTR, mol/s
F_0T	Total initial molar flowrate of materials entering into the CSTR, mol/s
FC, FCH_4, FCO,	
FCO_2, FH_2, FH_2O,	
FN_2, FO_2	Final molar flowrates of C, CH_4, CO, CO_2, H_2, H_2O, N_2 and O_2, respectively, leaving the CSTR, mol/s
FT	Total final molar flowrate of materials leaving the CSTR, mol/s
k_1, k_2, k_3, k_4	Rate constants for reaction R(1)
k_5, k_6, k_7	Rate constants for reaction R(2)
k_8, k_9, k_{10}, k_{11}, k_{12}	Rate constants for reactions R(3) to R(7), respectively
K_{eq}	Equilibrium constant of R(3)
M_C	Carbon molar weight, g/mol
R	The ideal gas constant, J/(mol K)
$r_1, r_2, r_3, r_4, r_5, r_6, r_7$	Rate equations for reactions R(1) to R(7), respectively, mol/(m^3s)
r_C, r_{CH4}, r_{CO}, r_{CO2},	
r_{H2}, r_{H2O}, r_{O2}	Net reaction rates for C, CH_4, CO, CO_2, H_2, H_2O, O_2, respectively, mol/(m^3s)
T	Absolute temperature, K
Po, P	Initial and final pressures in the reactor, Pa
Vo, V_R	Initial and final volumes of the reactor, m^3

v_0	Volume flowrate of materials through the CSTR, m^3
X	Carbon conversion
Greek letters	
$\zeta_1, \zeta_2, \zeta_3, \zeta_4, \zeta_5, \zeta_6, \zeta_7$	Extents of reactions R(1) to R(7), respectively, mol/s
ρ_{char}	Char density, kg/m^3
τ	Residence time, s

Acknowledgements

This work was supported in part by the National Science Foundation under Grant No. EPS-0814361 and the Oklahoma Agricultural Experiment Station.

5.6 References

Abelson, P.H. 1976. Energy from biomass. *Science*, **191**(4233), 1221.

Biba, V., Macak, J., Klose, E., Malecha, J. 1978. Mathematical Model for the Gasification of Coal under Pressure. *Industrial & Engineering Chemistry Process Design and Development*, **17**(1), 92-98.

Choi, Y.C., Li, X.Y., Park, T.J., Kim, J.H., Lee, J.G. 2001. Numerical study on the coal gasification characteristics in an entrained flow coal gasifier. *Fuel*, **80**(15), 2193-2201.

Corella, J., Sanz, A. 2005. Modeling circulating fluidized bed biomass gasifiers. A pseudo-rigorous model for stationary state. *Fuel Processing Technology*, **86**(9), 1021-1053.

Fogler, H.S. 1999. *Elements of chemical reaction engineering*. Prentice-Hall International London.

Gómez-Barea, A., Leckner, B. 2010. Modeling of biomass gasification in fluidized bed. *Progress in Energy and Combustion Science*, **36**(4), 444-509.

Goyal, A., Pushpavanam, S., Voolapalli, R.K. 2010. Modeling and simulation of co-gasification of coal and petcoke in a bubbling fluidized bed coal gasifier. *Fuel Processing Technology*, **91**(10), 1296-1307.

Hamelinck, C.N., Faaij, A.P.C. 2002. Future prospects for production of methanol and hydrogen from biomass. *Journal of Power Sources*, **111**(1), 1-22.

Inayat, A., Ahmad, M.M., Yusup, S., Mutalib, M.I.A. 2010. Biomass steam gasification with in-situ CO2 capture for enriched hydrogen gas production: A reaction kinetics modelling approach. *Energies*, **3**(8), 1472-1484.

Jenkins, B.M., Bhatnagar, A.P. 1991. On the Electric-Power Potential from Paddy Straw in the Punjab and the Optimal Size of the Power-Generation Station. *Bioresource Technology*, **37**(1), 35-41.

Jenkins, H.D.B. 2008. Le Chatelier's Principle. in: *Chemical Thermodynamics at a Glance*, Blackwell Publishing Ltd, pp. 160-163.

Jess, A., Popp, R., Hedden, K. 1999. Fischer-Tropsch-synthesis with nitrogen-rich syngas - Fundamentals and reactor design aspects. *Applied Catalysis a-General*, **186**(1-2), 321-342.

Klasson, K.T., Ackerson, M.D., Clausen, E.C., Gaddy, J.L. 1993. Biological conversion of coal and coal-derived synthesis gas. *Fuel*, **72**(12), 1673-1678.

Kumar, A., Jones, D.D., Hanna, M.A. 2009a. Thermochemical biomass gasification: A review of the current status of the technology. *Energies*, **2**(3), 556-581.

Kumar, A., Noureddini, H., Demirel, Y., Jones, D., Hanna, M. 2009b. Simulation of corn stover and distillers grains gasification with Aspen Plus. *Transactions of the ASAE*, **52**(6), 1989-1995.

Matsui, I., Kojima, T., Kunii, D., Furusawa, T. 1987a. Study of char gasification by carbon dioxide. 2. Continuous gasification in fluidized bed. *Industrial & Engineering Chemistry Research*, **26**(1), 95-100.

Matsui, I., Kunii, D., Furusawa, T. 1987b. Study of char gasification by carbon dioxide. 1. Kinetic study by thermogravimetric analysis. *Industrial & Engineering Chemistry Research*, **26**(1), 91-95.

Matsui, I., Kunii, D., Furusawa, T. 1985. Study of fluidized bed steam gasification of char by thermogravimetrically obtained kinetics. *Journal of Chemical Engineering of Japan*, **18**(2), 105-113.

Nikoo, M.B., Mahinpey, N. 2008. Simulation of biomass gasification in fluidized bed reactor using ASPEN PLUS. *Biomass and Bioenergy*, **32**(12), 1245-1254.

Pasangulapati, V., Kumar, A., Jones, C.L., Huhnke, R.L. 2012. Characterization of Switchgrass, Cellulose, Hemicellulose and Lignin for Thermochemical Conversions. *Journal of Biobased Materials and Bioenergy*, **6**(3), 249-258.

Patel, S.R., Bhoi, P.R., Sharma, A.M. 2006. Field-testing of SPRERI's open core gasifier for thermal application. *Biomass and Bioenergy*, **30**(6), 580-583.

Paviet, F., Chazarenc, F., Tazerout, M. 2009. Thermo chemical equilibrium modelling of a biomass gasifying process using ASPEN PLUS. *International Journal of Chemical Reactor Engineering*, **7**(7), 40.

Petersen, I., Werther, J. 2005. Experimental investigation and modeling of gasification of sewage sludge in the circulating fluidized bed. *Chemical Engineering and Processing: Process Intensification*, **44**(7), 717-736.

Puig-Arnavat, M., Bruno, J.C., Coronas, A. 2010. Review and analysis of biomass gasification models. *Renewable and Sustainable Energy Reviews*, **14**(9), 2841-2851.

Quaak, P., Knoef, H., Stassen, H.E. 1999. *Energy from biomass: a review of combustion and gasification technologies*. World Bank Publications.

Sharma, A.M., Kumar, A., Patil, K.N., Huhnke, R.L. 2013. Fluidization characteristics of a mixture of gasifier solid residues, switchgrass and inert material. *Powder Technology*, **235**, 661-668.

Sharma, A.M., Kumar, A., Patil, K.N., Huhnke, R.L. 2011. Performance evaluation of a lab-scale fluidized bed gasifier using switchgrass as feedstock. *Transactions of the ASABE*, **56**(6), 2259-66.

Spath, P.L., Dayton, D.C. 2003. Preliminary screening - technical and economic assessment of synthesis gas to fuels and chemicals with emphasis on the potential for biomass-derived syngas. NREL.

Umeki, K., Yamamoto, K., Namioka, T., Yoshikawa, K. 2010. High temperature steam-only gasification of woody biomass. *Applied Energy*, **87**(3), 791-798.

Wender, I. 1996. Reactions of synthesis gas. *Fuel Processing Technology*, **48**(3), 189-297.

Wenyi, T., Qin, Z. 2010. Simulation of Hydrogen Production in Biomass Gasifier by ASPEN PLUS. *Power and Energy Engineering Conference (APPEEC), 2010 Asia-Pacific*, 28-31 March 2010. pp. 1-4.

CHAPTER VI

NUMERICAL MODELING OF BIOMASS FLUIDIZED-BED GASIFICATION: INCORPORATING FLUIDIZATION CHARACTERISTICS AND REACTION KINETICS

This research paper is intended to be published as "Sharma, A.M., Kumar, A., Huhnke, R.L. Numerical modeling of biomass fluidized-bed gasification: Incorporating fluidization characteristics and reaction kinetics."

Abstract

A fluidized-bed gasification involves fluidization of bed-material and a series of gasification reactions which together influence the syngas yield and quality. Extensive gasification modeling studies using equilibrium and kinetics approaches have been reported to predict composition and yield of biomass generated syngas. However, the equilibrium and kinetics gasification models studied by several researchers did not consider the fluidization characteristics which are influenced by shape and size of materials present in the gasifier bed, and non-ideal behavior of gasifier. This study aimed to develop and validate a numerical gasification model based on reaction kinetics and fluidization using computational fluid dynamics (CFD) technique to predict syngas composition. Fluidization characteristics (effective particle size and effective density of bed materials) and kinetics of major gasification reactions were incorporated in the studied gasification model. Numerical simulations were performed using switchgrass as biomass feedstock and silica-sand as inert bed material. Biomass and air flowrates ranged from 3.4 to 3.9 kg/h and 4.5 to 6.5 kg/h, respectively. Properties of biomass and silica-sand were obtained from a previous experimental study using a fluidized-bed gasifier. The sensitivity analysis showed that with the change in equivalence ratio the model was able to predict syngas CO, H_2 and CO_2 contents within 32%, 47% and 42% errors, respectively. Compared to CO (3.6%) and H_2 (2.4%) contents observed without sand bed, the presence of sand in the bed showed higher syngas CO (11.2%) and H_2 (6.6%). The model also predicted the locations of drying, combustion and reduction zones of the gasifier, as well as revealed dominating reactions occurring in the fluidized-bed gasifier. Simulation results showed that the char combustion and char partial-oxidation reactions

were dominant in the combustion zone of the gasifier. The Boudouard and water-gas reactions contributed the most for CO production in the freeboard zone of the gasifier. Simulation results showed that the water-gas-shift reaction led to the decrease in CO content in the disengagement zone. The methane-steam-reforming reaction contributed the most for H_2 production in the gasifier.

Keywords: Fluidized-bed; CFD modeling; biomass gasification; syngas; fluidization characteristics; reaction kinetics

6.1 Introduction

Biomass, a lignocellulosic material, is a sustainable resource and potential energy feedstock for the production of green fuels, chemicals and power through thermochemical conversion process such as gasification. The gasification process thermally degrades biomass into a gaseous product called syngas, which is a building block for many fuels and chemicals (Ansys, 2011), and can be directly utilized to generate heat and power. Biomass gasification has been extensively studied using a fluidized-bed reactor (Campoy et al., 2008; Chen et al., 2004; Hanping et al., 2008; Jiang et al., 2003; Kumar et al., 2009a; Lim & Alimuddin, 2008; Mansaray et al., 1999; Sharma et al., 2011; Xu et al., 2006) as it offers better heat and mass transfers and efficient gas-solid reactions (Schmidt & Renz, 2000; Sharma et al., 2011; Yu et al., 2007) than a fixed-bed reactor. A fluidized-bed gasification process involves bed-material fluidization and a series of gasification reactions which influence the syngas quality. Although fluidized-bed gasification is a well-established process, thorough information on in-bed hydrodynamics and complex gasification reactions are still limited (Fakhim & Farhanieh, 2011; Lavoie et al., 2009) because experimental evaluation of such information is difficult and expensive. Several gasification modeling studies using equilibrium and kinetics approaches were reported to predict composition and yield of biomass generated syngas (Abdelouahed et al., 2012; Kumar et al., 2009c; Mann et al., 2004; Paviet et al., 2009; Puig-Arnavat et al., 2010; Radmanesh et al., 2006; Schuster et al., 2001; Wang & Kinoshita, 1993; Wenyi & Qin, 2010). However, these equilibrium and kinetics gasification models do not take into consideration the non-ideal behavior of the gasifier, and fluidization characteristics which are influenced by shape and size of materials

present in the gasifier bed (Sharma et al., 2013). Further, the equilibrium and kinetics gasification modeling approaches do not predict the temperature and species distributions along the height of the gasifier.

Computational fluid dynamics (CFD) is an advanced computational technique which is capable of modeling various physical and chemical processes such as a fluid flow through a complex system involving multiphase and multiple reactions (Sundaresan, 2000). Using CFD, it is possible to simulate a fluidized-bed gasification process which involves multiphase and several heterogeneous and homogenous reactions for optimization of gasifier design and operating conditions. Additionally, the CFD modeling technique provides visual details on non-ideal behavior of fluidized-bed gasifier and distribution of temperature and syngas constituents along the gasifier height.

Armstrong et al. (2011) simulated the fluidized-bed coal gasification using CFD model. The authors observed that the syngas composition was considerably influenced by height and composition (coal + limestone) as well as temperature of the gasifier bed (Armstrong et al., 2011). Deng et al. (2008) developed a CFD model of coal gasification process in a pressurized spout-fluidized-bed and reported that their model closely predicted the syngas composition and gasifier temperature distribution within 10% error as compared to experimental results (Armstrong et al., 2011).

Compared to coal, biomass exhibits different physiochemical properties, and contains high amounts of volatile matters, which make the biomass more reactive than coal (Basu, 2006). Thus, the biomass and coal both have different devolatization kinetics (activation energy and pre-exponential factor) and rates of gasification reactions.

However, the governing equations and modeling steps used in CFD modeling of coal gasification are also applicable to biomass gasification (Gómez-Barea & Leckner, 2010). Literature shows several CFD modeling studies on coal gasification while limited information is available on CFD gasification modeling of low bulk density biomass feedstock such as switchgrass. More importantly, most of the previous CFD studies on biomass gasification assumed that biomass decomposes into elemental materials (i.e. C, H, O, N and S), which can only occur in an extreme reaction environment far beyond the normal gasification conditions (Kumar et al., 2009c).

In this study, a novel methodology to decompose biomass into several possible devolatization products such as C, H_2O, CO, CO_2, CH_4 and H_2 was used along with experimentally-derived devolatization kinetics to develop the CFD-based biomass gasification model. Further, fluidization characteristics were also incorporated based on effective particle size (Eq. (1)) and effective density (Eq. (2)) of gasifier bed materials (i.e. a mixture of sand, switchgrass and gasifier solid residues (GSR)) (Sharma et al., 2013). The goal of this study was to develop and validate a numerical gasification model based on reaction kinetics and fluidization using computational fluid dynamics (CFD) technique to predict syngas composition, and distributions of syngas constituents and gasifier temperature within the fluidized-bed gasifier.

6.2 Materials and methods

6.2.1 Experimental setup and material characteristics

The diameter and height of the fluidized-bed gasifier, with throughput capacity of 5 kg/h, were 0.10 m and 1.52 m, respectively. The details of fluidized-bed gasifier, and experimental conditions and results are elucidated elsewhere (Sharma et al., 2011).

Gasification conditions and physical properties of materials are shown in Table 6.1. Kanlow switchgrass (a perennial grass native to Oklahoma) and silica sand (Oglebay Norton Industrial Sands, Inc., Brady, TX) were used as the biomass feedstock and inert bed material, respectively. Proximate and ultimate analyses of switchgrass are shown in Table 6.2. The calorific value of dry switchgrass was 18.83 MJ/kg. The mass of sand in the gasifier bed was 1.5 kg. The masses of switchgrass and GSR in the gasifier bed were determined using experimental data collected earlier (Sharma et al., 2011). Since fluidization was considerably influenced by the effective properties of materials present in the gasifier bed (i.e. a mixture of sand, switchgrass and GSR), the effective particle size (Eq. 1) and effective density (Eq. 2) of bed materials were determined and incorporated in the gasification model. The gasification model was studied by varying the equivalence ratio (*ER*), which is defined using following Eq. (3).

$$d_{peff} = k_1 d_{p1} \left\{ k_2 \left[\left(\rho_1 d_{p2} w_2 + \rho_1 d_{p2} w_3 \right) / \left(\rho_2 d_{p1} w_2 + \rho_3 d_{p1} w_3 \right) \right] \left(\rho_2 d_{p3} / \rho_3 d_{p2} \right)^{(w_3/w_2)} \right\}^{(w_2+w_3)/w_1} \quad \text{Eq.(1)}$$

$$\rho_{eff} = (w_1\rho_1 + w_2\rho_2 + w_3\rho_3)/(w_1 + w_2 + w_3) \quad \text{Eq.(2)}$$

where $k_1 = (20d_{p1} + 0.36)^{0.5}$ *and* $k_2 = (20d_{p2} + 0.36)^{0.5}$. w_1, w_2 and w_3 were the masses of sand, switchgrass, and GSR, respectively. ρ_1, ρ_2 and ρ_3 were the particle densities of sand, switchgrass, and GSR, respectively. d_{p1}, d_{p2} and d_{p3} were the particle sizes of sand, switchgrass, and GSR, respectively.

$$ER = \left(\frac{\textit{Air supplied for gasification per unit mass of biomass}}{\textit{Theoretical air required for complete combustion per unit mass of biomass}} \right) \quad \text{Eq.(3)}$$

Table 6.1. Experimental conditions used for model simulation

Gasification conditions (Sharma et al., 2011):			
ER	0.20	0.32	
Dry biomass feed rate, kg/h	3.9	3.4	
Air flowrate, kg/h	4.5	6.5	
Air temperature, °C	25.2	29.5	
Gasification temperature, °C	801	825	
Operating pressure, MPa	1.01	1.01	
Material properties (Sharma et al., 2013):			
Material	Silica sand	Switchgrass	GSR
Particle density (ρ), kg/m^3	2650	400	932
Bulk density (ρ_b), kg/m^3	1602	111	205
Particle size (d_p), mm	0.35	10.30	0.08

Table 6.2. Biomass properties (Sharma et al., 2011)

Proximate Analysis (wt. %, d.b.)[a]		Ultimate Analysis (wt. %, daf)[b]	
Moisture content	10.74	Carbon	49.02
Ash content	4.62	Hydrogen	6.04
Fixed carbon	15.02	Oxygen	44.44
Volatile matter	80.36	Nitrogen	0.19
		Sulfur	0.32

[a] Dry basis
[b] Dry ash-free

6.2.2 Numerical modeling approach

CFD methodology involves discretization of the whole domain of interest into a large number of finite elements of definite sizes and shapes, and then solution of governing equations such as conservation equations of mass, momentum, energy and

species for each element is integrated to obtain a solution for the whole domain (Fluent, 2009).

6.2.2.1 Governing equations

6.2.2.1.1 Conservation of mass equation

The general form of the conservation of mass (i.e. continuity) equation is shown using Eq. (4) in which S_m (source term) represents the addition of mass to the continuous (gas) phase from discrete (solid) phase (Fluent, 2009).

$$\frac{\partial \rho}{\partial t} + \nabla \cdot (\rho \vec{v}) = S_m \qquad \text{Eq.(4)}$$

6.2.2.1.2 Conservation of momentum equation

The general form of the conservation of momentum equation (i.e. Newton's second law) is shown using Eq. (5) wherein the terms $\vec{F}$, $\vec{v}$, p and $\bar{\bar{\tau}}$ represent external body forces, velocity vector, static pressure and stress tensor, respectively (Fluent, 2009).

$$\frac{\partial}{\partial t}(\rho \vec{v}) + \nabla \cdot (\rho \vec{v} \vec{v}) = -\nabla p + \nabla \cdot (\bar{\bar{\tau}}) + \rho \vec{g} + \vec{F} \qquad \text{Eq.(5)}$$

6.2.2.1.3 Conservation of energy equation

The general form of the conservation of energy equation is shown using Eq. (6). Where, E represents total energy, k_{eff} is the effective thermal conductivity, h_j and J_j terms are the sensible enthalpy and diffusion flux, respectively, of species j, $\bar{\bar{\tau}}_{eff}$ is the deviatoric stress tensor, and S_h term is the heat source due to chemical reactions (Fluent, 2009).

$$\frac{\partial}{\partial t}(\rho E) + \nabla \cdot \left(\vec{v} \cdot (\rho E + p)\right) = \nabla \cdot \left[\left(k_{eff} \nabla T\right) - \sum_J h_j J_j + \left(\bar{\bar{\tau}}_{eff} \cdot \vec{v}\right)\right] + S_h \qquad \text{Eq.(6)}$$

6.2.2.1.4 Species transport equation

The general form of the conservation of species equation is shown using Eq. (7). Where, Y_i is the mass fraction of species *i*, S_i is the rate of generation due to dispersed phase, and R_i is the net rate of change in species *i* by chemical reactions (Fluent, 2009; Singh et al., 2013).

$$\frac{\partial}{\partial t}(\rho Y_i) + \nabla \cdot (\rho \vec{v}\, Y_i) = \nabla \cdot \left(D \nabla (\rho Y_i)\right) + S_i + R_i \qquad \text{Eq.(7)}$$

6.2.2.2 Turbulence model

CFD technique contains various turbulence models to account for fluctuations in the fluid flow, i.e. variation in velocity and flow pattern with respect to time and space. The fluctuation in the fluid velocity is defined using eddy viscosity also known as turbulent viscosity. There are several approaches available to determine eddy viscosity using turbulent kinetic energy (*k*) and turbulence dissipation rate (*ε*). Unlike other turbulence models such as standard *k*-*ε* and renormalization group (RNG) *k*-*ε*, the realizable *k*-*ε* turbulence model included the new transport equation for *ε* making fluid turbulent viscosity more precise. Hence, the realizable k-ε turbulence model was used to determine eddy viscosity to account turbulence eddies resulting from fluidization hydrodynamics of gasification. The realizable *k*-*ε* turbulent model solves following two transport equations (Eqs. 8 and 9) to calculate *k* and *ε*, which are later used to determine eddy viscosity (μ_T) using Eq. (10) (Fluent, 2009).

6.2.2.2.1 Turbulent kinetic energy transport equation

$$\frac{\partial}{\partial t}(\rho k) + \nabla \cdot (\rho \vec{u} k) = \nabla \cdot \left[\left(\mu + \frac{\mu_T}{\sigma_k}\right) \cdot \nabla k\right] + G_k + G_b - \rho\varepsilon - Y_M + S_K \qquad \text{Eq.(8)}$$

where σ_k is the turbulent Prandtl number. G_k and G_b are turbulent kinetic energy generation terms attributed to mean velocity gradients and buoyancy, respectively. Y_M is the influence of fluctuating-dilation to overall dissipation rate. S_K is the user defined source term (Fluent, 2009).

6.2.2.2.2 Turbulent dissipation rate transport equation

$$\frac{\partial}{\partial t}(\rho\varepsilon) + \nabla \cdot (\rho\vec{u}\,\varepsilon)$$

$$= \nabla \cdot \left[\left(\mu + \frac{\mu_T}{\sigma_\varepsilon}\right) \cdot \nabla\varepsilon\right] + \rho c_1 S_\varepsilon - \rho c_2 \frac{\varepsilon^2}{k + \sqrt{\vartheta\varepsilon}} + c_{1\varepsilon}\frac{\varepsilon}{k} c_{3\varepsilon} G_b + S_\varepsilon \quad \text{Eq.(9)}$$

where σ_ε is the turbulent Prandtl number. c_1, c_2, $c_{1\varepsilon}$ and $c_{3\varepsilon}$ are constants. S_ε is the user defined source term (Fluent, 2009).

$$\mu_T = \rho C_\mu \frac{k^2}{\varepsilon} \quad \text{Eq.(10)}$$

6.2.2.3 Gasification chemistry

6.2.2.3.1 Biomass drying and devolatization

Biomass drying process (i.e. moisture evaporation) was included in the model using reaction R(1) with its Arrhenius equation parameters, i.e. activation energy (*E*) and pre-exponential factor (*A*) (Simone et al., 2013). In the model, moisture was included as one of inputs.

$$\text{Biomass drying:} \quad H_2O_{(l)} \rightarrow H_2O_{(v)} \quad \text{R(1)}$$

During devolatization process, the biomass disintegrates into char, i.e. fixed carbon (C), volatile products, moisture and ash (Fig. 6.1). The volatile matters further disintegrate into gaseous species (such as CO, CO_2, CH_4 and H_2) and impurities (such as tar, NH_3 and H_2S) as shown using reaction R(2). Thereby, the global reaction scheme of

biomass devolatization process can be described using reaction R(3) (Gómez-Barea & Leckner, 2010; Kumar et al., 2009c).

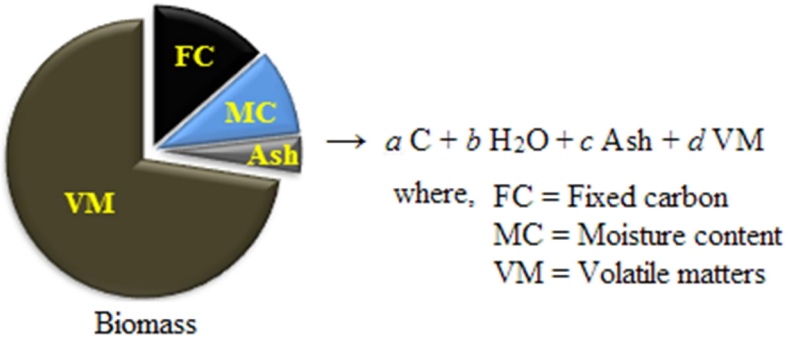

Fig. 6.1. Biomass decomposition into primary products

$$VM \rightarrow eCO + fCO_2 + gCH_4 + hH_2 + i\text{Tar} + jNH_3 + kH_2S \quad \text{R(2)}$$

$$\text{Biomass} \rightarrow aC + bH_2O + c\text{Ash} + eCO + eCO + fCO_2 + gCH_4 + hH_2 + i\text{Tar} + jNH_3 + kH_2S \quad \text{R(3)}$$

In this work, coefficients *a* to *d* (Fig. 6.1) were calculated using proximate analysis of switchgrass (Table 6.2). Proximate and ultimate analyses of switchgrass were used to determine coefficients *e* to *k* in reaction R(2) by balancing masses of C, H, O, N and S contents of the biomass and assuming CO/CO_2 ratio of 1 (Kumar et al., 2009c) while the quantity of tar was assumed known based on experimental results. The kinetics of switchgrass devolatization reaction (Table 6.3) were obtained from literature (Pasangulapati, 2012).

6.2.2.3.2 Biomass gasification reactions

Gasification process involves complex reaction mechanisms during which the solid char and gaseous products evolved during biomass devolatization process undergo series of gasification reactions. Table 6.3 shows the various heterogeneous (solid-gas) and homogeneous (gas-gas) gasification reactions (Kumar et al., 2009b; Sharma et al.,

2011) and their kinetics (Pasangulapati, 2012) used in the model. The heat released from exothermic reactions (such as methane oxidation R(7) and char combustion R(9) reactions) provide essential heat for biomass devolatization and other endothermic reactions such as Boudouard R(10) and water gas R(12) reactions.

Table 6.3. Gasification reactions and their kinetics (Pasangulapati, 2012; Simone et al., 2013)

Reactions		ΔH (kJ/mol)	A (1/s)	E (kJ/mol)
R(1)	Biomass drying	41	5.13×10^{10}	88
R(3)	Devolatization	118	3.88×10^{10}	122
R(4)	$CO + H_2O \leftrightarrow H_2 + CO_2$	-41	2.65×10^{-2}	66
R(5)	$CO + 1/2O_2 \rightarrow CO_2$	-338	8.83×10^{11}	100
R(6)	$H_2 + 1/2O_2 \rightarrow H_2O$	-242	3.09×10^{11}	100
R(7)	$CH_4 + 3/2O_2 \rightarrow CO + 2H_2O$	-519	1.58×10^{8}	202
R(8)	$CH_4 + H_2O \rightarrow CO + 3H_2$	206	3.02×10^{6}	125
R(9)	$C + O_2 \rightarrow CO_2$	-394	9.35×10^{4}	83
R(10)	$C + 1/2O_2 \rightarrow CO$	-111	6.47×10^{3}	167
R(11)	$C + CO_2 \rightarrow 2CO$	173	3.62×10	77
R(12)	$C + H_2O \rightarrow CO + H_2$	131	1.52×10^{4}	122
R(13)	$C + 2H_2 \rightarrow CH_4$	-75	4.20×10^{3}	19

6.2.2.4 CFD methodology

6.2.2.4.1 Geometry creation and discretization

Based on the physical dimensions of our lab-scale fluidized-bed gasifier, a two dimensional (2D) axisymmetric geometry of the gasifier (Fig. 6.2) was created using ANSYS Design-modeler. The gasifier geometry was imported to the ANSYS Mesh for discretization. Thereafter, the whole gasifier domain was discretized (also known as meshing) into large numbers of finite subdomains (i.e. elements) of quadrilateral shapes using a quadrilateral mesh method. The minimum and maximum element sizes used in the numerical grid were 0.0001 and 0.03 m, and the maximum face size of element was 0.025 m. This was because for the simple 2D geometry (Fig. 6.2), the quadrilateral mesh

contains lower skewness and offers better numerical grid and solution convergence compared to the other available mesh (i.e. triangular). The numerical grid of the gasifier domain under this study consisted of a total of 19096 nodes and 18450 elements. The advanced size function called proximity and curvature with curvature normal angle of 12° was used to generate numerical grid.

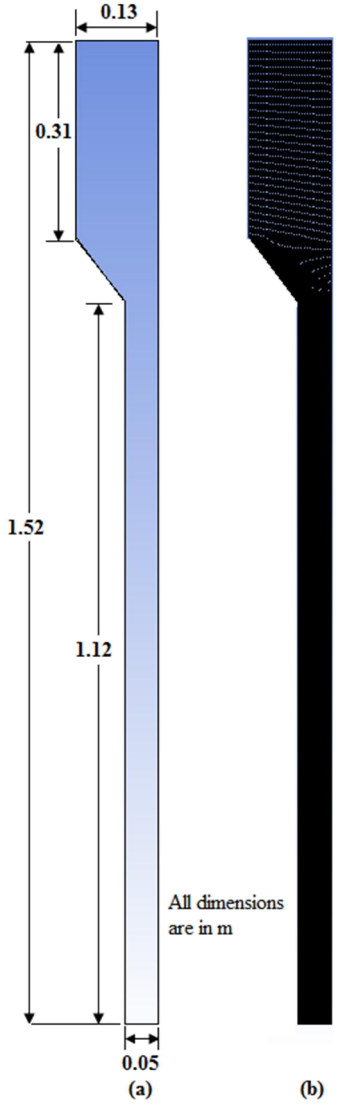

Fig. 6.2. Computational domain setup. (a) Geometry, and (b) discretization of gasifier domain

6.2.2.4.2 Boundary and initial conditions

In numerical simulation, establishing appropriate boundary conditions is key step to minimize convergence errors and achieve better simulation results. Since mass flow rates of biomass and air were known from the experimental study, a mass flow rate boundary condition was used for the gasifier inlet. A combined material stream, consisted of biomass's decomposed products and air, was defined at the inlet boundary. The total mass flow rate of combined material stream was calculated using the biomass decomposition procedure based on reactions R(2) and R(3). The gasifier was run at atmospheric pressure (Table 6.1); thereby a pressure outlet boundary condition was used by setting a zero gauge pressure (i.e. atmospheric pressure) as the outlet boundary condition. The no slip wall boundary condition was used for the velocity and axis boundary condition was used for the centerline of axisymmetric geometry. After setting up the essential boundary conditions, the numerical model was initialized to start the solver calculation. During initialization, a static bed of silica sand (0.106 m height) using volume fraction of 0.051 was patched at the bottom of the gasifier geometry (Fig. 6.2). Further, an initial temperature of 500°C was patched to the gasifier to initiate gasification process.

6.2.2.4.3 Simulation and convergence

ANSYS Fluent (release 14.5) was used to solve governing equations defined in the model of fluidized-bed gasifier. Eulerian multiphase flow, energy, viscous flow and species transport models were used in this study. Based on the experimental conditions (Tables 6.1 and 6.2), model inputs such as boundary and initial conditions were set during problem setup in ANSYS Fluent. In the Eulerian multiphase model, two phases

were used to define the input gaseous mixture stream (i.e. biomass plus air) as primary phase (phase-1) and the silica sand as secondary phase (phase-2). Syamlal-Obrien drag law was used to enable interaction between primary and secondary phases. As discussed earlier, the fluidization behavior depends on the size, shape and type of materials (i.e. a mixture of chopped switchgrass, silica sand and GSR) present in the gasifier bed. Hence, effective particle size (Eq. 1) and effective density (Eq. 2) of bed materials were used as particle size and density of phase-2. A time-step of 0.005 s and 50 iterations per time-step were used in the simulation run. The convergence absolute criterion for residual was set at 0.0001 for governing equations. Initially, a simulation run was performed with multiphase and viscous flow models and the whole fluid flow domain was calculated until the simulation reached steady state. Thereafter, other models (i.e. energy and species transport models) were also enabled and all governing equations were solved simultaneously until the convergence criterion was achieved. The model was validated using sensitivity analysis by varying ER. In the previous experimental study (Sharma et al., 2011), the best syngas composition and gasifier energy efficiency were observed at the ER of 0.32. Therefore, the model simulation and validation were performed using ER of 0.32. Based on the experimental condition shown in Table 6.1, another ER of 0.20 was selected for the sensitivity analysis of the studied model.

6.2.2.4.4 Model assumptions

The following assumptions were made in the numerical model of the fluidized-bed gasifier.

- Biomass decomposition was instant and the products of devolatization process were C, H_2O, CO, CO_2, CH_4, H_2 and ash.

- To avoid model complexity and reduce convergence time, gas impurities (i.e. tar, NH_3, and H_2S) and other lighter hydrocarbons (i.e. C_2H_2, C_2H_4 and C_2H_6) were assumed to be negligible.
- The effective particle size and effective density of bed materials were used for secondary phase (phase-2) for simulating fluidization hydrodynamics.
- An axisymmetric 2D numerical grid of fluidized-bed gasifier was selected to reduce the computational power required.

6.3 Results and Discussion

A 2D axisymmetric numerical model of fluidized-bed gasifier was developed using Eulerian multiphase flow approach. The model predictions in terms of syngas composition and distributions of syngas constituents, and gasifier temperature are discussed as follows.

6.3.1 Syngas composition

The distribution of syngas constituents (i.e. CO, H_2, CH_4, CO_2, O_2 and H_2O) within the gasifier for ER of 0.32 is shown in Fig. 6.3. The axial profiles of syngas constituents (Fig. 6.3) clearly indicated the locations of different zones (such as drying, pyrolysis, combustion and reduction) and revealed insight regarding dominating reactions that occurred in the fluidized-bed gasifier. The drying zone was located within the small bed-height (0.015 m above the gasifier inlet) in which evaporation of moisture occurred (Fig. 6.3(a)) leading to the production of H_2O vapor (Fig. 6.3(b)) though reaction R(1). In the drying zone, most of the biomass moisture (94%) was converted into H_2O vapor. It can be seen from Fig. 6.3(c and d) that most of the C and O_2 supplied to the gasifier rapidly reacted and consumed within a short bed-height (about 0.25 m above the gasifier

inlet), which disclosed that the char combustion reaction R(9) was predominant in this region as evident from the high CO_2 production (Fig. 6.3(e)). In addition, the CO oxidation reaction R(5) also contributed to CO_2 production in the combustion zone. As the products of combustion progressed up in the gasifier, the CO_2 content decreased from 14.7% to 14.1% in the reduction zone (i.e. the region located between the combustion zone and gasifier-top).

The CO distribution profile (Fig. 6.3(f)) showed 12.1% CO in the combustion zone, which indicated that the char partial-oxidation reaction (R(10)) was occurred in this zone leading to the production of CO. A further increase in the CO content from 12.1 to 12.8 was observed in the freeboard zone of the gasifier, which indicated that endothermic reactions such as Boudouard R(11) and water-gas R(12) occurred in the freeboard zone of the gasifier. Conversely, in the disengagement zone of the gasifier, the model showed decrease in the CO content from 12.8% to 11.2% which indicated that the water-gas-shift reaction R(4) might have occurred leading the decrease in the CO content. The H_2 distribution profile (Fig. 6.3(g)) indicated that methane-steam reforming reaction R(8) occurred in the combustion zone as exhibited by 7.8% H_2 production in this zone. In freeboard and disengagement zones, the H_2 content decreased from 7.8% to 6.6%, which indicated the H_2 oxidation reaction R(6) might have occurred producing H_2O vapor. The CH_4 distribution profile (Fig. 6.3(h)) indicated that most of the CH_4 consumed in the combustion zone, which indicated that CH_4 oxidation reaction R(7) was dominant in the combustion zone. The results indicated that the fluidization of sand in the gasifier-bed had enhanced the turbulence level, mixing characteristics, and heat and mass transfers

leading to the higher production of syngas CO (11.2%) and H_2 (6.6%) as compared to CO (3.6%) and H_2 (2.4%) contents observed without the sand bed.

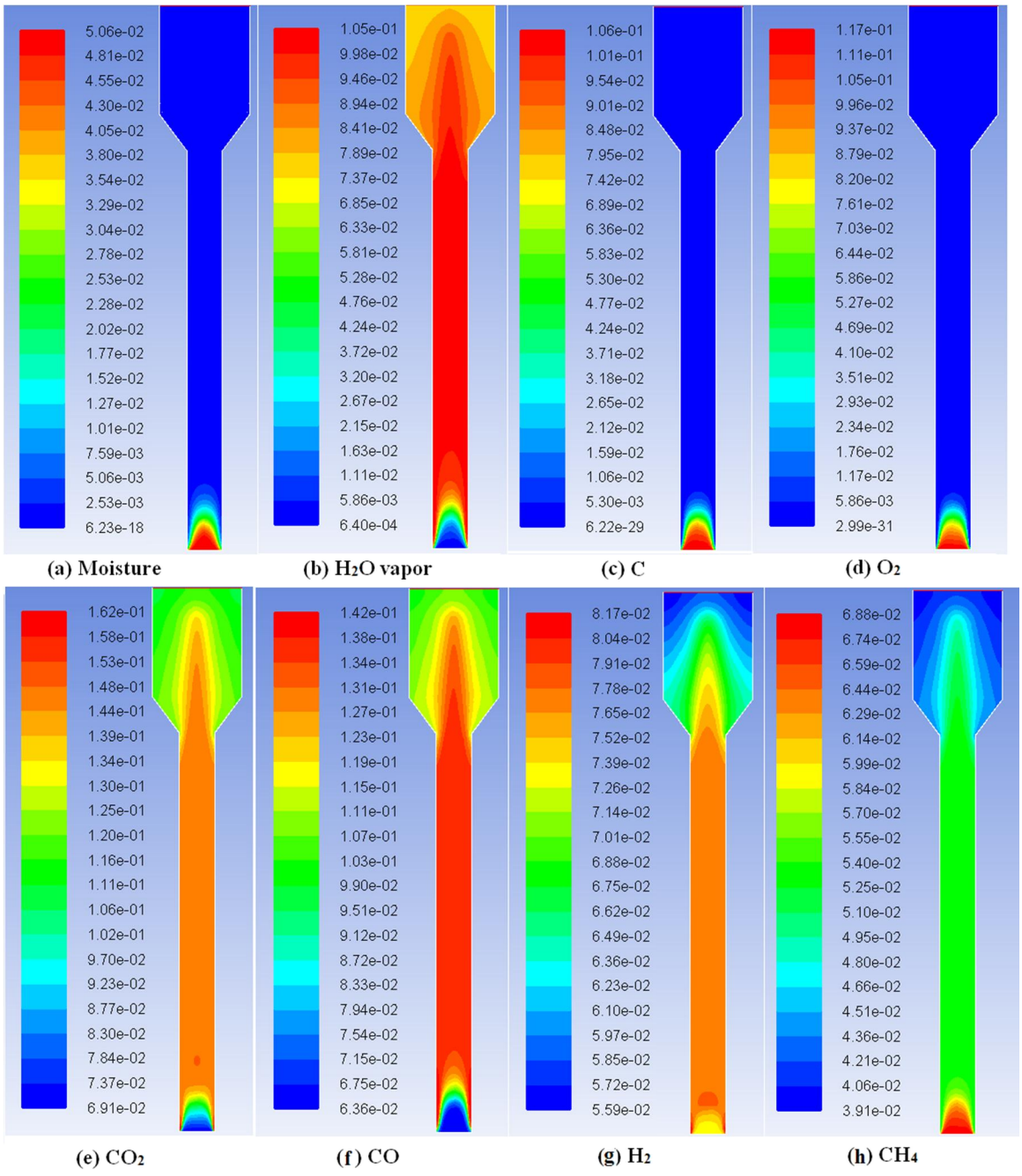

Fig. 6.3. Contour plots of syngas constituents (mole fraction) along the height of the gasifier for ER of 0.32

6.3.2 Gasifier temperature profile

Fig. 6.4 shows the predicted and experimental average temperature profile along the height of the gasifier. As described previously, the char combustion R(9) and char partial-oxidation R(10) reactions were dominant in the combustion zone (located in the gasifier-bed). As a result, the model predicted a higher temperature distribution within the gasifier-bed which attributed to the high heat release from exothermic reactions R(9)-R(10). Additionally, the presence of sand in the combustion zone enhanced the heat and mass transfer. As a result, the model showed few local hot spots in the combustion zone. The predicted maximum temperature in the combustion zone was 1995°C.

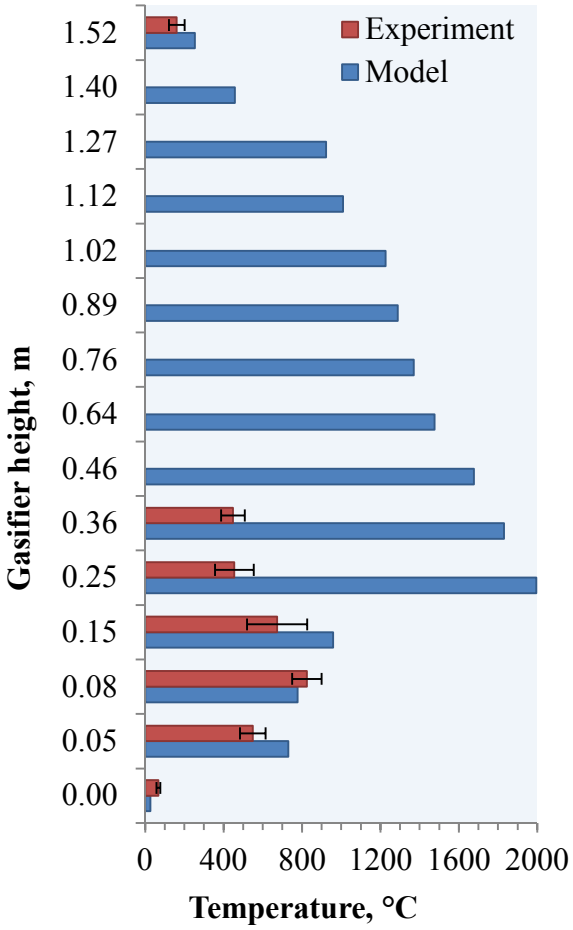

Fig. 6.4. Gasifier temperature profile along reactor height

As the products of combustion progressed upward in the freeboard and disengagement zones of the gasifier, the model predicted a continuous decrease in the temperature with an increase in the gasifier height above the bed. Such reduction in the gasifier temperature was mainly due to endothermic reactions such as Boudouard R(11), water-gas R(12) and methane-steam reforming R(8), which occurred in the freeboard and disengagement zones. These endothermic reactions consumed part of the process heat resulting in the overall decrease in the gasifier temperature as shown in Fig. 6.4. Considering the experimental results, the model closely predicted the temperature distribution for the bottom region of the gasifier-bed (located between gasifier inlet and up to 0.15 m of bed-height) and at the gasifier outlet while model showed much higher temperature in the region above 0.15 m, as well as in the freeboard zone as shown in Fig. 6.4. Such high temperature in the prediction might be attributed to the major assumption made in biomass devolatization. Since, the devolatization process is an endothermic reaction, the absence of devolatization step in this study might have caused over prediction of the temperature. Further, the kinetics of the reactions were not for the switchgrass rather they were adopted from literature (for cotton trash char), which might have resulted deviation between the predicted and experimental temperature.

6.3.3 Model validation

Comparison between experimental and predicted syngas CO, H_2, CH_4, CO_2 and N_2 contents at two ER conditions, i.e. 0.20 and 0.32, are shown in Fig. 6.5. At ER of 0.20, compared to the experimental result of CO (15.2 ± 2.1%), H_2 (5.9 ± 2.0%), CH_4 (2.5 ± 0.4%), CO_2 (14.3 ± 0.4%) and N_2 (60.1 ± 1.8%), the model predicted low CO (11.4%) and CO_2 (8.3%) while high H_2 (8.6%), CH_4 (4.8%) and N_2 (63.9%). At ER of

0.32, compared to the experimental result of CO (16.5 ± 1.1%), H_2 (9.3 ± 0.8%), CH_4 (2.2 ± 0.7%), CO_2 (12.2 ± 1.2%) and N_2 (56.7 ± 1.1%), the model predicted low CO (11.2%), H_2 (6.6%) and N_2 (54.4%) while high CH_4 (5.2%) and CO_2 (14.1%). The sensitivity analysis showed that with varying ER from 0.20 to 0.32, CO and H_2 decreased from 11.4 to 11.2% and from 8.6 to 6.6%, respectively; whereas CO_2 content increased from 8.3 to 14.1%.

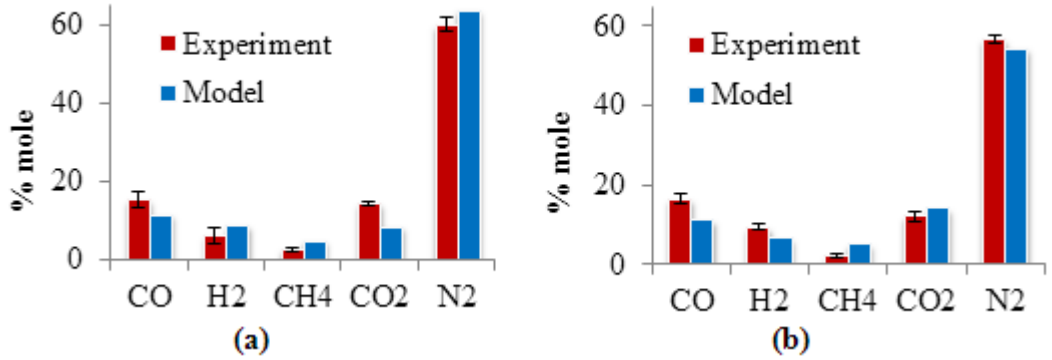

Fig. 6.5. Model validation - predicted and experimental syngas composition at ERs of (a) 0.20 and (b) 0.32

6.4 Conclusions

A 2D axisymmetric numerical model of biomass gasification was developed using an Eularian multiphase flow approach and by incorporating the reaction kinetics and fluidization characteristics. The model clearly indicated the locations of drying, combustion and reduction zones of the gasifier, as well as providing insight regarding dominating reactions occurring in the fluidized-bed gasifier. Simulation results showed that the char combustion and char partial-oxidation reactions were dominant in the combustion zone of the gasifier. The Boudouard and water-gas reactions contributed the most toward CO production in the freeboard zone of the gasifier. Simulation results showed that the water-gas-shift reaction led to the decrease in CO content in the

disengagement zone of the gasifier. The methane-steam-reforming reaction contributed the most H_2 production in the gasifier. The sensitivity analysis showed that the model was sensitive to the equivalence ratio and was able to predict syngas composition and the gasifier temperature with the change in equivalence ratio. The presence of sand in the bed increased syngas CO (from 3.6 to 11.2 %) and H_2 (from 2.4 to 6.6%) contents.

Acknowledgements

This work was supported in part by the National Science Foundation under Grant No. EPS-0814361 and the Oklahoma Agricultural Experiment Station. The authors also acknowledge the support of Vamsee Pasangulapati for assisting in the simulation work.

6.5 References

Abdelouahed, L., Authier, O., Mauviel, G., Corriou, J.P., Verdier, G., Dufour, A. 2012. Detailed Modeling of Biomass Gasification in Dual Fluidized Bed Reactors under Aspen Plus. *Energy & Fuels*, **26**(6), 3840-3855.

Ansys, A.F. 2011. 14.0 Theory Guide. in: *ANSYS inc*.

Armstrong, L.M., Gu, S., Luo, K.H. 2011. Parametric Study of Gasification Processes in a BFB Coal Gasifier. *Industrial & Engineering Chemistry Research*, **50**(10), 5959-5974.

Basu, P. 2006. *Combustion and gasification in fluidized beds*. CRC.

Campoy, M., Gomez-Barea, A., Villanueva, A.L., Ollero, P. 2008. Air-steam gasification of biomass in a fluidized bed under simulated autothermal and adiabatic conditions. *Industrial & Engineering Chemistry Research*, **47**(16), 5957-5965.

Chen, G., Spliethoff, H., Andries, J., Glazer, M.P., Yang, L.B. 2004. Biomass gasification in a circulating fluidised bed - Part 1: Preliminary experiments and modelling development. *Energy Sources*, **26**(5), 485-498.

Fakhim, B., Farhanieh, B. 2011. *Second Law Analysis of Bubbling Fluidized Bed Gasifier for Biomass Gasification*.

Fluent, A. 2009. Theory Guide. *US: ANSYS Inc*.

Gómez-Barea, A., Leckner, B. 2010. Modeling of biomass gasification in fluidized bed. *Progress in Energy and Combustion Science*, **36**(4), 444-509.

Hanping, C., Bin, L., Haiping, Y., Guolai, Y., Shihong, Z. 2008. Experimental investigation of biomass gasification in a fluidized bed reactor. *Energy & Fuels*, **22**(5), 3493-3498.

Jiang, H., Zhu, X.F., Guo, Q.X., Zhu, Q.S. 2003. Gasification of rice husk in a fluidized-bed gasifier without inert additives. *Industrial & Engineering Chemistry Research*, **42**(23), 5745-5750.

Kumar, A., Eskridge, K., Jones, D.D., Hanna, M.A. 2009a. Steam-air fluidized bed gasification of distillers grains: Effects of steam to biomass ratio, equivalence ratio and gasification temperature. *Bioresource Technology*, **100**(6), 2062-2068.

Kumar, A., Jones, D.D., Hanna, M.A. 2009b. Thermochemical biomass gasification: A review of the current status of the technology. *Energies*, **2**(3), 556-581.

Kumar, A., Noureddini, H., Demirel, Y., Jones, D., Hanna, M. 2009c. Simulation of corn stover and distillers grains gasification with Aspen Plus. *Transactions of the ASAE*, **52**(6), 1989-1995.

Lavoie, J., Chaouki, J., Drouin, G. 2009. Biomass gasification in a bubbling fluidized bed: Numerical modeling and experiments.

Lim, M.T., Alimuddin, Z. 2008. Bubbling fluidized bed biomass gasification - Performance, process findings and energy analysis. *Renewable Energy*, **33**(10), 2339-2343.

Mann, M.D., Knutson, R.Z., Erjavec, J., Jacobsen, J.P. 2004. Modeling reaction kinetics of steam gasification for a transport gasifier. *Fuel*, **83**(11–12), 1643-1650.

Mansaray, K.G., Ghaly, A.E., Al-Taweel, A.M., Hamdullahpur, F., Ugursal, V.I. 1999. Air gasification of rice husk in a dual distributor type fluidized bed gasifier. *Biomass & Bioenergy*, **17**(4), 315-332.

Pasangulapati, V. 2012. Devoltilization characteristics of cellulose, hemicellulose, lignin and the selected biomass during thermochemical gasification: Experiment and modeling studies, Vol. M.S. Thesis, Oklahoma State University.

Paviet, F., Chazarenc, F., Tazerout, M. 2009. Thermo chemical equilibrium modelling of a biomass gasifying process using ASPEN PLUS. *International Journal of Chemical Reactor Engineering*, **7**(7), 40.

Puig-Arnavat, M., Bruno, J.C., Coronas, A. 2010. Review and analysis of biomass gasification models. *Renewable and Sustainable Energy Reviews*, **14**(9), 2841-2851.

Radmanesh, R., Chaouki, J., Guy, C. 2006. Biomass gasification in a bubbling fluidized bed reactor: experiments and modeling. *Aiche Journal*, **52**(12), 4258-4272.

Schmidt, A., Renz, U. 2000. Numerical prediction of heat transfer in fluidized beds by a kinetic theory of granular flows. *International journal of thermal sciences*, **39**(9), 871-885.

Schuster, G., Löffler, G., Weigl, K., Hofbauer, H. 2001. Biomass steam gasification–an extensive parametric modeling study. *Bioresource Technology*, **77**(1), 71-79.

Sharma, A.M., Kumar, A., Patil, K.N., Huhmke, R.L. 2011. Performance evaluation of a lab-scale fluidized bed gasifier using switchgrass as feedstock. *Transactions of the ASABE*, **56**(6), 2259-66.

Sharma, A.M., Kumar, A., Patil, K.N., Huhnke, R.L. 2013. Fluidization characteristics of a mixture of gasifier solid residues, switchgrass and inert material. *Powder Technology*, **235**, 661-668.

Simone, M., Nicolella, C., Tognotti, L. 2013. Numerical and experimental investigation of downdraft gasification of woody residues. *Bioresource Technology*, **133**, 92-101.

Singh, R.I., Brink, A., Hupa, M. 2013. CFD modeling to study fluidized bed combustion and gasification. *Applied Thermal Engineering*, **52**(2), 585-614.

Sundaresan, S. 2000. Modeling the hydrodynamics of multiphase flow reactors: current status and challenges. *Aiche Journal*, **46**(6), 1102-1105.

Wang, Y., Kinoshita, C.M. 1993. Kinetic model of biomass gasification. *Solar Energy*, **51**(1), 19-25.

Wenyi, T., Qin, Z. 2010. Simulation of Hydrogen Production in Biomass Gasifier by ASPEN PLUS. *Power and Energy Engineering Conference (APPEEC), 2010 Asia-Pacific*, 28-31 March 2010. pp. 1-4.

Xu, G.W., Murakami, T., Suda, T., Matsuzawa, Y., Tani, H. 2006. Gasification of coffee grounds in dual fluidized bed: Performance evaluation and parametric investigation. *Energy & Fuels*, **20**(6), 2695-2704.

Yu, L., Lu, J., Zhang, X., Zhang, S. 2007. Numerical simulation of the bubbling fluidized bed coal gasification by the kinetic theory of granular flow (KTGF). *Fuel*, **86**(5), 722-734.

CHAPTER VII

RECOMMENDATIONS FOR FUTURE WORK

In this research a lab-scale autothermal fluidized-bed gasifier was designed, developed and experimentally optimized to maximize composition and yield of syngas generated from air and air-steam gasification of switchgrass. However, further modifications in the gasifier and change in the gasification conditions, such as increasing steam-to-biomass ratio (SBR) and steam injection temperature, would improve syngas composition and yields, as well as gasifier efficiencies. The reaction kinetics and computational fluid dynamics (CFD) gasification models developed in this research can also be improved by removing some of the model assumptions, such as CO/CO_2 ratio of 1.0 and devolatization products and kinetics of cotton trash char, used in this study, and thus, enabling the models to simulate the real conditions more closely. The following studies are recommended for further improving the quality and prediction of biomass-generated syngas suitable for the production of advanced biofuels, biochemicals and biopower.

1. In chapter three of the dissertation, a cold fluidization setup was used to study the fluidization behavior of bed consisted of a mixture of sand, biomass and gasifier solid residues (GSR). The study provided insights on fluidization behavior of a tertiary mixture with different particle size and shape. However,

since real gasification process occurs at high temperature, fluidization study at high temperature (600-800 °C) will be more informative.

2. In chapter four, since the autothermal fluidized-bed gasifier was limited by the maximum temperature it can reach, raising its temperature using external heaters and increasing steam-to-biomass ratio (SBR) to 1.0 can further improve syngas hydrogen and carbon monoxide contents. The high temperature and SBR would also help in the reduction of tars.
3. In chapter four, the temperature of the steam injected was lower (200°C) than that of the reactor bed (700-800°C). This resulted in reduced gasifier bed temperatures which affected the gasification process. Therefore, superheating steam up to gasification temperature or even higher would enhance steam-gasification reactions, and thus to improve syngas hydrogen and carbon monoxide yields.
4. Chapters five and six dealt with modeling of biomass gasification using reaction kinetics and computational fluid dynamics (CFD) approaches. In both of these modeling approaches, the biomass devolatization products were determined by balancing masses of C, H, O, N and S contents of the biomass with possible products and assuming CO/CO_2 ratio of 1. However, in reality, biomass devolatization depends on several factors such as biomass properties, temperature condition, and type of oxidizing agent. Hence, obtaining quantitative information on products of biomass devolatization is essential to improve reliability of gasification models.

APPENDICES

A.1 Biomass decomposition products used in simulation (chapters 5 and 6)

Table A.1.1. Products of biomass decomposition determined using mass balance for different gasification conditions

Gasification conditions :					
Equivalence ratio (ER)	0.20	0.29	0.32	0.40	0.45
Biomass moisture content, %	9.7	9.7	9.7	9.7	9.7
Biomass feed rate, kg/h	4.3	4.7	3.8	3.2	4.1
Dry biomass feed rate, kg/h	3.9	4.2	3.4	2.9	3.7
Air flow rate, kg/h	4.5	6.8	6.5	6.4	10
Air temperature, °C	25.2	29	29.5	29	32
Gasification temperature, °C	801	809	825	893	907
Gasification pressure, MPa	1.01	1.01	1.01	1.01	1.01
Syngas flow rate, Nm^3/h	4.61	7.23	6.99	6.43	9.25
Gasifier reactor volume, m^3	0.0272	0.0272	0.0272	0.0272	0.0272
Products of biomass decomposition (mol/s):					
C	0.0135	0.0146	0.0118	0.0101	0.0129
H_2O	0.0065	0.0070	0.0056	0.0048	0.0061
CO	0.0092	0.0095	0.0075	0.0065	0.0087
H_2	0.0107	0.0111	0.0088	0.0076	0.0102
CH_4	0.0093	0.0096	0.0076	0.0066	0.0088
CO_2	0.0092	0.0095	0.0075	0.0065	0.0087

B.1 Polymath code used for reaction kinetic gasification model (chapter 5)

Given below the example of polymath code for one gasification conditions (ER = 0.20).

```
# defining equations

f(x2) = (x1+x2+x6+x7)/v0+rA*t

x2(0) = 0

f(x1)= (x1+x3-2*x4+x5)/v0+rB*t

x1(0) = 0

f(x6)= (1.5*x4+x6+0.5*x7)/v0+rC*t

x6(0) = 0

f(x7)= (-x1-2*x2+x3-x4-x5-x7)/v0+rD*t

x7(0) = 0

f(x5)= (-x1-x3-3*x5)/v0+rE*t

x5(0) = 0

f(x4)= (x4+x5)/v0+rF*t

x4(0) = 0

f(x3)= (x2-x3-x6)/v0+rG*t

x3(0) = 0

# defining net rate of reaction for each participating species

rA = -r1-r2-r6-r7

rB = -r1-r3+2*r4-r5

rC = -1.5*r4-r6-0.5*r7

rD = r1+2*r2-r3+r4+r5+r7

rE = r1+r3+3*r5
```

rF = -r4-r5

rG = -r2+r3+r6

defining reaction rate equation for 7 reactions using literature data

r1 = 2*k1*(FH2O/v0)*0.045/(1+k2*(FH2O/v0)+k3*(FH2/v0)+k4*(FCO/v0))

r2 = 2*k5*(FCO2/v0)*0.045/(1+k6*(FCO2/v0)+k7*(FCO/v0))

r3 = k8*((FH2O/v0) *(FCO/v0)-(((FH2/v0)*(FCO2/v0))/Keq))*1

r4 = k9*(FCH4/v0)*(FO2/v0)

r5 = k10*((FCH4/v0)*(FH2O/v0)-((FCO/v0)*((FH2/v0)^2)/(0.0265*32900/(Tg+273))))

r6 = k11*(FC/v0)

r7 = k12*(FC/v0)*(FO2/v0)

defining reaction rate constants for 7 reactions using literature data

k1 = 239**EXP*(-129000/8.314/(Tg+273))

k2 = 0.0316**EXP*(-30100/8.314/(Tg+273))

k3 = 0.00536**EXP*(-59800/8.314/(Tg+273))

k4 = 8.25*(10^-5)**EXP*(-96100/8.314/(Tg+273))

k5 = 4.89*(10^-7)**EXP*(-268000/8.314/(Tg+273))

k6 = 0.066

k7 = 0.12**EXP*(-25500/8.314/(Tg+273))

k8 = 2.778**EXP*(-12560/8.314/(Tg+273))

Keq = 0.022**EXP*(34730/8.314/(Tg+273))

k9 = 5.16*(10^13)/((Tg+273)^-1)**EXP*(-130000/8.314/(Tg+273))

k10 = 3.1005**EXP*(-15000/(Tg+273))

k11 = 17.67*8.314*(Tg+273)**EXP*(-13600/(Tg+273))

k12 = 8710*EXP(-17967/(Tg+273))

FC = 0.0135-x1-x2-x6-x7

FH2O = 0.0065-x1-x3+2*x4-x5

FO2 = 0.0091-1.5*x4-x6-0.5*x7

FCO = 0.0092+x1+2*x2-x3+x4+x5+x7

FH2 = 0.0107+x1+x3+3*x5

FCH4 = 0.0093-x4-x5

FCO2 = 0.0092-x2+x3+x6

FN2 = 0.0342

FT_0 = 0.0135+0.0065+0.0091+0.0092+0.0107+0.0093+0.0092+0.0342

defining reactor volume, total molar flow rates entering and leaving the reactor

v0 = FT_0*(22.4/1000)*((25.2+273)/273)

FT = (FT_0+0.5*x4+2*x5-x6-0.5*x7)

Calculation or residence time based on the gasifier volume and gas volume flowrate

t = 0.0272/(4.61*(Tg+273)/(273*3600))

Defining gasifier temperature

Tg = 801

C.1 Numerical model parameters used for gasification CFD model (chapter 6)

Table C.1.1. Solver parameters used to develop gasification CFD model

Solution setup:		
Solver type	:	2D Pressure-Based
Velocity formulation	:	Absolute
Formulation	:	Implicit
Time	:	Transient
2D Space	:	Axisymmetric
Models:		
• Multiphase model	:	Eulerian multiphase flow (2 phases)
• Volume Fraction Parameters	:	Implicit
• Energy Equation	:	On
• Viscous model Near-Wall Treatment Turbulent multiphase model	:	Realizable k-e Standard Wall Fn. Mixture
• Species model Reactions Turbulence-Chemistry Interaction	:	Species transport Volumetric Finite-Rate/Eddy-Dissipation

Table C.1.2. Biomass-decomposition products and their properties used in the gasification CFD model (Chapter 6)

Properties		Biomass-decomposition products					
		C[a]	H_2O[b]	CO	CO_2	H_2	CH_4
Type	:	Fluid	Fluid	Fluid	Fluid	Fluid	Fluid
Density, kg/m^3	:	2000	998.2	1.123	1.788	0.082	0.668
Specific heat, j/kg-k	:	Piecewise-polynomial	Piecewise-linear	Piecewise-polynomial	Piecewise-polynomial	Piecewise-polynomial	Piecewise-polynomial
Molecular weight, kg/kmol	:	12.01	18.02	28.01	44.01	2.02	16.04
Standard state enthalpy, j/kgmol	:	7.17e+08	-2.86e+08	-1.11E+08	-3.94E+08	0	-7.49E+07
Standard state entropy, j/kgmol-k	:	157995	69902	197532	213720	130582	186040
Reference temperature, k	:	298	298	298	298	298	298

[a] Biomass fixed carbon content

[b] Biomass moisture content

VITA

Ashokkumar M. Sharma

Candidate for the Degree of

Doctor of Philosophy

Thesis: EXPERIMENTAL INVESTIGATION AND SIMULATION OF A FLUIDIZED-BED GASIFIER USING SWITCHGRASS

Major Field: Biosystems Engineering

Biographical:

Education:
Completed the requirements for the Doctor of Philosophy in Biosystems Engineering at Oklahoma State University, Stillwater, Oklahoma in December, 2013.

Completed the requirements for the Masters of Technology in Mechanical Engineering at Sardar Vallabhbhai National Institute of Technology, Surat, India in August, 2006.

Completed the requirements for the Bachelors of Engineering in Mechanical Engineering at Faculty of Technology and Engineering, Maharaja Sayajirao University of Baroda, Vadodara, India in August, 1998.

Experience:
Research Engineer (Biomass Thermochemical Conversion), Oklahoma State University, Stillwater, Oklahoma, September 2009 to Present.

Manager (Mechanical Engineering), Essar Steel Limited, Hazira, Surat, India, November 2007 to September 2009.

Faculty (Mechanical Engineering), Sarvajanik College of Engineering and Technology, Surat, India, July 2006 to November 2007.

Research Associate (Biomass Thermochemical Conversion), Sardar Patel Renewable Energy Research Institute (SPRERI), V.V. Nagar, India, July 2000 to July 2006.

Production Shift Engineer, Diamond Cables Limited, Vadodara, India, April 1999 to May 2000.

Trainee Engineer, Engineering Professional Groups, Surat, India, September 1998 to November 1998.

Professional Memberships:
Institute of Industrial Engineers (IIE)
American Society of Agricultural and Biological Engineers (ASABE)